An updated radiocarbon-based ice margin chronology for the last deglaciation of the North American Ice Sheet Complex

April S. Dalton[a,b], Martin Margold[b], Chris R. Stokes[a], Lev Tarasov[c], Arthur S. Dyke[d,e], Roberta S. Adams[f], Serge Allard[g], Heather E. Arends[h], Nigel Atkinson[i], John Attig[j], Peter J. Barnett[k], Robert Langdon Barnett[l,m], Martin Batterson[n], Pascal Bernatchez[l], Harold W. Borns, Jr[o], Andrew Breckenridge[p], Jason P. Briner[q], Etienne Brouard[r,s], Janet E. Campbell[t], Anders E. Carlson[u], John J. Clague[v], B. Brandon Curry[w], Robert-André Daigneault[x], Hugo Dubé-Loubert[y,z], Don J. Easterbrook[aa], David A. Franzi[bb], Hannah G. Friedrich[h†], Svend Funder[cc], Michelle S. Gauthier[dd], Angela S. Gowan[ee], Ken L. Harris[ff], Bernard Hétu[l], Tom S. Hooyer[gg†], Carrie E. Jennings[hh], Mark D. Johnson[ii], Alan E. Kehew[jj], Samuel E. Kelley[kk], Daniel Kerr[t], Edward L. King[ll], Kristian K. Kjeldsen[cc,mm], Alan R. Knaeble[ee], Patrick Lajeunesse[r], Thomas R. Lakeman[nn], Michel Lamothe[s], Phillip Larson[oo], Martin Lavoie[r], Henry M. Loope[pp], Thomas V. Lowell[qq], Barbara A. Lusardi[ee], Lorraine Manz[ff], Isabelle McMartin[t], F. Chantel Nixon[rr], Serge Occhietti[x], Michael A. Parkhill[ss], David J. W. Piper[ll], Antonius G. Pronk[tt], Pierre J. H. Richard[uu], John C. Ridge[vv], Martin Ross[ww], Martin Roy[z], Allen Seaman[g], John Shaw[ll], Rudolph R. Stea[xx], James T. Teller[yy], Woodrow B. Thompson[zz], Harvey L. Thorleifson[ee], Daniel J. Utting[aaa], Jean J. Veillette[t], Brent C. Ward[v], Thomas K. Weddle[zz], Herbert E. Wright, Jr[hh†]

Author affiliations

[a]Department of Geography, Durham University, Durham, United Kingdom

[b]Department of Physical Geography and Geoecology, Charles University, Prague, Czech Republic

[c]Department of Physics and Physical Oceanography, Memorial University, St. John's, Newfoundland, Canada

[d]Department of Earth Sciences, Dalhousie University, Halifax, Nova Scotia, Canada

[e]Department of Anthropology, McGill University, Montreal, Quebec, Canada

[f]Madrone Environmental Services Ltd, Abbotsford, British Columbia, Canada

[g]New Brunswick Department of Energy and Mines, Geological Surveys Branch, Fredericton, New Brunswick, Canada

[h]Division of Lands and Mineral, Minnesota Department of Natural Resources, St. Paul, Minnesota, USA

[i]Alberta Geological Survey, Edmonton, Alberta, Canada

[j]Wisconsin Geological and Natural History Survey, Madison, Wisconsin, USA

[k]Harquail School of Earth Sciences, Laurentian University, Sudbury, Ontario, Canada

[l]Département de biologie, chimie et géographie & Centre for Northern Studies (CEN), Université du Québec à Rimouski, Rimouski, Québec, Canada

[m]Geography, College of Life and Environmental Sciences, University of Exeter, Exeter, United Kingdom

[n]Geological Survey of Newfoundland and Labrador, St. John's, Newfoundland, Canada

[o]School of Earth and Climate Sciences, University of Maine, Orono, Maine, USA

[p]Natural Sciences Department, University of Wisconsin–Superior, Superior, Wisconsin, USA

[q]Department of Geology, University at Buffalo, Buffalo, New York, USA

[r]Département de géographie and Centre d'études nordiques, Université Laval, Québec, Québec, Canada

[s]Département des sciences de la Terre et de l'atmosphère, Université du Québec à Montréal, Montréal, Québec, Canada

[t]Geological Survey of Canada, Natural Resources Canada, Ottawa, Ontario, Canada

[u]College of Earth, Ocean, and Atmospheric Science, Oregon State University, Corvallis, Oregon, USA

[v]Department of Earth Sciences, Simon Fraser University, Burnaby, British Columbia, Canada

[w]Illinois State Geological Survey, Prairie Research Institute, University of Illinois at Urbana-Champaign, Champaign, Illinois, USA

[x]Département de géographie, Université du Québec à Montréal, Montréal, Québec, Canada

[y]Ministry of Energy and Natural Resources of Quebec, Val-d'Or, Quebec, Canada

[z]Département des Sciences de la Terre et de l'atmosphère, Centre de recherche GEOTOP, Université du Québec à Montréal, Montréal, Québec, Canada

[aa]Department of Geology, Western Washington University, Bellingham, Washington, USA

[bb]Center for Earth and Environmental Science, State University of New York Plattsburgh, Plattsburgh, New York, USA

[cc]Centre for GeoGenetics, Natural History Museum of Denmark, Copenhagen, Denmark

[dd]Manitoba Geological Survey, Winnipeg, Manitoba, Canada

[ee]Minnesota Geological Survey, University of Minnesota, St. Paul, Minnesota, USA

[ff]North Dakota Geological Survey, Bismarck, North Dakota, USA

[gg]Department of Geosciences, University of Wisconsin, Milwaukee, Wisconsin, USA

[hh]Department of Earth and Environmental Sciences, University of Minnesota, Twin Cities, Minnesota, USA

[ii]Department of Earth Sciences, University of Gothenburg, Sweden

[jj]Department of Geological and Environmental Sciences, Western Michigan University, Kalamazoo, Michigan, USA

[kk]School of Earth Sciences, University College Dublin, Dublin, Ireland

[ll]Natural Resources Canada, Geological Survey of Canada (Atlantic), Bedford Institute of Oceanography, Dartmouth, Nova Scotia, Canada

[mm]Department of Glaciology and Climate, Geological Survey of Denmark and Greenland (GEUS), Copenhagen, Denmark

[nn]Geological Survey of Norway, Trondheim, Norway

[oo]Swenson College of Science and Engineering, University of Minnesota Duluth, Duluth, Minnesota, USA

[pp]Indiana Geological and Water Survey, Indiana University, Bloomington, Indiana, USA

[qq]Department of Geology, University of Cincinnati, Cincinnati, Ohio, USA

[rr]Department of Geography, Norwegian University of Science and Technology, Trondheim, Norway

[ss]New Brunswick Department of Energy and Mines, Geological Surveys Branch, Bathurst, New Brunswick, Canada

[tt]Geological Survey, Energy and Resource Development, Fredericton, New Brunswick, Canada

[uu]Département de géographie, Université de Montréal, Montréal, Québec, Canada

[vv]Department of Earth and Ocean Sciences, Tufts University, Medford, Massachusetts, USA

[ww]Centre for Groundwater Research, University of Waterloo, Waterloo, Ontario, Canada

[xx]Stea Surficial Geology Services, Halifax, Nova Scotia, Canada

[yy]Department of Geological Sciences, University of Manitoba, Winnipeg, Manitoba, Canada

[zz]Maine Geological Survey, Augusta, Maine, USA

[aaa]Alberta Energy Regulator, Calgary, Alberta, Canada

[†]deceased

Keywords

Quaternary; glaciation; North America; ice margin chronology; radiocarbon

Abstract

The North American Ice Sheet Complex (NAISC; consisting of the Laurentide, Cordilleran and Innuitian ice sheets) was the largest ice mass to repeatedly grow and decay in the Northern Hemisphere during the Quaternary. Understanding its pattern of retreat following the Last Glacial Maximum is critical for studying many facets of the Late Quaternary, including ice sheet behaviour, the evolution of Holocene landscapes, sea level,

atmospheric circulation, and the peopling of the Americas. Currently, the most up-to-date and authoritative margin chronology for the entire ice sheet complex is featured in two publications (Geological Survey of Canada Open File 1574 [Dyke et al., 2003]; 'Quaternary Glaciations – Extent and Chronology, Part II' [Dyke, 2004]). These often-cited datasets track ice margin recession in 36 time slices spanning 18 ka to 1 ka (all ages in uncalibrated radiocarbon years) using a combination of geomorphology, stratigraphy and radiocarbon dating. However, by virtue of being over 15 years old, the ice margin chronology requires updating to reflect new work and important revisions. This paper updates the aforementioned 36 ice margin maps to reflect new data from regional studies. We also update the original radiocarbon dataset from the 2003/2004 papers with 1,541 new ages to reflect work up to and including 2018. A major revision is made to the 18 ka ice margin, where Banks and Eglinton islands (once considered to be glacial refugia) are now shown to be fully glaciated. Our updated 18 ka ice sheet increased in areal extent from 17.81 to 18.37 million km^2, which is an increase of 3.1% in spatial coverage of the NAISC at that time. Elsewhere, we also summarize, region-by-region, significant changes to the deglaciation sequence. This paper integrates new information provided by regional experts and radiocarbon data into the deglaciation sequence while maintaining consistency with the original ice margin positions of Dyke et al. (2003) and Dyke (2004) where new information is lacking; this is a pragmatic solution to satisfy the needs of a Quaternary research community that requires up-to-date knowledge of the pattern of ice margin recession of what was once the world's largest ice mass. The 36 updated isochrones are available in PDF and shapefile format, together with a spreadsheet of the expanded radiocarbon dataset (n = 5,195 ages) and estimates of uncertainty for each interval.

1 Introduction

The North American Ice Sheet Complex (NAISC) consisted of the Laurentide, Cordilleran, Innuitian and Greenland ice sheets that coalesced at the Last Glacial Maximum (LGM) during Oxygen Isotope Stage 2. As the largest ice mass of the Northern Hemisphere, the NAISC played an important role in the evolution of Quaternary climate, sea levels, atmospheric circulation, and the peopling of the Americas (e.g. Goebel et al., 2008; Carlson and Clark, 2012; Löfverström et al., 2014; Böhm et al., 2015; Waters et al., 2015; Löfverström and Lora, 2017; Potter et al., 2018; Waters, 2019). Accordingly, Quaternary scientists require knowledge of former ice positions over time for a broad range of disciplines. These isochrones also provide useful analogues of ice sheet behaviour that go beyond the observational record of modern ice sheets (e.g. Stokes et al., 2016) and are therefore critical for the calibration of numerical models to study past ice sheet change in response to climate (e.g. Tarasov et al., 2012; Batchelor et al., 2019).

Fifty years ago, the first substantial attempts at reconstructing the NAISC combined glacial geomorphology, stratigraphy and radiocarbon dating to reconstruct the pattern of ice retreat from 18 ka through the Holocene (Bryson et al., 1969; Prest, 1969). These pioneering maps were subsequently updated to reflect more detailed mapping of the Quaternary geology of North America and the consequent increase in the number and quality of relevant radiocarbon dates (Dyke and Prest, 1987; Dyke et al., 2003; Dyke, 2004). Currently, a Geological Survey of Canada Open File Report containing 36 time slices spanning 18 ka to 1 ka (all ages in this study are reported in uncalibrated radiocarbon years; see Section 2) is widely regarded as the authoritative source for deglaciation isochrones for the NAISC (Dyke et al., 2003). This work was also published the following year in Ehlers and Gibbard's 2004 book: 'Quaternary Glaciations – Extent and Chronology, Part II' (Dyke, 2004) with a brief interpretation of the pattern of deglaciation.

Given the continued growth in the size and diversity of chronological data (Stokes et al., 2015) a revision of the NAISC margin chronology is overdue. For example, recent marine geophysical work and mapping of ice streams (Brouard and Lajeunesse, 2017; Shaw and Longva, 2017; Margold et al., 2018) suggests an expansion of the LGM ice margin onto the continental shelf well beyond that depicted by Dyke et al. (2003). In addition, new regional reconstructions of post-18 ka ice dynamics and ice streaming have been produced (De Angelis and Kleman, 2007; Ross et al., 2012; Hogan et al., 2016; Gauthier et al., 2019) and there has been a surge in the use of non-radiocarbon dating methods (e.g. cosmogenic exposure and optically stimulated luminescence; Wolfe et al., 2004; Briner et al., 2009; Munyikwa et al., 2011; Lakeman and England, 2013; Ullman et al., 2015; Ullman et al., 2016; Corbett et al., 2017b; Margreth et al., 2017; Dubé-Loubert et al., 2018b; Leydet et al., 2018; Barth et al., 2019; Corbett et al., 2019). All these data provide additional information on ice extent and the dynamics of ice margin retreat.

Here, we integrate new information provided by regional experts, along with new radiocarbon data, into the North American deglaciation sequence. Where new information is lacking, we maintain the original ice margin positions of Dyke et al. (2003). Working from the original Dyke et al. (2003) isochrones and retaining them where new information is lacking prevents us from integrating non-radiocarbon dating methods. We first describe major updates to the 18 ka ice margin. We then summarize significant changes to the deglaciation sequence, region by region (see Fig. 1). Included in this update are 1,541 radiocarbon ages to the radiocarbon dataset of Dyke et al. (2003) with work undertaken from 2003 to 2018 (Fig. 2; Table A1). Because the dates were originally reported as uncalibrated by Dyke et al. (2003), we keep this practice and show all new dates as uncalibrated. However, the maps we present also indicate a calibrated age for each given ice-marginal line. The relation between calibrated and uncalibrated ages is shown in Table 1. We consider this to be a pragmatic solution that satisfies the needs of a Quaternary research community that requires up-to-date knowledge of the pattern of ice margin recession over North America. We conclude by outlining strategies for creating a new generation of deglaciation isochrones that is independent of Dyke et al. (2003).

2 Methods, estimates of uncertainty and limitations

Our starting point for each of the 36 isochrones is the pattern of ice retreat suggested by Dyke et al. (2003) and we make changes to the ice margins based on recent work. Updates were largely accomplished by overlaying data from regional studies and/or manually editing the ice margins to fit recently mapped landforms of known age (e.g. moraines in the Canadian Prairies). We also make adjustments based on a review of relevant publications addressing NAISC margins and configuration since 2002 and compiled a radiocarbon dataset that includes relevant dates that have been published from 2002 to 2018 (n = 5,195 radiocarbon dates). In some areas, we present new interpretations of the deglaciation sequence (e.g. the Des Moines Lobe; Section 4.12). In regions where there are few geochronological constraints on which to interpret the pattern of ice retreat, we build the new ice margin around a few reliable data points. Regions and time slices not mentioned here retain the ice margin of Dyke et al. (2003). Notably, the isochrones from 5 ka to 1 ka are largely unchanged from Dyke et al. (2003). We discuss all major adjustments in the text below and, for clarity, the new maps (see Figs. B1-2) show the overlap between the original and updated isochrones.

Keeping with the conventions of Dyke et al. (2003), this manuscript and the accompanying appendices use uncalibrated radiocarbon years. In cases where multiple radiocarbon ages are available for the same site, we generally include the oldest date in what may be a stratigraphic series of dates. Some data were excluded from the dataset if suggested to be incorrect by authors of the original publication. This includes several radiocarbon ages on freshwater ostracods from Ontario/Quebec (hard water contamination; Daubois et al., 2015) and a bulk lacustrine sediment sample from Baffin Island (suspected incorporation of old carbon; Narancic et al., 2016). However, no thorough evaluation of radiocarbon dates is presented here.

All radiocarbon ages are normalized to a $\delta^{13}C$ value of −25‰, following the conventions of Stuiver and Polach (1977). Marine corrections generally follow the work of Dyke et al. (2003), but several important updates are included. Notably, shells from the Arctic and subarctic regions are corrected according to the work of Coulthard et al. (2010), and we use a correction of 1 kyr for shells from New England (following Thompson et al., 2011) and a 1.8 kyr correction for shells marking the inception of Champlain Sea near Montreal (following Occhietti and Richard, 2003; Richard and Occhietti, 2005). Justification for each marine reservoir correction is specified in Table A1.

2.1 Estimates of uncertainty for each isochrone

Users requiring estimates of min/max uncertainty for each isochrone are directed to our suggested guidelines in Table 1. We base our uncertainties on our best estimate for each interval and we expect the ice margin to have been located within the suggested min/max for the given time interval. However, this may not be the case in areas where the ice margin is poorly understood or drawn based on limited data. For example, along the continental shelves, given the sometimes limited constraints, the ice margin should be considered as maximum grounded ice.

2.2 Limitations and uncertainties

Although some new regional interpretations are presented in this paper, our work is not a systematic re-interpretation of deglaciation of North America. Instead, this work is best viewed as a series of critical updates to the previous work of Dyke et al. (2003). Thus, users of these data should bear in mind the following caveats and considerations.

2.2.1 Our updated ice margins are intended for use at continental scale

In some regions, we present a highly refined ice margin that is likely to be accurate to within several meters (e.g. placement of the ice margin at moraines in the Canadian Prairies; see Section 4.13). However, in other areas, the ice margin remains generalised or unchanged from the work of Dyke et al. (2003). In other cases still, the ice margin was interpolated or inferred from regional studies (e.g. several isochrones from 17 ka to 13 ka along the Arctic coastline). Owing to this patchwork approach, ice margins from this manuscript are not intended for use at a high spatial resolution (e.g. scales of 1:1,000,000 or finer). If such high-resolution information is required, the reader is encouraged to visit the most recent local studies. For the same reason, the ice margins provided here are not prescriptive for determining outlets, spillways or pinch points for proglacial lakes.

2.2.2 Ice margin positions are averaged over the interval of interest

Our decision to maintain the same time steps as Dyke et al. (2003) necessarily results in time-averaging some short-lived fluctuations of the ice sheet margin. For example, the Cochrane re-advance (Veillette et al., 2017) that likely occurred in the 0.3 kyr immediately preceding the collapse of the Hudson Bay Ice Saddle (Hughes, 1965; Hardy, 1977; Roy et al., 2011; Godbout et al., 2019) and immediately preceding the drainage of Lake Agassiz-Ojibway. Moreover, in some cases, the discrete time steps in this paper give the impression that ice lobes acted synchronously. This is particularly notable in the Des Moines Lobe (see Section 4.12). Readers should note these ice lobes were in fact highly dynamic, typically thin and occurred over a deformable substrate. Overall recession of the ice margin associated with some of these lobes generally followed a pattern of advance, followed by an interval of retreat/stagnation, then a re-advance to a lesser position (see Section 4.12). Thus, the updated ice margins may not reflect the independent behaviour of the Lake Michigan, Saginaw and Huron-Erie lobes.

Another artefact of this time-averaging is that, occasionally, some ice margins may appear incompatible with the local landscape (e.g. an unrealistically smooth ice margin over a highly dynamic surface). Time-averaging of the ice margins may also yield some ice dynamics that are difficult to explain from a glaciological standpoint (e.g. rapid ice surge over a large lake with no obvious source of mass displacement). Moreover, some ice margins are inferred or interpolated. For example, when a significant update to the ice margin resulted in an abrupt discontinuity at the boundary between a regional compilation and Dyke's ice margin, we smoothly connected the ice margins. In some cases, manual interpolation of the ice margins was necessary; this was accomplished by equally distributing the ice margins (e.g. ice margins between 18 ka to 13 ka along the entire Arctic coastline). Users of these updated ice margins should bear in mind these considerations.

2.2.3 Some marine ice margins are undated

Since the publication of Dyke et al. (2003), the study of marine regions has grown substantially (e.g. seismic surveys, mapping of the geomorphological record) and much evidence now suggests a highly dynamic ice margin over many continental shelf regions of the Arctic and Atlantic coastlines at 18 ka (see Section 3). While these marine-based data clearly suggest the presence of ice near the shelf break in most Arctic and Atlantic regions, we stress these landforms are largely undated. As such, the timing and depiction of ice sheet recession is assumed, interpolated or inferred from adjacent land-based evidence. In the above example, we cannot rule out the possibility that these ice margins represent a pre-LGM ice position. The reader should be aware of the uncertainty that this introduces to our ice margins and hence there is potential for future work to refine these margins further.

2.2.4 <u>We make no changes to Iceland, Greenland or Cordilleran ice sheets</u>

The decision to retain the ice margins of Dyke et al. (2003) for the Iceland, the Greenland and (for a large part of) the Cordilleran ice sheets was made on a pragmatic basis. Although recent work has taken place in these regions (Winsor et al., 2015; Sinclair et al., 2016; Corbett et al., 2017a; Larsen et al., 2017; Levy et al., 2017; Dyke et al., 2018), the resulting glacial chronologies are heavily reliant on cosmogenic exposure dating and thus include assumptions and sources of error not discussed in this largely radiocarbon-based review. Readers interested in updated ice margin maps from these regions are encouraged to read local studies.

2.2.5 <u>The Last Glacial Maximum was asynchronous</u>

For consistency with Dyke et al. (2003), our maps begin the deglaciation sequence at 18 ka. However, the LGM extent was reached at different times in each region (Dyke et al., 2002; Clark et al., 2009; Ullman et al., 2015; Stokes, 2017). Notably, our maps miss the maximum ice extent in the Great Lakes area (occured prior to 22.5 ka; Heath et al., 2018; Loope et al., 2018), Labrador (maximum ice extent reached prior to 30 ka; Roger et al., 2013) and the Atlantic Canada margin (occured at ~20 ka; Baltzer et al., 1994). Our maps also record ice sheet advance in some western areas (ice advance as late as 15.5 ka; Lacelle et al., 2013).

2.2.6 <u>Our work does not show the extent of proglacial lakes</u>

We recognize that ice-dammed lakes are critical for delineating the position of an ice margin in a given region. However, calculating the extent of such lakes requires a thorough examination of the relationships between ice-marginal positions, lake levels, dated shorelines and spillways (Lewis and Anderson, 1990; Teller and Leverington, 2004; Breckenridge, 2015; Hickin et al., 2015) that is beyond the scope of this primarily ice margin paper. At the same time, it is inappropriate to overlay the proglacial lakes of Dyke et al. (2003) onto our updated ice margins since the outlines of these lakes are often not aligned with the updated ice margin. Thus, we made a practical decision to remove proglacial lakes from our ice margin reconstructions. Note that, while we do not explicitly plot proglacial lakes, our updated ice margins and the position of marine re-entrants (calving embayments) take into considerations evidence for these landscape features (e.g. re-drawing of the deglaciation of the Labrador Dome; Section 4.8).

3 Overall changes to the 18 ka ice margin

Some of the most substantive updates that we make are to the 18 ka ice margin. In this section, updates are presented in a clockwise direction starting in the northwest Arctic, moving to the Arctic Islands, Atlantic coastline and finally to terrestrial regions (Figs. 1 and 2). Compared to Dyke et al. (2003), our updated 18 ka ice sheet increased in areal extent from 17.81 to 18.37 million km^2, which is 3.1% more spatial coverage of the NAISC at that time (Table 1). All changes to the ice margin following 18 ka are discussed in Section 4.

In Arctic Canada, Dyke et al. (2003) depicted an 18 ka ice margin that largely followed the outer coastline of the Canadian Arctic Archipelago. The major exception to this pattern was the western Queen Elizabeth Islands (Prince Patrick, Eglinton, and Melville islands) and Banks Island, depicted as supporting only local ice caps or as ice-free glacial refugia, respectively, at 18 ka (Fig. 3). For reasons we describe in the next paragraph, a major feature of our update is the extension of this ice margin to the continental shelf edge along the entire western Arctic coastline. This includes an extension of ice 100 km northward to shelf-break in the Beaufort Sea and glaciation across mid Yukon Shelf (King et al., 2019) as well as a substantial extension of 18 ka ice in the northwestern Arctic (by >200 km near Banks Island) over what was depicted by Dyke et al. (2003) for the same interval. Farther north along the Arctic coastline, we adjust the 18 ka ice margin to the shelf edge on the basis of geomorphological records showing pronounced modification of the continental shelf by ice streams draining the Innuitian Ice Sheet (Margold et al., 2015).

We present three key pieces of evidence for the shift of 18 ka ice to the continental shelf. (1) Seismic surveys from Amundsen Gulf and adjacent Beaufort Sea identify ice stream bedforms and deposits extending to the shelf edge and upper slope (Batchelor et al., 2014; King, 2015; MacLean et al., 2015). (2) Recent seismic surveys from the vicinity of Beaufort Shelf including the outermost Yukon Shelf suggest that ice was fed from the marine realm and not across the coastline (King et al., 2019). (3) The presence of thick tills in the Amundsen Gulf, indicating an ice extent to the outer eastern Beaufort Shelf. Moreover, recent marine surveying confirmed the confluence of the Laurentide and Innuitian ice sheets in M'Clure Strait (e.g. immediately northeast of Banks Island) with a shelf break ice margin (King, 2015).

We also extend the 18 ka ice margin seaward near Greenland and Baffin Island. In the extreme far north, the junction of the Greenland and Innuitian ice sheets is placed to the shelf edge following the suggestion of Funder et al. (2011). In the eastern Arctic, a similar expansion of the 18 ka ice margin offshore of Baffin Island is suggested by geomorphology, cosmogenic nuclide dating and marine-based work (Fig. 3). Extensive cosmogenic work and mapping of glacial features on Baffin Island initiated this idea (e.g. Briner et al., 2005; Miller et al., 2005). Additional support is provided by marine-based work such as acoustic profiles and core samples (mapping of an ice-contact submarine drift; Praeg et al., 2007), sedimentological evidence of a grounding line (Li et al., 2011), the presence of ice margin diamicts (Jenner et al., 2018) and a suite of geophysical evidence (e.g. lateral moraines, ice-contact evidence; Brouard and Lajeunesse, 2017, 2019; Lévesque et al., 2020). Following the aforementioned studies, we extend the 18 ka ice margin to the continental shelf edge along the coast of Baffin Island and Labrador (Fig. 3). In this region, we show ice remaining near the continental shelf (east coast of Baffin Island) from 18 ka to ~12 ka prior to moving on land (Jenner et al., 2018). These edits require a manual interpolation of the 17.5 ka to 13.5 ka ice margins to fit between the new 18 ka and existing 13 ka isochrones (see Section 4.3).

Along the coast of Labrador, we draw the local LGM at the shelf break (Josenhans et al., 1986) and assign it to 18 ka. However, locally, this may have been considerably earlier. The 18 ka ice limit is delineated by the extent of 'till 3a' in Josenhans et al. (1986) (not shown in Fig. 3). In Atlantic Canada, we adjust the 18 ka ice margin to cover most of the Grand Banks and Scotian Shelf (Piper and Macdonald, 2001). The updated ice margin now extends to a depth of over 500 m at the continental shelf edge (Hundert and Piper, 2008) and shows an ice front in the Laurentian Channel at the shelf edge (Shaw et al., 2006). We also extend 18 ka ice to cover the Notre Dame Trough as suggested by recent examination of glaciomarine landforms (Robertson, 2018); this embayment was previously depicted as ice-free at 18 ka (Dyke et al., 2003). Because the 18 ka ice margin falls ~0.5 kyr after Heinrich Event 2, our 18 ka margin depicts ice pulled back from the shelf edge in places such as Hudson Strait and Trinity Trough. As such, the true timing of extent of ice cover across this region is largely lacking; retreat may have initiated at least 2 ky prior to 18 ka (depicted by a red dashed line; Fig. 3). At the extreme southeastern extent of the 18 ka ice margin, near Long Island, we adjust the ice margin inland by ~20 km to align with recent mapping of glacial deposits (Stone et al., 2005).

We also make adjustments to the 18 ka ice margin south of the Great Lakes. At the time of Dyke et al. (2003), ice margin constraints in this region were limited. As a result, most ice margins were generalized. Since then, recent work has contributed significant refinement to recession of the 18 ka ice margin in this region. We update the 18 ka ice lobe in Indiana and Ohio to follow recent work on the rate of glacial retreat in this area (Heath et al., 2018; Loope et al., 2018). For example, the updated 18 ka limit in central Indiana now follows the Crawfordsville Moraine (not shown in Fig. 3, see: Wayne, 1965; Loope et al., 2018) which ranges from 10 to 50 km inboard of the previous 18 ka ice extent. Overall, adjustments to the Huron-Erie Lobe range between 10 km and 200 km inboard of the ice margins of Dyke et al. (2003). Significant changes are also made to the Lake Michigan Lobe, based largely on improved sedimentology and chronology of moraine deposits and associated paleo ice-marginal lakes. To better fit with recent chronology work in this area, we align the 18 ka ice margin with the Marseilles Morainic Complex (not shown in Fig. 3, see: Curry and Petras, 2011; Curry et al., 2014; Curry et al., 2018).

Finally, we adjust 18 ka ice in the extreme northwest region of the former ice sheet. In Alaska, we replace the 18 ka isochrone with the isochrones from Kaufman et al. (2011). Key updates include the refinement of ice extent over the Brooks Range, along with the complete removal of ice from the extreme western area of the Brooks Range (known as the De Long Mountains). We also reduce ice over the Ahklun Mountains, and we modify the ice limit on the continental shelf along the southern coast of Alaska (Fig. 3). In Southeast Alaska, we adjust the 18 ka ice margin by ~30 km inboard to align with recent work suggesting the maximum extent of ice in this area was reached after 17 ka (Heaton and Grady, 2003; Lesnek et al., 2018). We also make a minor adjustment to the ice margin in the extreme west of the Northwest Territories following Lacelle et al. (2013). In that case, we adjust the local ice margin inboard by ~25 km between 18 ka to 15.5 ka to reflect a ‘stillstand’ (see Lacelle et al., 2013).

Prior to our update of the 18 ka ice margin (herein), Margold et al. (2018) showed an 18 ka ice margin in the Canadian Artic that was similarily extended to the continental shelf. The purpose of their 18 ka ice margin was to fit the reconstructed drainage network of the Laurentide Ice Sheet within the ice sheet outline; in that case, updates were made on an ad-hoc basis to conform with the position and dynamics of ice streams as well as tentative suggestions from the literature (Briner et al., 2006; England et al., 2006; Shaw et al., 2006; Lakeman and England, 2012; Jakobsson et al., 2014; Brouard and Lajeunesse, 2017). Because our work is based on regional expertise, coastal radiocarbon dates and a geologic framework for sediments on the continental shelf, our 18 ka ice margin is different than that of Margold et al. (2018). For example, in the Beaufort Sea area, Margold et al. (2018) inferred a more extensive glacier cover than what we show.

4 Additional post-18 ka changes to the ice margin

Updates to the ice margins of Dyke et al. (2003) are also warranted following the 18 ka interval. These updates are presented in a clockwise direction starting in the northwest Arctic region (see Fig. 1 for overview of each location). Note that Figs. 4-14 do not show all changes described in this section. Rather, these figures contain brief summaries of key regional changes to the ice margin at select intervals. The reader is referred to Figs. B1-2 in Appendix C, which contain all updated isochrones in PDF and shapefile formats.

Readers interested in the broad, continental-scale changes to the ice margin are referred to Table 1. In this table, we present a summary of changes to each isochrone, as well as a comparison of areal extent of the updated ice sheets compared to the original of Dyke et al. (2003) for each timestep. Estimates of uncertainty for each isochrone are also provided in Table 1.

4.1 Banks, Melville, Eglinton islands and M’Clure Strait

New seismic evidence and limited sampling in M’Clure Strait and offshore Banks Island since 2014 compliments the extension of 18 ka ice over Banks, Melville and Eglinton islands (Section 3), requiring an entirely new depiction of the timing, pattern, and dynamics of subsequent ice margin retreat in this region. Our updated ice margins show a stepwise deglaciation from 18 ka based largely on undated geomorphological and marine-based records (Figs. 4 and Figs. B1-2). For example, during the deglaciation sequence, the flank of the M'Clure ice stream cut the northern edge of Banks Island, then splayed southward forming a marked scarp to within kilometres of the shelf break (King et al., 2014). This resulted in exceptionally thick stratified material on Banks Shelf, none of which has a recognizable glacier sole imprint, further indicating that ice emanating from Banks Island was limited, perhaps to the innermost shelf (Fig. 4). In this region, a marine margin (or its timing) is not yet recognized despite overconsolidated mud (glacially loaded?) on an extensive low stand-related terrace (King et al., 2014) and recognition of drumlins of unknown stratigraphic position beyond it. With the only time constraint of 12 ka on an ice margin trending north-south across the central interior of Banks Island (Lakeman and England, 2012, 2013), we manually interpolate a pattern of ice retreat between these two timesteps (17.5 ka and 12.5 ka) taking into consideration ice-lateral meltwater channels and other geomorphic features (Lakeman and England, 2013). Additional radiocarbon age constraints indicate final ice sheet withdrawal from Banks Island and Amundsen Gulf by ~10.5 ka (Dyke and Savelle, 2000; Lakeman and England, 2012; Lakeman et al., 2018).

The Innuitian Ice Sheet (Fig. 3) was largely erosional (no retreat moraines) with a notable exception in a massive mid-trough moraine off Eglinton Island, apparently in reaction to a loss of pinning with the collapse of the M'Clure ice stream before retreat to land. On nearby Melville Island, we show that ice persisted for longer than what was suggested by Dyke et al. (2003). Following Nixon and England (2014), we show remnant ice in the form of island-based ice caps, especially in western Melville Island, which has some high-elevation plateaux (Fig. 4). Our updated maps show a near-synchronous ice retreat from eastern M'Clure Strait and western Viscount Melville Sound at ~11.5 ka (England et al., 2009). We make further refinements on Melville Island between 12 ka and 10 ka to follow extensive mapping, geomorphology and radiocarbon work (Nixon and England, 2014). We also retain a remnant ice lobe over northeastern Melville Island until 9 ka following the work of Hanson (2003).

4.2 Beaufort Sea and Amundsen Gulf

In the Beaufort Sea, we extend the ice margin between 18 ka and 15.5 ka northward by ~100 km compared to Dyke et al. (2003). The updated ice margin now lies at the shelf-break as opposed to remaining at the coastline (Figs. B1-2). The shelf break position between the trough mouths is based on subtle mass-wasting features attributed to a glacial margin, but we note the timing and duration of this ice margin is undated. This updated ice margin is further marked by evidence of a floating glacier in over 500 m (present water depth) with a large ice component sweeping the outer Yukon Shelf and at least one mid-shelf still-stand or minor re-advance (King et al., 2019). The pattern of retreat from this position follows ice-marginal features at the mouth of Mackenzie Trough, notably moraines that, until now, were considered to date to the LGM. We assign this retreat event to 15 ka based on radiocarbon ages from near to the shoreline (Figs. B1-2). Note that ice margins on the central Beaufort Shelf are inferred because marine transgression would have removed most evidence.

Similar features lead us to begin the shelf-break retreat at Amundsen Gulf at around the same time as the Beaufort Sea (~15 ka). However, in some cases, the timing is more precise in Amundsen Gulf because it can be linked to ice-rafted debris pulses (Lakeman et al., 2018). Retreat of ice from the Amundsen Gulf was punctuated, marked by a large moraine spanning the trough between Banks Island and Franklin Bay (Fig. 4) and a thin ice tongue occupying the bay. Collapse was rapid, dated by far-travelled ice rafted detritus events constraining three margins (Lakeman et al., 2018). Additional radiocarbon age constraints indicate final ice sheet withdrawal from Banks Island and Amundsen Gulf by 10.5 ka (Dyke and Savelle, 2000; Lakeman and England, 2012; Lakeman et al., 2018). Immediately following outer trough retreat, a thick, stacked till tongue complex demonstrating multiple fluctuations emanated from the adjacent bank, flowing northward into Amundsen Gulf. This cannot have been maintained without ice cover across the Beaufort Shelf.

Despite significant progress in refining ice margins in the Beaufort Sea and Amundsen Gulf, some elements of our reconstruction remain speculative. For example, around 13 ka, discrepancies arise in the southern Amundsen Gulf trough-mouth when attempting to reconcile the marine records with land-based evidence for the ice sheet; the marine record contains too many margin fluctuations and apparent longevity to form from the ice tongue depicted at ca. 13 ka (Fig. 4). However, our ice depiction can be satisfied if the main Amundsen Gulf ice stream periodically floated across the deep reaches between here and Banks Island at earlier stages.

4.3 Central and Eastern Queen Elizabeth Islands

England et al. (2006) presented an updated interpretation of the deglaciation of the Innuitian Ice Sheet (see Fig. 3) suggesting that the pattern of ice retreat in this region may have been more rapid than what was suggested by Dyke et al. (2003). This new interpretation depicted many of the Central and Eastern Queen Elizabeth Islands as hosts to local ice dispersal centres at 18 ka (England et al., 2006; England et al., 2009; Nixon and England, 2014). We adopt these changes to the broad region of the Innuitian Ice Sheet, mostly consisting of minor adjustments to the ice margin and the most substantive change being an accelerated rate of ice retreat over marine regions at ~9 ka (Figs. 5 and Figs. B1-2). We further refine the pattern of ice retreat around the Amund and Ellef Ringnes islands, as well as southern Ellesmere Island to reflect detailed work that has taken place in those regions (after Atkinson, 2003; England et al., 2004). The result is a much refined ice margin and more persistent ice masses on these islands over the generalized work of Dyke et al. (2003).

We also make changes to deglaciation of the Nares Strait, the region of separation of the Innuitian and Greenland ice sheets (Fig. 5). North of Nares Strait, marine core evidence from the coast of Greenland suggests that retreat of the ice sheet from the edge of the continental shelf began as early as 16 ka (Larsen et al., 2010) and had reached the central area of the Nares Strait by ~8.5 ka (Jennings et al., 2011a). We update the pattern of ice retreat to incorporate these constraints, the most substantive of which are expansions of the ice margin by ~150 km northward at 16 ka (Figs. B1-2). Similarly, in the southern Nares Strait, the oldest radiocarbon age in a marine core suggests the separation of the Innuitian and Greenland ice sheets occurred between 8.5 ka and 6.5 ka (Georgiadis et al., 2018) and we update the relevant isochrones to reflect this increased rate of deglaciation (Figs. 5 and B1-2). We also make minor adjustments (largely < 10 km) to the ice margin along the western coast of Greenland (only in the area immediately adjacent to the Nares Strait) to reflect radiocarbon ages (e.g. extensive dating of shell deposits on coastal Greenland; Bennike, 2002). No other changes were made to the Greenland Ice Sheet.

4.4 Barrow Strait and Lancaster Sound

The Northwest Passage is a major marine waterway in the Canadian Arctic consisting of the Barrow Strait, Lancaster Sound and Viscount Melville Sound (Fig. 5). Here, we make refinements to the deglaciation sequence of Lancaster Sound, located in the eastern Northwest Passage, based on several recent studies of grounding zone wedges, marine sedimentology, geochemistry and paleoproxy data that refine the pattern of ice retreat in this region (Ledu et al., 2010; Pieńkowski et al., 2012; Bennett et al., 2013; Pieńkowski et al., 2014; MacLean et al., 2017; Furze et al., 2018). Radiocarbon dates from these marine cores provide evidence for a more accelerated deglaciation of eastern Lancaster Sound than previously understood. Notably, Li et al. (2011) assign a 13.5 ka age (~16 ka calibrated) to the latest till tongue in deep water on Lancaster Fan (easternmost Lancaster sound, reaching into northern Baffin Bay) suggesting that initial retreat began at this time from the LGM. As a result, we extend the ice margin at 13.5 ka by ~150 km and the updated 13.5 ka ice limit is based on their seismic control (Figs. B1-2). The subsequent westward deglaciation of Lancaster Sound is updated to reflect several successive but largely undated retreat margins, mainly marked by grounding zone wedges suggesting punctuated westward retreat (Figs. 5 and B1-2). Chronology, though limited, conforms to land-based studies and is based on extrapolated dates to the basal diamict in two cores (Pieńkowski et al., 2013). In this region, the maximum adjustment of the ice margin over what was depicted by Dyke et al. (2003) was ~200 km at 10 ka. Our updated isochrones are based largely on the new pattern of ice retreat presented in Pieńkowski et al. (2014).

Our updated ice margins in the vicinity of Barrow Strait (Fig. 5) reflect the presence of several stacked till sheets, undated except for the uppermost. At ~9.5 ka, we show ice from the Wellington Channel splaying southward toward Prince Regent Inlet (MacLean et al., 2017); this re-advance postdated retreat in the Viscount Melville Sound region and is dated through extrapolation of the Pieńkowski et al. (2013) age model. We also make adjustments to ice margins in Barrow Strait, but do not recognize any stepwise retreat deposits in the channels south of Lancaster Sound. Further, between 10 ka and 9 ka, our updated ice margins show Innuitian ice from Wellington Channel streaming in a southerly direction and meeting Barrow Strait ice, which caused an overdeepening of the strait along a syncline. This likely afforded the preservation of multiple local tills, demonstrating dynamic mid-channel margin fluctuations though margin reconstruction from the till remnants remain indefinite. We add a margin marking the uppermost till edge tracing across Barrow Strait and recognize a re-advance (through mega-scale glacial lineations) emanating southwestward from Wellington Channel and overriding earlier till deposits (Figs. B1-2). This was likely a reaction to calving of Barrow Strait, just as for Regent Sound. We adjust the margin that built a distinct grounding-zone wedge at the mouth of Wellington Channel and now recognize further northward, stepped retreat with at least two other (undated) arcuate till bodies crossing

Wellington Channel within an otherwise deposit-sparse area. Large extrapolation of core dates from Pieńkowski et al. (2012) place the uppermost Barrow Strait till about 9.6 ka, possibly older (Figs. 5 and B1-2). Further westward retreat in Barrow Strait saw several minor stillstands marked by small moraine fields, rare eskers, and thin grounding-zone wedges in an otherwise very thin Quaternary cover. In this region, chronological constraints are from land only.

4.5 Labrador Shelf and Hudson Strait

As described earlier (Section 3), along the coastline of Labrador, we adjust the 18 ka ice margin to the local LGM at the shelf break (Josenhans et al., 1986). The retreat from this maximum extent filled only the coast-marginal trough, along the entire Labrador offshore, and went partially into most of the shelf-crossing troughs ('till 3b' in Josenhans et al., 1986). However, without known ages, we rather arbitrarily assigned this margin to 16 ka and manually adjusted time slices accordingly (See Figs. B1-2). We also extent ice eastward from Hudson Strait and Frobisher Bay to the shelf break, its margin marked by the extent of an undated till from the final ice lobe here ('till 3c' in Josenhans et al., 1986). It is also assigned a rather arbitrary age to be compatible with a later “Gold Cove” event at 9.9 ka and subsequent “Noble Inlet” re-advance at 8.9 ka, both spilling across Meta Incognita Peninsula, the southernmost Peninsula on Baffin Island (Manley, 1996; Manley and Jennings, 1996). This was followed by retreat of ice along the deepest Hudson Strait axis by 8.4 ka to leave marine ice emanating from Ungava Bay and outer Meta Incognita Peninsula (Jennings et al., 1998). Cosmogenic dating on land explained by weathered erosional remnants beneath cold-based ice (Marsella et al., 2000), helped reconcile the differences with the ice margin minimal versus maximum extents.

4.6 Hudson Bay region

Keeping with the ice margin depictions of Dyke et al. (2003), one of the first areas to become ice-free during the deglaciation of Hudson Bay was Ungava Peninsula (Fig. 6). We retain this general chronology here. However, in this section we describe several key adjustments to the ice margin along the Quebec coastline, Ungava Peninsula and Southampton Island. Our updates include a significant reduction in the ice margin between 9 ka and 7 ka (Fig. 6). We update all isochrones affected by new mapping work (precise ice margins shown in Daigneault, 2008). Note that the focus of this section is on the general deglaciation of the Hudson Bay region; the independent Labrador Dome is discussed in Section 4.8.

Several key adjustments are necessary to the pattern of ice retreat between 8 ka and 7 ka on Foxe Peninsula, Baffin Island. Using a combination of field evidence and new chronology, Utting et al. (2016b) suggested this region deglaciated more rapidly than what was depicted by Dyke et al. (2003). We update the deglaciation isochrones accordingly, which amounts to mostly minor changes on the range of 10 km to 20 km inland (Fig. 6). Similarly, on Southampton Island, Ross et al. (2012) presented a suite of radiocarbon dates from shells that offer new resolution on the timing of deglaciation. Notably, these new data suggest the northern region of Southampton Island was ice-free by 7 ka, which amounts to a shift in the ice margin of Dyke et al. (2003) by >200 km inland toward Foxe Basin (Fig. 6). Isochrones elsewhere on Southampton Island are adjusted inland by ~20 km toward a remnant ice cap over the central uplands until 6.5 ka (Figs. B1-2). In this region, we also modify the ice margin at 7.6 ka to represent the initiation of the opening of Foxe Basin, and at 7.2 ka to show the retreat toward Frozen Strait, which is linked also to the ice flow reversal towards Repulse Bay (McMartin et al., 2015).

Inland of northwestern Hudson Bay, recent extensive mapping projects in Eastern Keewatin (McMartin and Henderson, 2004; Little, 2006; McMartin et al., 2015) have led to higher-resolution mapping of glacial features (moraines, striations, streamlined landforms) and provided new radiocarbon dates to constrain marine invasion against the retreating ice margins between 8.5 ka and 7.6 ka (Figs. 6 and B1-2). West of Committee Bay, we adjust the 8.5 ka ice margin to the northeast by < 15 km to match a recently mapped moraine from this area (Giangioppi et al., 2003; Little, 2006) and we shift the 8 ka to 7.6 ka ice margins inland by several km to match the Chantrey Moraine System (moraines not shown in Fig. 6, see: Campbell et al., 2013). These changes better account for the near 1.5 kyr difference between ages north and south of the Chantrey Moraine System, reflecting a significant still stand/retreat position. A retreat position farther north at 7.2 ka also leaves time and space for an ice flow reversal to occur toward Repulse Bay before the ice margin pulls back in Rae Isthmus (McMartin et al., 2015). Further west, in central Keewatin, we also extend the Chantrey Moraine System positions at 8.0 and 7.8 ka to match the MacAlpine Moraine System (moraines not shown in Fig. 6, see: Dredge and Kerr, 2013; Levson et al., 2013; Campbell et al., 2019) and to reflect migrating ice divide positions (cf. McMartin and Henderson, 2004). We also add a small, <50 km extension to the northern part of the Keewatin dome, and a small remnant ice cap at 6.5 ka. Our rationale for the latter adjustments is recent mapping in the region on either side of Wager Bay (Dredge and McMartin, 2007; McMartin et al., 2015) which suggests the last position of the ice divide was located farther north than what is suggested by Dyke et al. (2003).

4.7 Southern Hudson Bay

Recent and emerging work hints at a different mechanism for the drainage and timing of Hudson Bay over what is depicted by Dyke et al. (2003); this work is detailed below. However, in an effort to present a single set of deglaciation ice margins for the entire North

American Ice Sheet complex, we made a pragmatic decision to present a model that is largely unchanged from that of Dyke et al. (2003). Accordingly, ice margin retreat in southern Hudson Bay is marked by the collapse of an ice saddle over the Hudson Bay basin (termed the Hudson Bay Ice Saddle), and coeval drainage of glacial Lake Agassiz-Ojibway around ~7.55 ka (Barber et al., 1999). The Sakami Moraine (moraines not shown on Fig. 6), a prominent feature of north-central Quebec, was formed partially during the collapse and drainage of glacial Lake Ojibway and subsequent transgression of the Tyrrell Sea (Hillaire-Marcel et al., 1981). The oldest marine shells along this moraine, collected in 1975, provide an ice-margin age of 7.6 ka, which is why we retain this chronology. Here, we adjust ice margins in Manitoba between 8.5 ka and 7.2 ka based on extensive fieldwork and eleven new deglacial radiocarbon ages obtained on marine and lacustrine shells sampled from postglacial sediments (Table A1; Fig. 6). These changes better capture updated mapping of late-stage ice-flow patterns (Trommelen et al., 2012; Gauthier et al., 2019) and the position and age of lacustrine deposits impounded by ice (Gauthier, 2016; Gauthier et al., *in review*). However, as noted below, work in this region is ever-evolving, and we strongly encourage users to consult the most recent publications regarding ice margins in this area.

In Manitoba, we modify the 8.5 ka ice margin to allow for lacustrine deposition at 8.46 ka near the Whitecap moraine (Gauthier et al., *in review*), as well as the formation of the Trout Lake flowset into an ice-marginal lake (prior to the Quinn Lake Ice Stream; Gauthier et al., 2019). We also refine the position of the 8.0 ka ice margin over Manitoba by 20 to 60 km to encompass the entire Quinn Lake glacial terrain zone, and also to reflect new mapping that indicates the South Knife Lake moraine formed at the same time as the ice stream (Fig. 6). Following Gauthier et al. (2019), the 8.0 ka and 7.8 ka isochrones are extended southwest and westward, to reflect a late-deglacial west to northwest surge of the Stephen Lake sublobe into an ice-marginal lake. Finally, the 7.6 ka and 7.2 ka isochrones are extended into northern

Manitoba to account for southeastward ice-flow into the ocean (Trommelen et al., 2012). Note that several of the aforementioned landscape features are not shown in Fig. 6.

As noted above, emerging work signals a different mechanism for the drainage and timing of this event. Notably, some recent work in Ontario and Manitoba suggests a collapse of the Hudson Bay Ice Saddle in northwestern Ontario rather than in the area of James Bay. Importantly, extensive fieldwork in northern Ontario on former ice marginal positions (Barnett and Yeung, 2012 and associated maps) suggest an alternative deglaciation of the southern Hudson Bay Lowlands, based largely on the distribution and pattern of ice-marginal landforms mapped and the large area of erosion or possibly non-deposition of Stage 2 glacial deposits to the west of Fort Severn, Ontario. Also, recent work based on new radiocarbon ages and geomorphic mapping suggests that the collapse of the Hudson Bay Ice Saddle may have potentially occurred over a period of ~400 years (Lochte et al., 2019; Gauthier et al., *in review*) ending around 7.2 or 7.1 ka (Roy et al., 2011; Jennings et al., 2015; Gauthier et al., *in review*). If correct, these interpretations suggest a collapse of the Hudson Bay Ice Saddle that is incompatible with Dyke's models which we present here (Fig. 6). The reader is encouraged to consult the most recent publications for this region.

4.8 Labrador Dome

Following the collapse of the Hudson Bay Ice Saddle, the Labrador Dome became an independent entity. This section describes updates to this dome from ~7.7 ka onward. Overall, our updated ice margins show a more pronounced pattern of retreat and significant reduction in ice extent toward the late stages of deglaciation as compared to Dyke et al. (2003). They are now more in line with scenario C of Clark et al. (2000). We organize our updates into the Ungava Peninsula, western Quebec coastline and eastern flank of the Labrador Dome. Note: because of the relatively low resolution of Fig. 7, it is not possible to plot several of the landscape features mentioned below (e.g. spillways, glacial lake locations, drift belts).

On the Ungava Peninsula, following earlier work (Lauriol and Gray, 1987; Gray et al., 1993), Daigneault (2008) suggests a deglaciation pattern that involves a significant reduction in the ice margin between 9 ka and 7 ka. We update all isochrones and ice margin locations for northern Ungava based on regional mapping of Daigneault (2008). In this sector, eskers and evidence of proglacial lakes suggest that the ice margin retreated westward up to the area previously occupied by the northern extension of the New-Quebec ice divide (Daigneault and Bouchard, 2004). One of the most substantive changes in this area is at 7 ka where we refine the ice margin by ~100 km inland on the Ungava Peninsula (Fig. 7).

Along the western Quebec coastline (bordering Hudson Bay), we update several ice margin positions based on mapping of glacial and geomorphological features along with cosmogenic nuclide dating of shorelines and spillways (Fig. 7). Notably, following radiocarbon work of Lajeunesse (2008), we adjust the 7.6 ka ice margin inland by ~150 km to conform to the present-day shoreline in this region (e.g. position of the Nastapoka Drift Belt). As shown in Figs. B1-2, the 7.6 ka ice margin now aligns with the position of the Sakami Moraine, Nastapoka Drift Belt, and extends northwest to the Ottawa Islands (Lajeunesse, 2008). Along the western Quebec coastline, we also update the 7.2 ka ice margin by ~10 km inland to accommodate detailed mapping of moraine belts and new radiocarbon dates (Lajeunesse and Allard, 2003; Lajeunesse, 2008; Lavoie et al., 2012). At 7.0 ka, we show two prominent re-entrants (calving embayments) to accommodate the development of glacial lakes in major river valleys (Lac Payne and Lac Minto; see: Lauriol and Gray, 1987; Gray et al., 1993; Dubé-Loubert et al., 2018a). By 6.5 ka and 6 ka, we add another re-entrant farther south to acknowledge evidence for an additional glacial lake in the basin of Lac à l'Eau-Claire (Allard and Seguin, 1985). In the absence of geochronological data and field-based mapping constraints for the core-area of the Labrador Sector, all isochrones post-dating the 6 ka interval remain speculative and are here adjusted to fit an ice withdrawal pattern that follows the outlines of the updated margins. Moreover, ice during these intervals is absent from major river valleys because we know that there were no more glacial lakes.

Refinements to the eastern flank of the Labrador Dome were based on mapping and geochronological constraints on the large ice-dammed Lake Naskaupi (Dubé-Loubert et al., 2015, 2016; Dubé-Loubert and Roy, 2017; Dubé-Loubert et al., 2018b). One of the most substantive updates is at 7.2 ka, where we adjust the ice margin by ~50 km inland to follow the mapping of shoreline sequences and spillways, along with cosmogenic nuclide dating of shorelines that provide a firm constraint on the lake main stage and thereby the position of the damming ice margin (Fig. 7). At the same time, in Labrador, we similarly adjust the ice margin inland by ~50 km to acknowledge the occurrence of meltwater channels going south across the continental drainage divide (Ungava Bay/Labrador Sea), which imply that part of this region was ice-free at this time (Dubé-Loubert and Roy, 2017). Also for this time interval, we adjust the ice margin inland at the opening of Ungava Bay to better conform with the occurrence of large glaciomarine deltas mapped in recent regional surveys (Dubé-Loubert and Roy, 2014). These esker-fed glaciomarine deltas rest directly on fine-grained marine sediments and suggest that the ice margin retreated in contact with the postglacial marine incursion (Iberville Sea, not plotted in Fig. 7) at this time further south in the Ungava Bay lowlands. To maintain a stepwise pattern of deglaciation and to comply with recent mapping constraints, we revise the ice margin immediately prior to 7.2 ka (7.6 ka) by 50 km inland along the eastern flank of the Labrador Dome (see Figs. B1-2). All isochrones post-7.2 ka are adjusted to fit within the constraints of the updated margin, as well as evidence for ice-dammed lakes in the region.

4.9 Atlantic Canada

Assessing the pattern of marine-based ice retreat in Atlantic Canada is challenging. There is evidence that all the shelf-crossing troughs in this region supported ice streams that extended to the shelf-break (Margold et al., 2015), some with numerous deposit remnants. However, most are entirely inaccessible to sampling. For example, the Laurentian Channel (Fig. 8) has at least 16 stratigraphically differentiated till units that are partly preserved, of which only the latest four or five record the last glacial and progressive retreat (King, 2012). Using a combination of marine shelf topography, chronology and inferences on ice sheet dynamics, Shaw et al. (2006) presented a conceptual framework for the pattern of ice sheet retreat of Atlantic Canada. In that paper, ice margin features constraining glacial margin reconstructions are generally robust, however the timing is largely interpolated. Thus, is difficult to adjust the ice margins based on this work. Instead, we combine the work of Shaw et al. (2006) with recently emerged bathymetric-morphological renderings, improved margin deposit recognition and progress on chronologies to present an updated interpretation of ice sheet dynamics in this region.

Key updates to the work of Dyke et al. (2003) include a stepwise deglaciation of the continental shelves between 18 ka and 14 ka, governed by deep water ice calving of ice stream fronts. With notable exceptions, we show that retreat was progressive but with minor still-stands and re-advances as tributary ice stream sources locally adjusted to over-steepened profiles following rapid calving of the main streams (Fig. 8). More than ten moraine complexes within 20 km of the Atlantic shore of Nova Scotia are time transgressive, starting at ca. 15 ka in the west, younging eastward (King, 1996) but we stress that many have poor chronological constraint. A ca. 15 ka meltwater-rich re-advance laid the foundation for Sable Island (King, 2001) and water-rich ice persisted on the eastern shelf with stepwise retreat emanating from what eventually diminished to a cap over Cape Breton (Figs. 8 and B1-2).

By 14 ka, a marine re-entrant (calving embayment) advanced northwestward into the Laurentian Channel toward the Gulf of St Lawrence. In this region, we present several unpublished radiocarbon dates (see Table A1) that make it possible to specify the pattern of deglaciation in the northern part of the Gulf of St. Lawrence. Following these data, the west of Anticosti Island and the eastern tip of the Gaspé Peninsula (Percé sector) became ice-free as early as 13 ka. By 12.5 ka, the eastern section of the Gaspé Peninsula, including Gaspé Bay, and the entire periphery of Anticosti Island was ice-free (Figs. 8 and B1-2). However, the highlands through the centre of Anticosti Island remained occupied by an autonomous ice cap that continued to persist for at least another 0.5 kyr (Hétu et al., in preparation). At 12 ka, coastlines surrounding the Gaspé Peninsula were entirely deglaciated. Our updated maps show these adjustments to the ice margin (Fig. 8). Also in the Gulf of St Lawrence, on the Magdalen Islands (small archipelago located northeast of Prince Edward Island), we show deglaciation at ~13.5 ka (2 kyr earlier than Dyke et al., 2003) to better align with recently published dates from optically stimulated luminescence analysis of cryopediment and coastal deposits which suggest that deglaciation of this island archipelago occurred around that time (Rémillard et al., 2016).

New information about ice retreat through the Bay of Fundy, located between New Brunswick and Nova Scotia, as the ice margin approached land (around 13 ka) was provided by Todd et al. (2007) and Todd and Shaw (2012) who mapped the extent of nearby glaciomarine landforms and dated the onset of marine sedimentation in the cores collected from the sea floor. We update the pattern of ice retreat between 18 ka and 13 ka following this work, the most substantive change being the extension of ice by ~100 km beyond what is depicted by Dyke et al. (2003) to cover the entire Bay of Fundy at 13.5 ka (Figs. B1-2).

By ~13 ka, the ice margin in Atlantic Canada had largely moved on land. A key exception is, in southern Newfoundland, an ice tongue emanating 20 to 50 km from the shoreline at 12.5 ka to satisfy late-stage grounded ice and outburst flooding observations, but the long tongue may have had lateral buttressing from floating ice. Also at 12.5 ka, we adjust isochrones in New Brunswick by ~150 km southward toward the Bay of Fundy to accommodate the aforementioned marine sediment records from that area (Todd et al., 2007; Todd and Shaw, 2012) (Figs. B1-2). On land, from 13 ka to 8 ka, we update the deglaciation largely to follow the work of Stea et al. (2011). Most adjustments to the ice margins are minor (<20 km) compared to what was presented in Dyke et al. (2003). For example, we slightly reduce the size of remnant ice bodies over Nova Scotia at ~12 ka to accommodate new chronological constrains (e.g. onset of peat accumulation at Petite Bog; Charman et al., 2015). One of the more substantive updates is a re-advance between 11 ka and 10.5 ka over Nova Scotia and Prince Edward Island (Figs. B1-2). This Younger Dryas ice configuration is based on extensive radiocarbon dates that underlie till or ice-marginal deposits (Stea and Mott, 2005; Stea et al., 2011). We also maintain remnant ice caps over central New Brunswick for 0.75 kyr longer than what is suggested by Dyke et al. (2003). In Newfoundland, we reduce the size of remnant ice caps from 13 ka to 9 ka by ~30% to better align with the position of fjord-mouth moraines along the coastline (Shaw et al., 2006).

4.10 New England and southern Quebec

Renewed work on varve records in proglacial lakes (North American Varve Chronology; Ridge, 2012; Ridge et al., 2012) and site-specific studies (e.g. radiocarbon dating of plant remains in the initial, inorganic sediment of small lakes) refine the pattern of ice retreat between 18 ka and 11.5 ka in New England and southern Quebec (Stone et al., 2005; Oakley and Boothroyd, 2012) and in New York (Franzi et al., 2016). Following this work, we make minor adjustments to the ice margin between 18 ka and 13 ka in New York and New Hampshire (after Ridge, 2003, 2004, 2012; Ridge et al., 2012). Note that, because of the scale of Fig. 9, it is not possible to plot several of the landscape features mentioned below (e.g. glacial lake locations, moraine belts, fjord locations).

More substantive updates to New England are the result of radiocarbon ages of shells from glaciomarine sediments (Borns et al., 2004) as well as a reservoir correction of at least 1 kyr applied to marine shells (Thompson et al., 2011). Notably, we expand the 13 ka ice margin by ~90 km coastward (Fig. 9). The updated 13 ka ice margin covers the majority of Maine, except parts of the eastern and western coastal zone (e.g. Sargent Mountain Pond, a mid-coastal mountain pond that likely became deglaciated before the surrounding lowlands). We similarly adjust the 12.5 ka Maine ice margin coastward by ~90 km to better align with several ages on both sides of the major Pineo Ridge Moraine System (moraines not plotted on Fig. 9, see: Borns et al., 2004) and with varve chronology in New Hampshire to the west. The updated 12.5 ka isochrone also depicts a major re-advance of ice ~50 km southward along several river valleys of New Hampshire and New York State (following Ridge, 2003, 2004; Ridge et al., 2012; Franzi et al., 2016). In addition, the 12 ka ice margin is shown at a re-advance position in the Connecticut Valley (Thompson et al., 2017) and is extended between 10 km to 60 km southward into the Champlain Valley and surrounding areas to better reflect evidence of the persistence of ice in that region (Fig. 9; Chapdelaine and Richard, 2017).

We make significant adjustments to the 11.5 ka and 11 ka ice margin in Quebec. Cross-dating of marine and terrestrial-derived sources (Occhietti and Richard, 2003; Richard and Occhietti, 2005) suggests a more appropriate marine reservoir correction for this area, thus settling a long-standing controversy over the age of the Champlain Sea, the marine incursion immediately following deglaciation of this region (Rayburn et al., 2005; Cronin et al., 2012). Combined with the information from Thompson et al. (1999) in northern New Hampshire and Borns et al. (2004) in northern Maine, this prompted a major change in the ice position on the 11.5 ka map (Fig. 9). The updated 11.5 ka ice margin in this area is drawn after Chapdelaine and Richard (2017); this ice front occupied the Maine-Quebec boundary, corresponding to the so-called Frontier Moraine (see: Parent and Occhietti, 1999). From recent work on the northern side of the St. Lawrence lower estuary, downstream the Saguenay Fjord (Occhietti et al., 2015), the coast of the upper part of the lower estuary was deglaciated and inundated by Goldthwait Sea waters by 11.3 ka until the Younger Dryas re-advance. Current work upstream of the Saguenay Fjord, in Charlevoix (by workers Occhietti, Govare, Bhiry et al.), indicates that the St. Lawrence Ice Stream remained active in the middle estuary until about 11.2 ka and the opening to marine waters of Goldthwait Sea, shortly before to the Champlain Sea incursion, with short lived lateral lakes preceding the marine invasion (Fig. 9). On the southern shore of the middle estuary, it seems that the late ice stream was bordered by an early arm of Goldthwait Sea in the downstream part and by the ephemeral Chaudière-Etchemin Lake in the upstream part, immediately prior to the Champlain Sea incursion in the central St. Lawrence valley.

Immediately following 11.5 ka, highly dynamic events took place in the central St. Lawrence valley region. Remnant ice briefly remained over the Montreal lowland area prior to shifting eastward at ~11.25 ka and lying adjacent to the topographic high of Warwick, on the Appalachian piedmont. This was likely the last ice position prior to the incursion of the Champlain Sea. Unfortunately, this ~11.25 ka ice margin is not captured in our relatively low-resolution maps, but we present an approximate position for this ice margin in the 11 ka interval (orange line; Fig 9) because it provides important context for the deglaciation of this region. Regardless, by 11.1 ka, the ice margin had receded sufficiently to allow incursion of the Champlain Sea. The 11 ka ice margin therefore lies north of the St. Lawrence River (Fig. 9). At this time in the broader region, the ice margin remained along the shore of the St. Lawrence lower estuary, except in southernmost Labrador and downstream of the Saguenay Fjord. Minor adjustments to the 11 ka ice margin follow Occhietti et al. (2011).

In addition to the changes described above, we also update the timing of the marine re-entrant (calving embayment) in the lower St. Lawrence estuary from a progressive calving from 13 ka to 11.5 ka (as depicted by Dyke et al., 2003) to a rapid embayment at 11.5 ka (Fig. 9) in accordance with the ice stream evidence upstream in the mid estuary. We also make this change because of recent work in New York State that suggests ice lobes remained active until ~11.5 ka, and were able to re-advance and also act as a barrier to the drainage of glacial Lake Iroquois in the Ontario Basin (Franzi et al., 2016). These ice lobes required a continuous ice supply that would not be likely if the calving embayment occurred as early as 13.5 ka and spread westward prior to 11.5 ka (Ross et al., 2006).

One to three centuries after 11 ka was the onset of the Younger Dryas cold episode and the emplacement of the St. Narcisse Moraine at the southeastern margin of the Canadian Shield and on the north shore of the St. Lawrence Estuary and Gulf (Occhietti, 2007; Occhietti et al., 2011). Accordingly, we update the position of the 10.5 ka isochrone to reflect the position of the main ridges of the St. Narcisse Morainic Complex (Fig. 9). We note that the configuration of remnant ice masses in northern Maine is very approximate during these intervals. In drawing these ice margins, we have considered recent work by Dieffenbacher-Krall et al. (2016), along with previous workers such as Borns et al. (2004), who have found stratigraphic evidence of a Younger Dryas glacial re-advance. Evidence of a Younger Dryas climate cooling also occurs as a lithic zone in many of the dated lake sediment cores from northern Maine, and sites that preserve this record must have remained deglaciated during the Younger Dryas. Finally, we make minor changes, generally < 10 km, to the retreating ice margin in Quebec between 11 ka and 9 ka following Occhietti (2007) and Occhietti et al. (2011).

Our work provides significant updates to the deglaciation of New England and southern Quebec. However, some conflicts remain and some elements of our reconstruction are somewhat speculative. For example, the updated marine reservoir correction in this region causes a discord between the ice margin and several terrestrial radiocarbon ages, causing the terrestrial radiocarbon ages to appear too old. Possible explanations include (1) derivation from bulk samples prior to the availability of accelerator mass spectrometry dating; (2) the influence of carbonate rocks that underlie parts of this region; and (3) the predominantly meltwater environment. A notable example of this discord is at 12.5 ka, where the updated ice margin conflicts with a few terrestrial radiocarbon ages (Fig. 9). We consider this issue unavoidable to get a realistic active ice sheet margin. To maintain an objective research approach, we retain these radiocarbon data points on our maps. However, we do not use them as control points for drawing our ice margin.

4.11 Great Lakes

At the time of Dyke et al. (2003), chronological constraints were limited in the area south of the Great Lakes. As a result, most ice margins in that study area were generalized. Since then, recent work has contributed significant refinement to the recession of the ice margin in this region. We first update the recession of the Huron-Erie Lobe in Ohio and Indiana based on minimum ages on organic matter that formed in shallow depressions in moraines (Glover et al., 2011). The most substantial adjustment is the refinement of this ice lobe in Indiana between 18 ka and 16 ka (Fig. B1-2; Heath et al., 2018). As seen in Fig. 10 and Figs. B1-2, adjustments to the Huron-Erie Lobe range between 10 km to 200 km inboard of the ice margins of Dyke et al. (2003).

Significant changes are also made to the Lake Michigan Lobe. Minimum moraine ages are given through more than 200 accelerator mass spectrometry ages of tundra plant macrofossils preserved in periglacial and ice-marginal lakes (Curry and Petras, 2011; Curry et al., 2014; Curry et al., 2018). We align the 18 ka to 16.5 ka ice margin with the Marseilles Morainic Complex, Barlina Moraine, and Gilman Moraine (Fig. 10). We also adjust the 16 ka ice margin to the Rockdale moraine in Illinois and continue eastward into Indiana and Michigan. Note that the aforementioned moraines are not shown in Fig. 10.

Overall, we show the deglaciation of the Lake Michigan region occurring ~1 kyr sooner over what is depicted by Dyke et al. (2003); our justification for this change is improved radiocarbon work and landscape analysis related to erosion caused by a dramatic meltwater event (Kankakee Torrent; Curry et al., 2014). This meltwater event is well-constrained to 15.69 ka and its sources included meltwater of the Lake Michigan, Saginaw, and Huron-Erie Lobes in southwestern Michigan (Curry et al., 2014). New radiocarbon dates indicate the torrent skirted the southern margin of the Valparaiso Morainic System, which we align with the 15.5 ka margin. We align the 15 ka ice margin to the Tinley Moraine of the Valparaiso Morainic System in Illinois and Indiana (moraine positions not shown, see Fig. 10). While our updates represent significant refinement to the deglaciation sequence for the Lake Michigan and Huron-Erie Lobes, we stress that ice margin ages in Michigan and northern Indiana remain speculative because many areas are not mapped in detail and the ages of moraines are often poorly constrained.

Another notable update to the pattern of ice retreat in the southern Great Lakes is at 15.5 ka. A this time, Dyke et al. (2003) depicted a short-lived yet dramatic recession of the margin by ~400 km (the Erie Interstadial), leaving large parts of the Great Lakes region briefly ice-free (see Figs. B1-2). The Erie Interstadial is well-documented in the stratigraphic record (Fullerton, 1980; Barnett, 1992; Karrow et al., 2000). However, Dyke (2004) acknowledged that the timing of this dramatic oscillation in the ice margin remained unclear and could range from ~16.5 ka to 14.5 ka. Recent work on dating this interstadial event has focused on meltwater routing as a result of glacially-induced drainage shifts (Carlson and Clark, 2012; Porreca et al., 2018). Yet, the timing of this event remains enigmatic. For this reason, we remove the Erie Interstadial from the 15.5 ka isochrone. The updated 15.5 ka ice margin north and east of Lake Michigan now lies approximately midway between the 16 ka and 15 ka ice margins (Fig. 10).

Farther west, we also make updates to the deglaciation of Lake Superior. Our updates align with recent work on ^{10}Be-dating, varve records, radiocarbon data and drainage basin mapping (Breckenridge et al., 2004; Hyodo and Longstaffe, 2011; Breckenridge, 2015; Ullman et al., 2015), which suggest a much later ice retreat from the basin than shown in Dyke et al. (2003). Following the aforementioned studies, we re-draw the ice margins between 10 ka an 8 ka to better align with the onset of varved records in various sub basins of the lake (updated ice margins follow Breckenridge, 2013). Major updates include the expansion of ice by ~200 km southward at 9.6 ka and 9.5 ka to cover a large area of Lake Superior (Figs. B1-2). We also show ice remaining in the northern area of the watershed at the Nakina moraine until ~9 ka. The updated ice margin lies north of the Lake Superior drainage basin by 8 ka (Figs. B1-2).

Finally, we make adjustments to the west of Lake Superior. Ice margins in this region are contentious because they relate to the drainage of Lake Agassiz. For example, a ^{10}Be-based deglaciation chronology (Leydet et al., 2018) suggests a much older withdrawal of the Rainy Lobe than interpreted from radiocarbon dates (Lowell et al., 2009). For the purposes of this continental-scale update to the ice margin, we adjust the 11.5 ka ice margin by ~50 km southward to better align with the Vermilion Moraine, a prominent feature in the region (Figs. B1-2). We also adjust the 11 ka and 10.5 ka ice margins to better align with the position of the Eagle Finlayson Moraine (adjustments of <10 km and ~50 km, respectively). Lastly, we make minor changes (<10 km) to the 10.25 ka and 10 ka isochrones to better align with the position of the Dog Lake Moraine. It was not possible to plot the aforementioned moraines on Figs. B1-2.

4.12 Des Moines Lobe

The James Lobe (JL) and Des Moines Lobe (DML) were terrestrially terminating ice lobes (Patterson, 1998; Colgan et al., 2003) active in the Midwestern United States between 18 ka and 12 ka. Our updated interpretation of these ice lobes is based largely on improved statistical correlation of regional till sheets along with sediment-landform associations, both of which have been verified and strengthened using lithological and textural data in recent years (e.g. Harris, 1998; Lusardi et al., 2011). Not all maps are cited here and the reader is encouraged to visit state survey websites for indices to detailed mapping and relevant studies (e.g. detailed ice sheet reconstructions for Michigan; Mickelson and Attig, 2017). Note that it was not possible to plot some of the mentioned landscape features in Figs. 11 and B1-2.

The updated isochrones depict the JL at or near its maximum extent in South Dakota between 18 ka and 14 ka (Figs. 11 and B1-2). This position is consistent with chronostratigraphic evidence suggesting that the JL covered North Dakota between 17 ka to 15 ka (Burnstad and Fresh Lake Phase; Clayton, 1966; Clayton and Moran, 1982) as well as the deposition of the upper Peoria loess in western Iowa and eastern Nebraska (Muhs et al., 2013). The 13 ka to 11 ka interval then represents the narrowing and northward recession of the JL (Figs. B1-2). However, it is possible that this recession was punctuated briefly by a southward advance of at least 160 km to near its maximum position at some point between 13 ka and 12 ka (see Lepper et al., 2007; Lundstrom, 2013). Radiocarbon dates on wood pieces that were deeply buried by up to 58 m of late Wisconsin glacial deposits, mainly till, also support ice advance at this time (Lundstrom, 2013).

The updated isochrones depict the DML covering a large swath of Minnesota and extending into northern Iowa from 18 ka to 16 ka (Figs. 11 and B1-2). At the same time, it is likely that a central region of Minnesota remained ice-free (Fig. 11). This highly dynamic ice margin is supported by the distribution of a surface till with a unique matrix texture and lithology (Patterson, 1997; Lusardi et al., 2011). The maximum southern extent of the DML was reached between 15 ka and 14 ka, resulting in the well-dated Bemis moraine >200 km south of the Minnesota-Iowa border (Clayton and Moran, 1982; Hallberg and Kemmis, 1986). However, the maximum southerly advance is not necessarily related to the maximum ice volume of the ice sheet or the ice lobe. From 14 ka to 13 ka, the DML alternated between intervals of advance, stagnation and re-advance to lesser positions as documented by moraines in Iowa dated to between 14 ka to 13 ka (e.g. Algona moraine in Iowa; Bettis and Hoyer, 1986). At around 13 ka the Grantsburg sublobe advanced through the Twin Cities lowland to the northeast into Wisconsin where it dammed the St. Croix River forming glacial Lake Grantsburg, which lasted about 100 years prior to drainage due to ice retreat (Figs. B1-2) (Cooper, 1935; Wright et al., 1973; Johnson and Hemstad, 1998). Following this maximum ice extent, the DML retreated (e.g. repeatedly advanced and stagnated with each advance being less extensive) in a northwesterly direction from 13 ka to 12 ka. However, this retreat was punctuated by several ice advances, whose stagnation phases formed high-relief hummocky areas with minimum ages of 12.43 ka (Jennings et al., 2011b). By 12 ka, the DML had retreated from Minnesota northwestward into North Dakota as suggested by several radiocarbon ages in the region that was recently covered by the DML (e.g. radiocarbon age from Dead Tree Lake; Lepper et al., 2007). The DML had largely receded from the midwestern United States by 11 ka.

4.13 Canadian Prairies

Recent projects have resulted in a much improved knowledge of ice marginal positions in the Canadian Prairies. Important advances in this region include the interpretation of landform features using remote imagery and DEMs, surficial mapping compilations and targeted field studies, all of which have led to improved identification of deglaciation between ~15 ka and ~9 ka in Alberta (Atkinson et al., 2014; Evans et al., 2014; Atkinson et al., 2016; Atkinson et al., 2018), Saskatchewan (Norris et al., 2017; Norris et al., 2018) and Manitoba (McMartin et al., 2012).

An increased availability of deglacial radiocarbon ages adds further refinement to the pattern of ice retreat (Fisher et al., 2009; Anderson, 2012). Moreover, progress has been made identifying the imprints of paleo-ice streams, which evolved across central and southern Alberta and adjacent Saskatchewan due to a succession of spatially and temporally transgressive reorganizations in ice sheet geometry and dynamics during regional deglaciation (Evans et al., 1999; Evans et al., 2008; Ross et al., 2009; Ó Cofaigh et al., 2010; Lusardi et al., 2011; Evans et al., 2012; Evans et al., 2014). Based on these advances and new data we make minor adjustments (e.g. shifts of less than 50 km) to ice margins in the Canadian Prairies. The more substantive updates include an adjustment in Alberta of the 12 ka, 11.5 ka and 11 ka ice margins by up to ~200 km inland (Figs. 12 and B1-2) to better align with regional topography and major mapped moraines. Although not shown on our maps, the updated ice margins also align with recent work on the formation of proglacial lakes along the retreating ice margin in this region (Utting et al., 2016a). In Saskatchewan, more substantive changes include an increased region of unglaciated terrain from 18 ka to ~14 ka to better align with previous surficial mapping of the unglaciated terrain and ice marginal features (Klassen, 1991, 1992; Klassen, 2002). From 14 ka to 12.5 ka, we incorporate recent work on ice streams (Ross et al., 2009; Lusardi et al., 2011) which results in a nunatak in southeastern Saskatchewan. In addition, the updated 11 ka isochrone is noteworthy because it shows an elongated ice lobe in central Saskatchewan (Fig. 12). This is derived from mapping of specific flow sets and follows topographic lows in this region (Ross et al., 2009) and matching it to the extent of the ice streams immediately to the east. Finally, in Manitoba, we adjust the position of the 10 ka to 9.5 ka ice margins by 50 to 100 km inland at subtle moraine segments north of Lake Winnipeg (Figs. 12 and B1-2).

4.14 Alaska and Pacific Coastline

In northern Alaska, between 18 ka and 12 ka, we replace ice over the Brooks Range and Ahklun Mountains with the 'LGM' extent suggested by Kaufman et al. (2011) as part of the Alaska PaleoGlacier Atlas (developed by INSTAAR, University of Colorado; Fig. 13). We also remove ice entirely from these regions from 11.5 ka onwards to be most compatible with existing data and ongoing work in the area (Briner and Kaufman, 2008). In southern Alaska (Alaska Range extending westward to the Aleutian Range), we replace the 18 ka to 16 ka ice margins with the 'LGM' extent suggested by Kaufman et al. (2011). This updated ice configuration is maintained from 18 ka to 16 ka. Subsequent isochrones follow Dyke et al. (2003).

Radiocarbon ages on seal bones from Southeast Alaska (Shuká Káa cave; Heaton and Grady, 2003) and coastal British Columbia (Port Eliza cave; Ward et al., 2003) suggest that westward advance and maximum limit of the Cordilleran Ice Sheet occurred in some areas of the Pacific coastline after 17 ka. The timing of this ice advance was also confirmed via cosmogenic ^{10}Be exposure dating from this coastline (Lesnek et al., 2018). As a result of these new constraints, we adjust the 18 ka, 17.5 ka and 17 ka coastal ice margins in Southeast Alaska by ~30 km inland (Figs. B1-2). We then show maximum ice extent (following Kaufman et al., 2011) in these areas between 17 ka to 15 ka. Farther south, near Vancouver, chronostratigraphic work on sediments from the Chehalis River valley document a brief retreat of regional ice around 15.5 ka, followed by a relatively late advance to maximum ice extent in the area around 14 ka (Figs. B1-2; Ward and Thomson, 2004). We adopt the ice margins suggested by this work, which amounts to adjustments of the ice margin in the Vancouver area by ~50 km inland. We also adjust the ice margin in the Puget Lowland area, Washington, between 14.5 ka and 11.5 ka by ~50 km inland to accommodate recent radiocarbon ages (largely on marine shells) and ongoing work in this area (e.g. Easterbrook, 2015; Riedel, 2017).

5 Conclusions and future work

We present an update to the 36 North American deglaciation isochrones of Dyke et al. (2003) along with an up-to-date (c. 2018) dataset of n = 5,195 radiocarbon ages that document the timing of landscape emergence along the retreating ice margin (see Table A1). Our starting point for this work was the pattern of ice retreat suggested by Dyke et al. (2003). Updates were largely accomplished by overlaying data from regional studies and/or manually editing the ice margins to fit recently mapped landforms and/or to fit renewed radiocarbon work. A major update is the expansion of the ice margin to the continental shelf in most marine areas at 18 ka based largely on undated geomorphological and marine-based records (see Section 3). Other updates to terrestrial regions are presented on a region-by-region basis. These updated isochrones are a solution to satisfy the needs of a broad Quaternary research community that requires knowledge of former ice positions, as well as ice sheet modelers (Tarasov et al., 2012; Kageyama et al., 2018).

The next reconstruction of the pattern of ice retreat of the NAISC should follow the precedent set by the recent ice-margin chronology for the Eurasian ice sheets (Hughes et al., 2016; Clark et al., 2018). This work should be presented in a calendar year time scale, which will allow for the integration of other dating methods, most importantly cosmogenic nuclide exposure and optically stimulated luminescence ages, and a thorough assessment of uncertainties for the ice sheet margin for every given time step (see also Small et al., 2017). However, applying these methods to the much larger landscape of North America will be a lengthy process. For example, from a data collection standpoint, integration of cosmogenic nuclide exposure ages will require extensive recalculation to determine an appropriate ^{10}Be production rate and scaling (Heisinger et al., 2002; Corbett et al., 2017a), as well as correcting for glacial isostatic adjustment (Ullman et al., 2016; Leydet et al., 2018; Jones et al., 2019). Moreover, the integration of optically stimulated luminescence dates may be challenging due to a history of poor solar resetting of sediments in glacial settings (e.g. improper solar resetting owing to sediment-rich water; Larsen et al., 2014).

Solutions must also be found for conflicting ice margin interpretations. Notable examples include (1) different geochronological techniques yield contrasting ages for the formation of glacial Lake Wisconsin (Attig et al., 2011; Ullman et al., 2015), (2) discrepancies on the formation/draining of glacial Lake Agassiz (age differences of >1.5 ka between 10Be and 14C; Teller et al., 2005; Lowell et al., 2009; Teller, 2013; Leydet et al., 2018), and (3) conflicting information on the deglaciation of the Labrador dome based on ^{14}C and recent cosmogenic work (Ullman et al., 2016). We also note that collapse of the Hudson Bay Ice Saddle is an area of emerging research that may undergo revision in the future. We strongly encourage the reader to consult with the most recent publications for information about these critical regions of deglaciation. Future work should also consider the effects of ice dynamics with some regions of the ice being much thinner and more dynamic (ice streams and their outlets) than others, as well as the precise timing of known ice margin oscillations (e.g. the Erie Interstadial and Younger Dryas). Notwithstanding these issues, our new maps represent the most up-to-date knowledge of ice margin recession and capture important revisions to both the pattern and rate of deglaciation in North America.

Acknowledgements

This work was initiated by the MOCA (Meltwater routing and Ocean-Cryosphere-Atmosphere response) project, which was a joint network project of the INQUA (International Union for Quaternary Research), PALCOM (Paleoclimate) and TERPRO (Terrestrial Processes) Commissions. We are grateful for financial support for MOCA project workshops from INQUA over the 2009 to 2012 interval. We also acknowledge funding from the DIFeREns2 Junior Research Fellowship (no. 609412; funded by European Union / Durham University) to ASD; the Natural Environment Research Council (no. NE/J00782X/1) to CRS; the International Postdoctoral Fellowship (no. 637-2014-483) from the Swedish Research Council to MM, and the Czech Science Foundation (no. 19-21216Y) to MM. We thank the PALSEA (a PAGES / INQUA) working group for useful discussions at the 2019 meeting (Dublin, Ireland). We also thank the USGS-supported STATEMAP and Great Lake Geologic Mapping Consortium for providing funding for coring and new dates. Maps were created in ArcGIS Pro 2.3.2 using basemap data from Esri, DigitalGlobe, GeoEye, Earthstar Geographics, CNES/Airbus DS, USDA, USGS, AeroGRID, IGN, and the GIS User Community. Finally, we thank the constructive feedback from Lynda Dredge as well as two anonymous reviewers who greatly improved the manuscript.

Data availability

The 36 updated isochrones are available in PDF and shapefile format, together with a spreadsheet of the expanded radiocarbon dataset (n = 5,195 ages) and estimates of uncertainty for each interval.

Table 1. Isochrones (n=36) showing the pattern of ice retreat of the North American Ice Sheet Complex (NAISC) along with estimates min/max uncertainties and a comparison of areal extent as compared to Dyke et al. (2003). All updated isochrones are available as PDFs and shapefiles in the Appendices.

	Estimates of uncertainty and calibration		Comparison of areal extent (x1,000,000 km^2)			
Isochrone (ka ^{14}C)	Recommended isochrone for ± uncertainty (lower//upper)	Calibrated age (cal. ka)[a]	Dyke et al. (2003)	current publication	difference in area (%)	Qualitative overview of changes having greatest impact on areal extent[b]
18 ka	17 ka // 18 ka	≈21.7	17.81	18.37	3.14	+ extension of ice onto continental shelf in Arctic, Atlantic and Alaska (Section 3) – reduction of ice over some regions of Alaska, Great Lakes and Atlantic Canada (Section 3)
17.5 ka	16.5 ka // 18 ka	≈21.1	17.67	18.30	3.58	+ extension of ice onto continental shelf in Arctic, Atlantic and Alaska (Section 4.1-4.5 and 4.9) – reduction of ice over some regions of Atlantic Canada, Great Lakes and Alaska (Section 4.9, 4.11 and 4.14)
17 ka	16 ka // 18 ka	≈20.5	17.69	18.24	3.10	+ extension of ice onto continental shelf in Arctic, Atlantic and Alaska (Section 4.1-4.5, 4.9, 4.13) – reduction of ice over some regions of Atlantic Canada, Great Lakes and Alaska (Section 4.9, 4.11 and 4.14)
16.5 ka	15.5 ka // 17.5 ka	≈19.9	17.69	18.19	2.83	+ extension of ice onto continental shelf in Arctic, Atlantic and Alaska (Section 4.1-4.5, 4.9, 4.13) – reduction of ice over some regions of Atlantic Canada, Great Lakes and Alaska (Section 4.9, 4.11 and 4.14)
16 ka	15 ka // 17 ka	≈19.3	17.60	17.99	2.22	+ extension of ice onto continental shelf in Arctic, Atlantic and Alaska (Section 4.1-4.5, 4.9, 4.13) – reduction of ice over some regions of Atlantic Canada, Great Lakes and Alaska (Section 4.9, 4.11 and 4.14)
15.5 ka	14.5 ka // 16.5 ka	≈18.7	16.76	17.72	5.65	+ extension of ice onto continental shelf in Arctic, Atlantic and Alaska (Section 4.1-4.5, 4.9, 4.13) + removal of Erie Interstadial and adjustment of 15.5 ka ice margin to midway between the 16 ka and 15 ka ice margins (Section 4.11) – reduction of ice over some regions of Atlantic Canada, Great Lakes and Alaska (Section 4.9, 4.11 and 4.14)
15 ka	14 ka // 16 ka	≈18.0	17.18	17.42	1.38	+ extension of some ice onto continental shelf in Arctic and some parts of Canada (Section 4.1-4.5 and 4.9) – reduction of some ice in the Great Lakes region (Section 4.9, 4.11 and 4.14)
14.5 ka	13.5 ka // 15.5 ka	≈17.4	16.97	17.12	0.91	+ extension of some ice onto continental shelf in Arctic regions (Section 4.1-4.5) – reduction of some ice in the Great Lakes region (Section 4.9, 4.11 and 4.14)
14 ka	13 ka // 15 ka	≈16.8	16.59	16.84	1.51	+ extension of some ice onto continental shelf in Arctic regions (Section 4.1-4.5) – reduction of some ice in the Great Lakes region (Section 4.9, 4.11 and 4.14)
13.5 ka	12.5 ka // 14.5 ka	≈16.1	16.08	16.36	1.74	+ extension of some ice onto continental shelf in Arctic regions (Section 4.1-4.5)
13 ka	12 ka // 14 ka	≈15.5	15.34	15.74	2.63	+ extension of ice to cover Brooks Range, Alaska (Section 4.14) + extension of ice in the James and Des Moines lobes (Section 4.12)
12.5 ka	11.5 ka // 13.5 ka	≈14.9	14.83	15.01	1.22	+ extension of ice to cover Brooks Range, Alaska (Section 4.14)
12 ka	11 ka // 13 ka	≈14.2	13.73	13.98	1.82	+ extension of ice to cover Brooks Range, Alaska (Section 4.14) + extension of ice in the James and Des Moines lobes (Section 4.12) – reduction and refinement of ice in the Canadian Prairies (Section 4.13)

11.5 ka	10.5 ka // 12.5 ka	≈13.5	12.93	13.02	0.67	+ extension of ice in New England and Southern Quebec (Section 4.10) – reduction and refinement of ice in the Canadian Prairies (Section 4.13) Minor refinements of ice margin over Canadian Arctic Archipelago (Section 4.1-4.4)
11 ka	10 ka // 12 ka	≈12.8	11.84	11.88	0.30	Minor refinements of ice margin over Canadian Arctic Archipelago (Section 4.1-4.4)
10.5 ka	9.5 ka // 11.5 ka	≈12.1	10.88	11.02	1.24	+ extension of ice into Great Lakes region (Section 4.11) Minor refinements of ice margin over Canadian Arctic Archipelago
10.25 ka	9.5 ka // 11 ka	≈11.8	9.97	9.99	0.17	Minor refinements of ice margin over Canadian Arctic Archipelago
10 ka	9.5 ka // 10.5 ka	≈11.5	9.80	9.71	-0.84	– reduction of ice margin over Canadian Arctic Archipelago (Section 4.1-4.4)
9.6 ka	9 ka // 10.25 ka	≈11.0	9.01	9.10	1.06	+ extension of ice into Great Lakes region (Section 4.11)
9.5 ka	9 ka // 10.25 ka	≈10.9	8.89	8.98	0.96	+ extension of ice into Great Lakes region (Section 4.11)
9 ka	8.5 ka // 9.5 ka	≈10.3	8.12	8.18	0.71	+ extension of ice into Great Lakes region (Section 4.11) – reduction of over the Canadian Arctic Archipelago (Section 4.1-4.4)
8.5 ka	8 ka // 9 ka	≈9.6	6.97	6.97	0.08	Minor refinements of ice margin over the Canadian Arctic Archipelago (Section 4.1-4.4)
8 ka	7.8 ka // 8.5 ka	≈9.0	6.06	6.12	0.94	+ extension of the Keewatin Dome (Section 4.6)
7.8 ka	7.7 ka // 8 ka	≈8.8	5.66	5.69	0.57	+ extension of the Keewatin Dome (Section 4.6)
7.7 ka	7.6 ka // 8 ka	≈8.7	4.94	4.90	-0.69	+ extension of the Keewatin Dome (Section 4.6) – reduction of Labrador Dome (Section 4.8)
7.6 ka	7.2 ka // 7.8 ka	≈8.5	4.35	4.24	-2.64	+ extension of the Keewatin Dome (Section 4.6) – reduction of Labrador Dome (Section 4.8) and removal of ice from Southampton Island (Section 4.6)
7.2 ka	7 ka // 7.6 ka	≈8.1	3.82	3.74	-2.20	– reduction of Labrador Dome (Section 4.8) and removal of ice from Southampton Island (Section 4.6)
7 ka	6.5 ka // 7.2 ka	≈7.9	3.54	3.28	-7.43	– reduction of Labrador Dome (Section 4.8) and removal of ice from Southampton Island (Section 4.6)
6.5 ka	6 ka // 7 ka	≈7.3	2.91	2.75	-5.41	– reduction of Labrador Dome (Section 4.8)
6 ka	5.5 ka // 6.5 ka	≈6.8	2.53	2.45	-2.92	– reduction of Labrador Dome (Section 4.8)
5.5 ka	5 ka // 6 ka	≈6.3	2.40	2.31	-3.50	– reduction of Labrador Dome (Section 4.8)
5 ka	4 ka // 5.5 ka	≈5.7	2.27	2.19	-3.57	– reduction of Labrador Dome (Section 4.8)
4 ka	3 ka // 5 ka	≈4.5	2.12	2.17	2.66	Minor refinements of ice margin over the Canadian Arctic Archipelago (Section 4.1-4.4)
3 ka	2 ka // 4 ka	≈3.2	2.10	2.16	2.64	Minor refinements of ice margin over the Canadian Arctic Archipelago (Section 4.1-4.4)
2 ka	1 ka // 3 ka	≈2.0	2.10	2.15	2.14	Minor refinements of ice margin over the Canadian Arctic Archipelago (Section 4.1-4.4)
1 ka	1 ka // 2 ka	≈0.9	2.14	2.13	-0.69	Minor refinements of ice margin over the Canadian Arctic Archipelago (Section 4.1-4.4)

[a] Obtained using IntCal 13 (Reimer et al., 2013) using the ^{14}C age and 10% error.

[b] This should not be taken as a comprehensive list of edits to the ice margin as some significant updates are not described here (e.g. refinements to New England and Southern Quebec [Section 4.10], the James and Des Moines lobes [Section 4.12], and Canadian Prairies [Section 4.13]).

Rather, this list is a qualitative overview of changes having greatest impact on areal extent of the ice margin. The reader is referred to the text as well as Fig. 1B for a comprehensive view of all changes to the ice margin.

Fig. 1. Map of North America showing locations discussed in the text. White boxes and text indicate the location of Figs. 4 to 14. Elevation data from United States Geological Survey's Center for Earth Resources Observation and Science (EROS) (2010). Light blue ocean bathymetry represents the continental shelf (less than 1000 m depth). For ease of comparison between time slices and to allow proper orientation to each region, all figures in this paper contain the same base layer showing modern-day topography, landscape and political boundaries. Readers should bear in mind these features were not static over time and, in many cases, were highly influenced by the deglaciation of continental ice (e.g. gradual formation of the Great Lakes; dynamics of isostatic rebound on the marine shorelines).

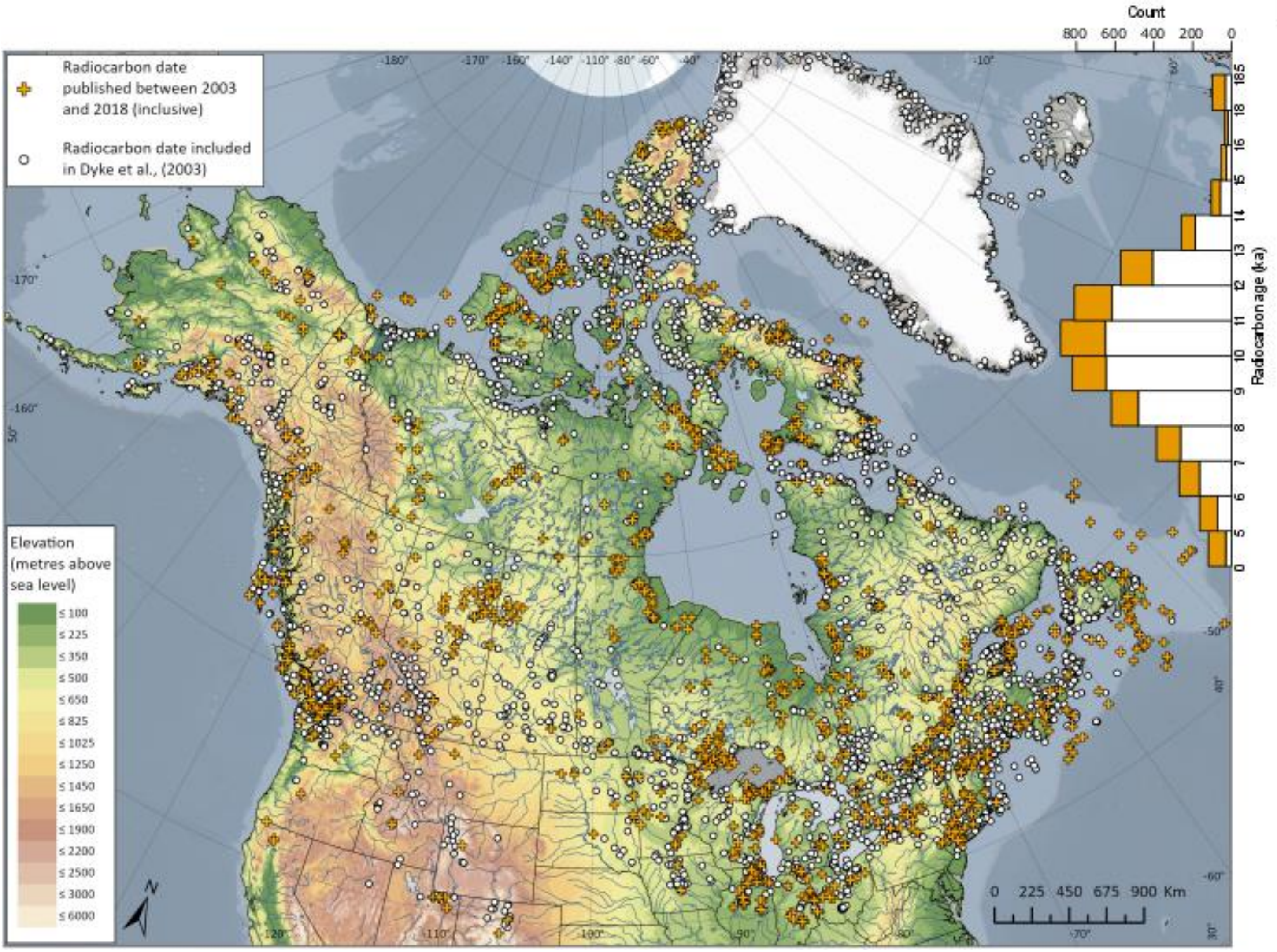

Fig. 2. Radiocarbon data (n = 5,195) used in the construction of isochrones. This study contributes 1,541 new ages to reflect work taken place up to and including 2018. Barplot on top right shows the distribution of data from Dyke et al. (2003)(white) and new radiocarbon dates (orange) compiled for this study. Table A1 documents these data points along with relevant references for each site. Additional notes on topography, bathymetry and the base layer are detailed in the caption for Fig. 1.

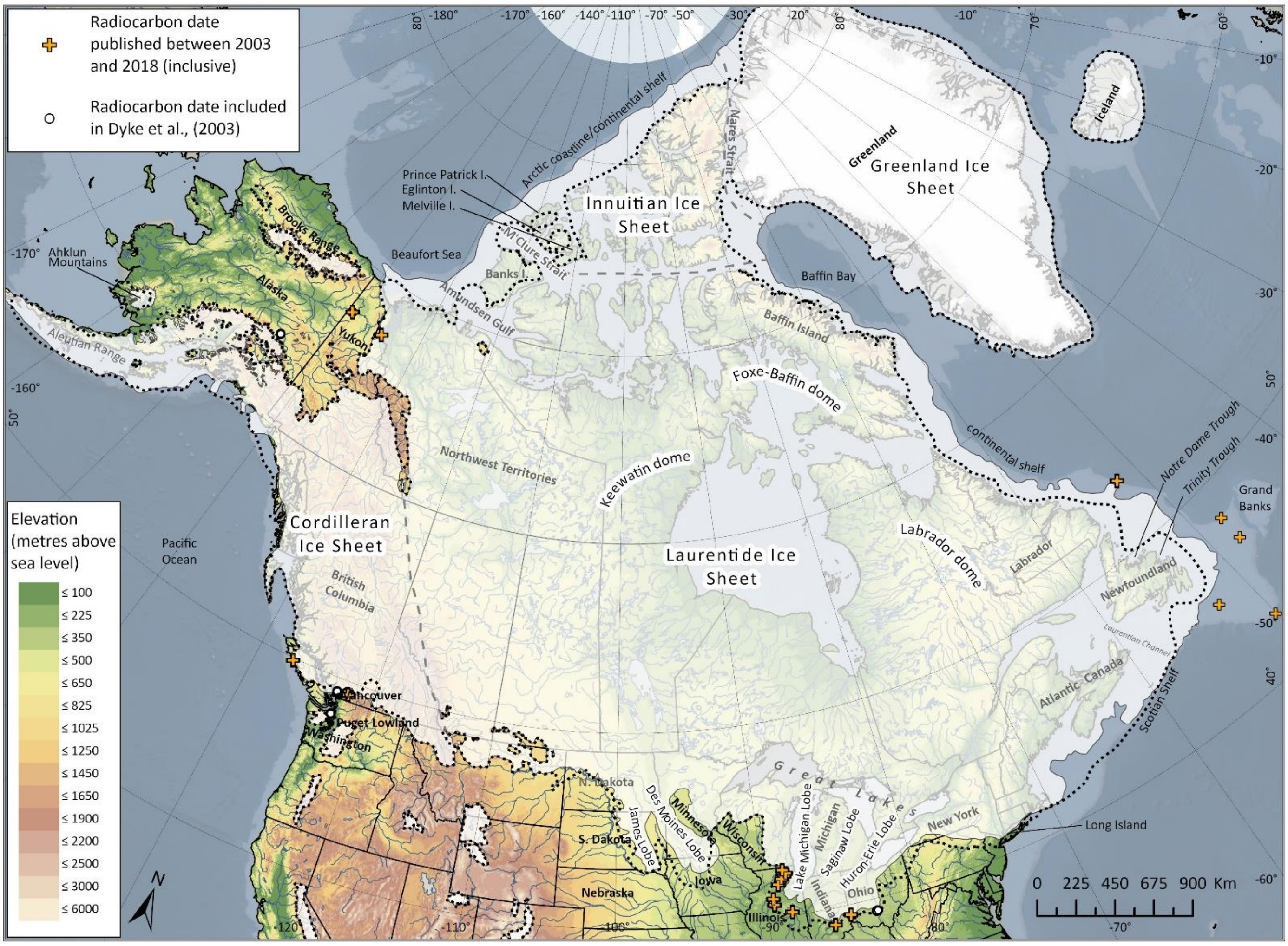

Fig. 3. Updated 18 ka ice margin overlain with the previous 18 ka isochrone of Dyke et al. (2003) (black dashed line). Key updates include the expansion of ice to the continental shelf in the Arctic and Eastern Canada (details in Section 3). Note that the Last Glacial Maximum was asynchronous, occurring at different times in each region. For example, the Last Glacial Maximum in Atlantic Canada and along the Labrador coastline (depicted by the red dashed line) occurred prior to 18 ka (see King, 1996; Shaw et al., 2006). The locations of key glacial features (sheets, domes, lobes) are also shown. Note that proglacial lakes are excluded from this map. Data points and colour scheme are described in Fig 2. Additional notes on topography, bathymetry and the base layer are detailed in the caption for Fig. 1.

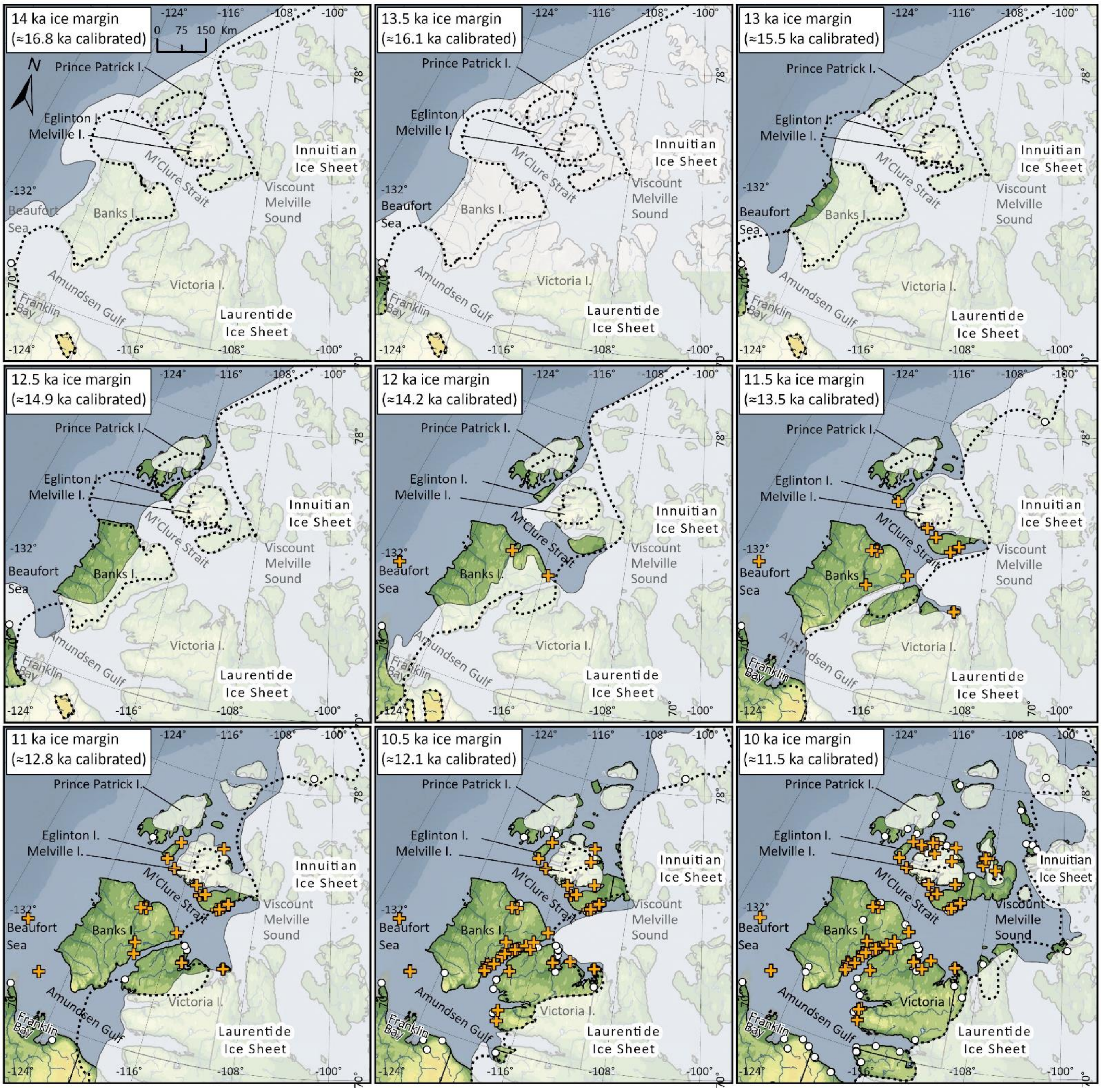

Fig. 4. Updated ice margins (opaque white) showing the deglaciation of Banks, Melville, Eglinton islands and M'Clure Strait at selected intervals. Our updated ice margins show a stepwise deglaciation from the new 18 ka ice margin based largely on undated geomorphological and marine-based records (see Section 4.1). In the Beaufort Sea and Amundsen Gulf, our updated ice margins show a stepwise retreat to land that is marked by moraines (see Section 4.2). Previous isochrones of Dyke et al. (2003) shown as black dashed line. Data points and colour scheme are described in Fig. 2. Additional notes on topography, bathymetry and the base layer are detailed in the caption for Fig. 1.

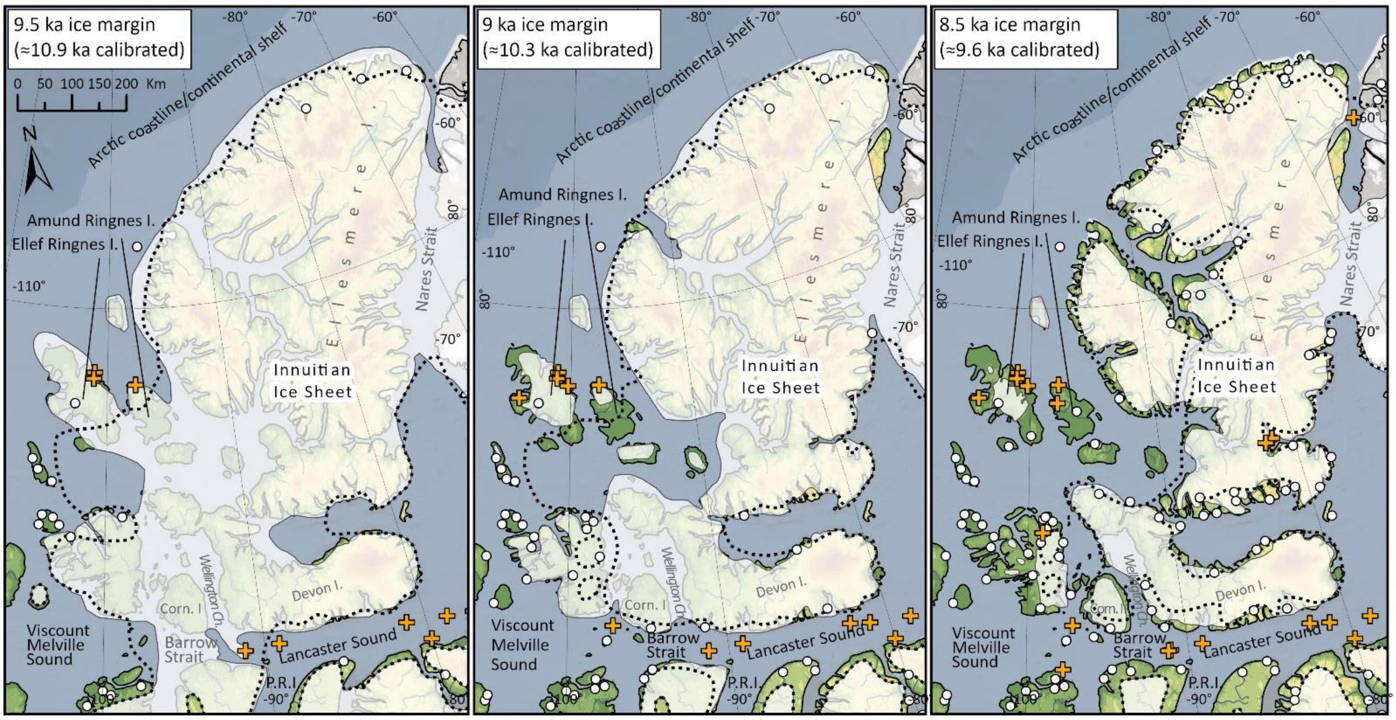

Fig. 5. Updated ice margins (opaque white) showing the deglaciation of the Central and Eastern Queen Elizabeth Islands at selected intervals. Our updated interpretation of the deglaciation of the Innuitian Ice Sheet suggests the pattern of ice retreat in this region may have been more rapid than what was suggested by Dyke et al. (2003) (see Section 4.3). We also make adjustments to ice retreat in Lancaster Sound based on several recent studies of grounding zone wedges, marine sedimentology, geochemistry and paleoproxy data (see Section 4.4). Previous isochrones of Dyke et al. (2003) shown as black dashed line. Data points and colour scheme are described in Fig. 2. Additional notes on topography, bathymetry and the base layer are detailed in the caption for Fig. 1. “P.R.I” = Prince Regent Inlet.

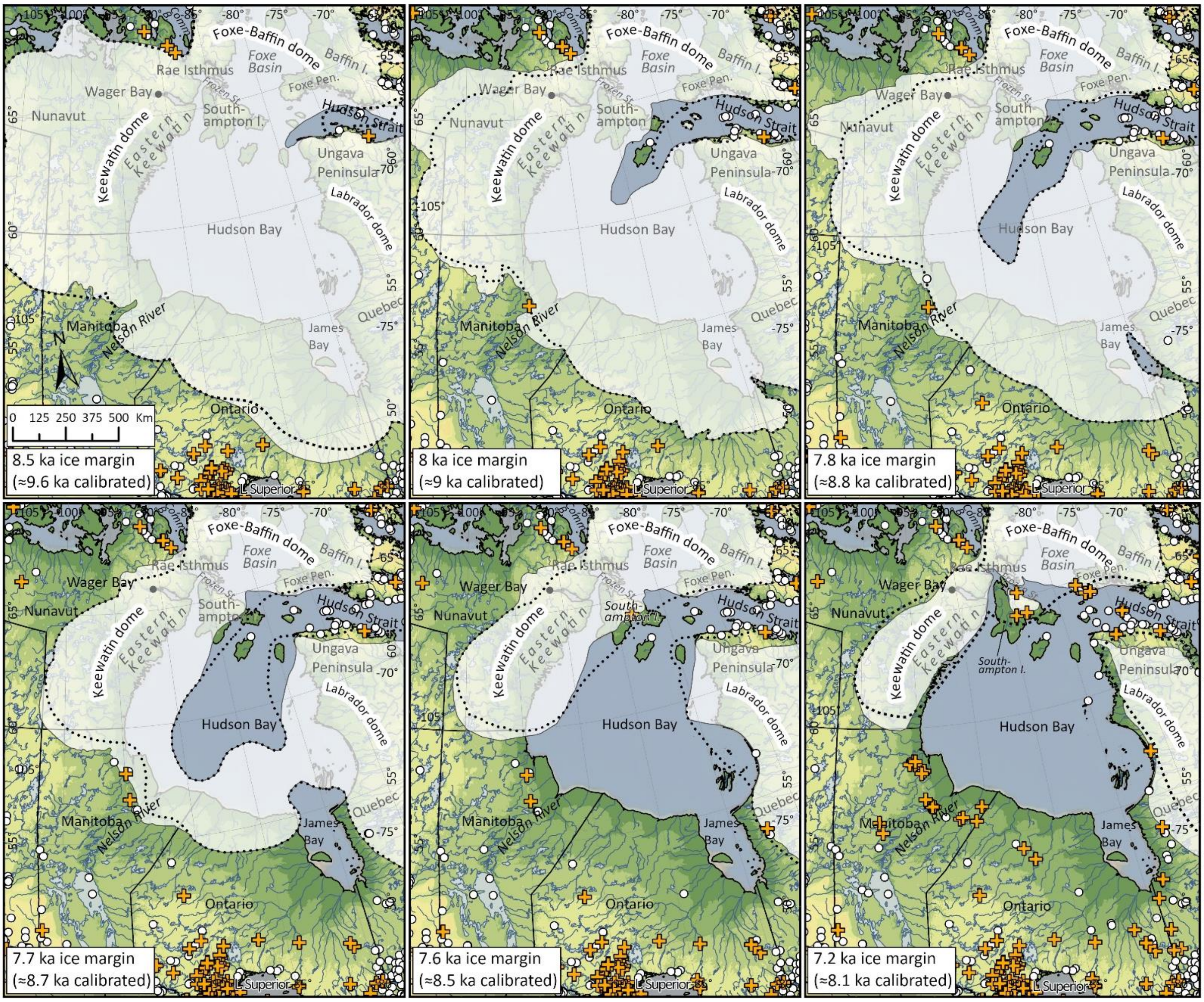

Fig. 6. Updated ice margins (opaque white) showing the deglaciation of the Hudson Bay region at selected intervals. We adjust ice margins based on extensive fieldwork in coastal and terrestrial settings, as well as many new deglacial radiocarbon ages obtained on marine and lacustrine shells sampled from postglacial sediments (see Section 4.5, 4.6, 4.7). Previous isochrones of Dyke et al. (2003) shown as black dashed line. Data points and colour scheme are described in Fig. 2. Additional notes on topography, bathymetry and the base layer are detailed in the caption for Fig. 1. “Comm. B.” = Committee Bay.

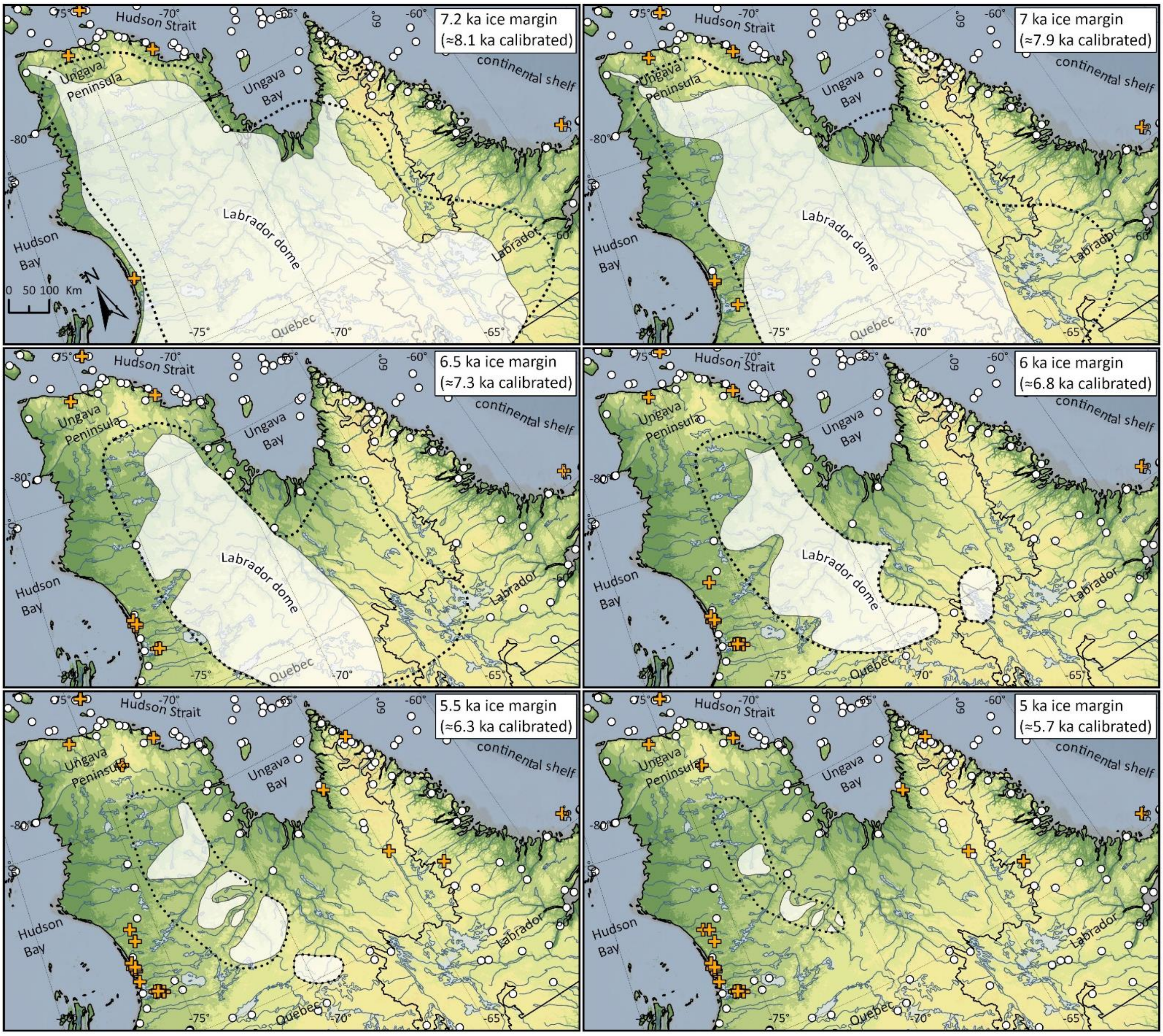

Fig. 7. Updated ice margins (opaque white) showing the deglaciation of the Labrador Dome at selected intervals. In this region, we update several ice margin positions based on mapping of glacial and geomorphological features along with cosmogenic nuclide dating of shorelines and spillways (see Section 4.8). Previous isochrones of Dyke et al. (2003) shown as black dashed line. Data points and colour scheme are described in Fig. 2. Additional notes on topography, bathymetry and the base layer are detailed in the caption for Fig. 1.

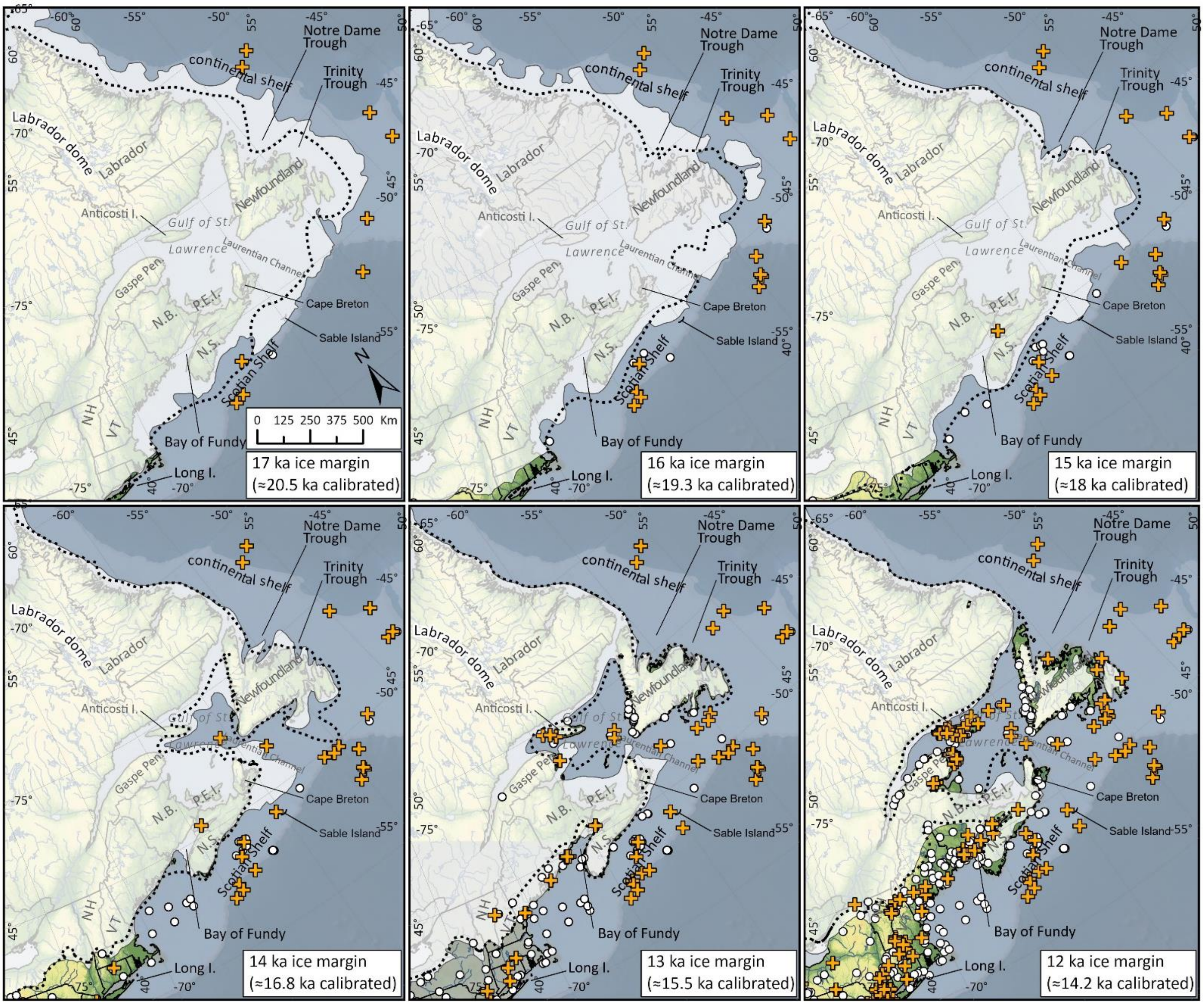

Fig. 8. Updated ice margins (opaque white) showing the deglaciation of Atlantic Canada at selected intervals. Key updates include stepwise deglaciation of the continental shelves between 18 ka and 14 ka, governed by deep water ice calving of ice streaming (see Section 4.9). Previous isochrones of Dyke et al. (2003) shown as black dashed line. Data points and colour scheme are described in Fig. 2. Additional notes on topography, bathymetry and the base layer are detailed in the caption for Fig. 1. "P.E.I" = Prince Edward Island; "N.B" = New Brunswick; "N.S" = Nova Scotia; "NH" = New Hampshire; "VT" = Vermont.

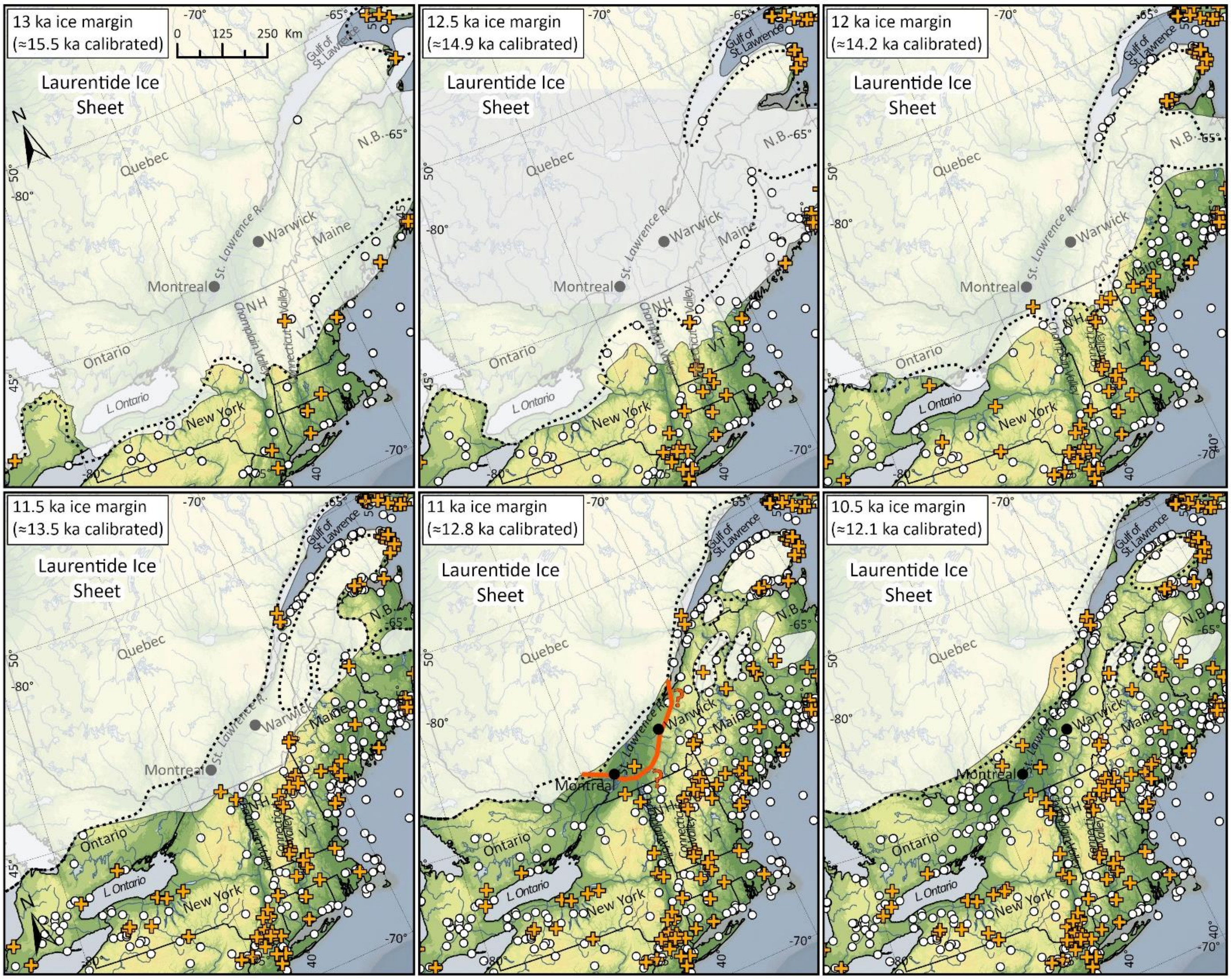

Fig. 9. Updated ice margins (opaque white) showing the deglaciation of New England and southern Quebec at selected intervals. Key updates include a significant expansion of the 11.5 ka ice margin as well as adjustments to the timing of the marine re-entrant (calving embayment) in the St. Lawrence lower estuary from a progressive calving from 13 ka to 11.5 ka (as depicted by Dyke et al., 2003) to a rapid embayment at 11.5 ka (see Section 4.10). Orange line signifies the likely position of ice at 11.25 ka. Previous isochrones of Dyke et al. (2003) shown as black dashed line. Data points and colour scheme are described in Fig. 2. Additional notes on topography, bathymetry and the base layer are detailed in the caption for Fig. 1. "N.B" = New Brunswick; "NH" = New Hampshire; "VT" = Vermont.

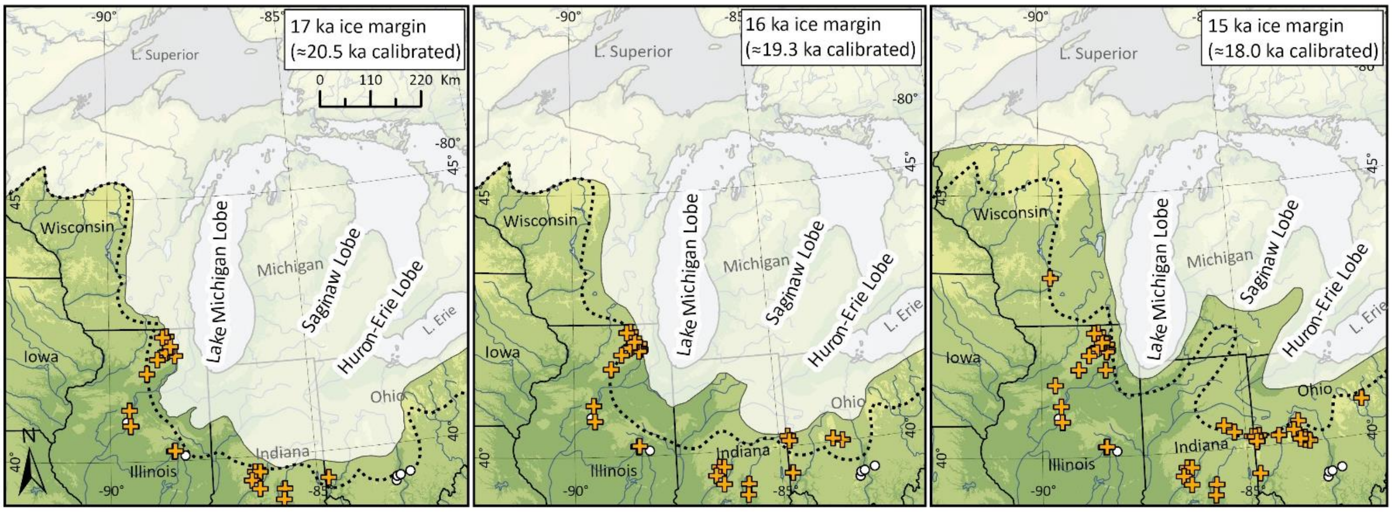

Fig. 10. Updated ice margins (opaque white) showing the deglaciation of the southern Great Lakes at selected intervals. A major update is the overall adjustment of ice inboard of the previous ice margin (based on minimum-limiting radiocarbon ages) for most time intervals (see Section 4.11). Previous isochrones of Dyke et al. (2003) shown as black dashed line. Data points and colour scheme are described in Fig. 2. Additional notes on topography and the base layer are detailed in the caption for Fig. 1.

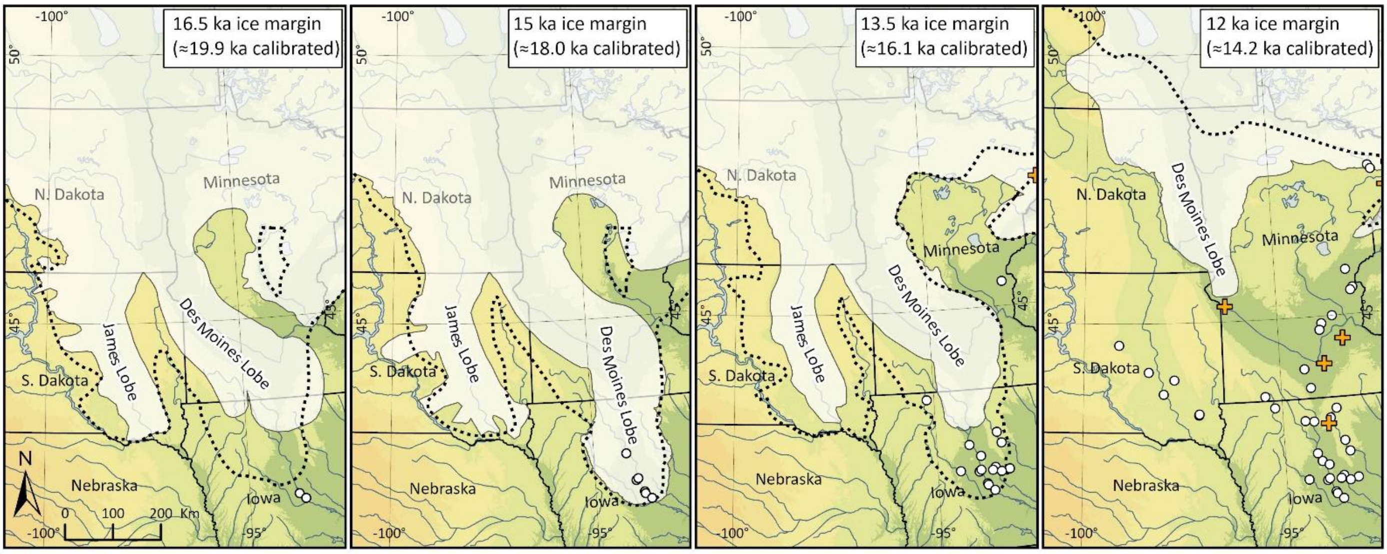

Fig. 11. Updated ice margins (opaque white) showing the deglaciation of the Des Moines and James lobes at selected intervals. Updates are based on improved statistical correlation of regional till sheets along with sediment-landform associations, both of which have been verified and strengthened using lithological and textural data in recent years (see Section 4.12). Note that the Grantsburg sublobe underwent a short-lived advance into Wisconsin at 13 ka; a time slice that is not featured in this figure. The reader is referred to Figs. B1-2 which contain the 13 ka time slice (see also section 4.12). Previous isochrones of Dyke et al. (2003) shown as black dashed line. Data points and colour scheme are described in Fig. 2. Additional notes on topography and the base layer are detailed in the caption for Fig. 1.

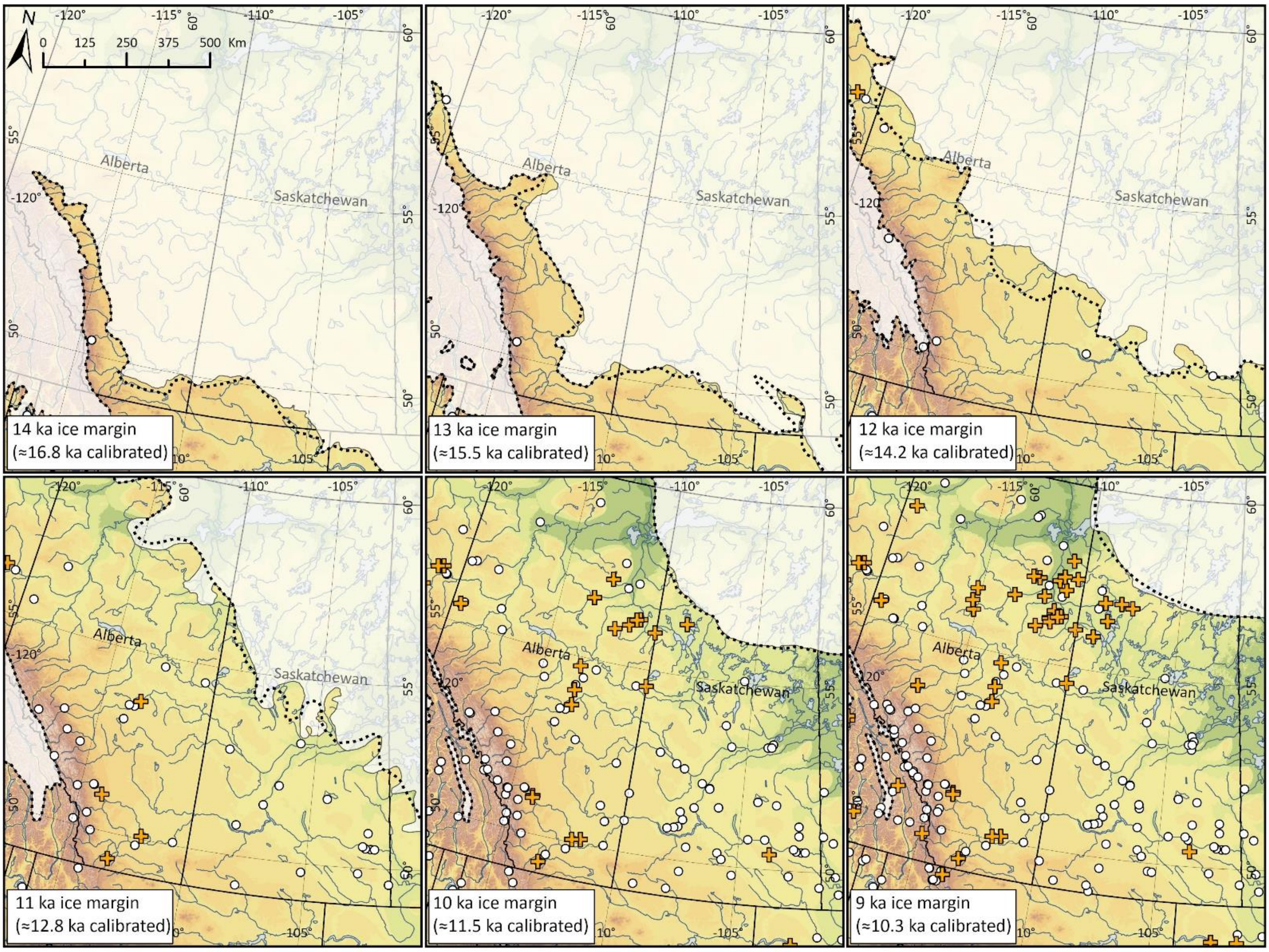

Fig. 12. Updated ice margins (opaque white) showing the deglaciation of the Canadian Prairies at selected intervals. Updates to the ice margin are the result of recent digitization of landform features, surficial mapping compilations and targeted field studies in this region (see Section 4.13). Previous isochrones of Dyke et al. (2003) shown as black dashed line. Data points and colour scheme are described in Fig. 2. Additional notes on topography and the base layer are detailed in the caption for Fig. 1.

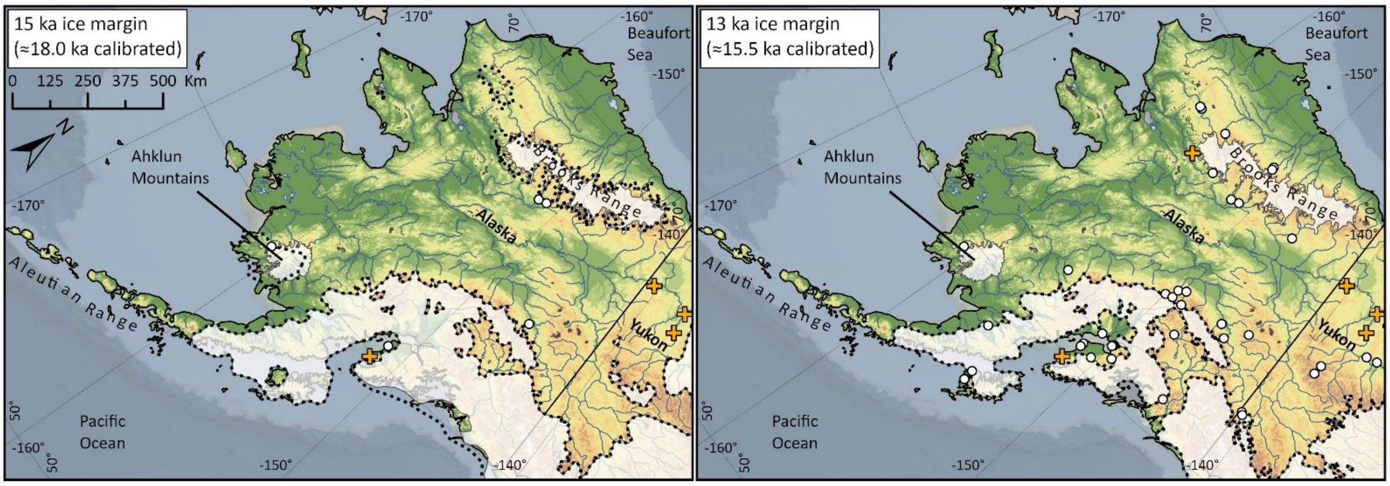

Fig 13. Updated ice margins (opaque white) showing the deglaciation of Alaska at selected intervals. Key updates include a more refined ice extent on the Pacific coastline at 15 ka (see Section 4.14). Previous isochrones of Dyke et al. (2003) shown as black dashed line. Data points and colour scheme are described in Fig. 2. Additional notes on topography, bathymetry and the base layer are detailed in the caption for Fig. 1.

Appendices (see attached files)

Table A1. Table containing all radiocarbon ages used in this study (n = 5195). Data are arranged from east to west. Errors are presented in 1-sigma, however “GSC-” ages are at 2-sigma. All radiocarbon ages were reported as normalized to a $\delta^{13}C$ of -25‰. This involved editing marine shells by ~0.4 kyr, however, if $\delta^{13}C$ information was available, the correction was adjusted accordingly. Following the suggestion in many Government of Canada radiocarbon reports, marine whales were assigned a reservoir correction of 0.15 kyr and other marine mammals were assigned 0.4 kyr regardless of region. The column ‘Median calibrated age’ was calculated using IntCal 13 (Reimer et al., 2013). The “Reference” column indicates the publication or report where the data were published. Some unpublished ages instead indicate the scientist who originally targeted the site or facilitated the dating. In the case of radiocarbon dates from marine cores, uncertainties include vague marine reservoir correction, laboratory analysis and calibration recalculation errors but these are generally outweighed by the necessity to extrapolate, via an age model, to deeper horizons, usually well beyond the core penetration, to a seismically defined deposit or event. Generally, sedimentation rate trails exponentially with time, especially through the Holocene, with the effect that small dating errors are exaggerated with extrapolation. PC=Piston Core, JPC= jumbo Piston Core, GC=Gravity Core, VC=Vibrocore.

Fig. B1. Individual maps of each updated isochrone in this study (36 PDF maps) overlain with the original isochrones of Dyke et al. (2003) for the same interval. Note that proglacial lakes are excluded from these maps. Minimum radiocarbon ages for each interval are shown. For ease of comparison between time slices and to allow proper orientation to each region, all figures in this paper contain the same base layer showing modern-day topography, landscape and political boundaries. Readers should bear in mind these features were not static over time and, in many cases, were highly influenced by the deglaciation of continental ice (e.g. gradual formation of the Great Lakes; dynamics of isostatic rebound on the marine shorelines). Elevation data from United States Geological Survey's Center for Earth Resources Observation and Science (EROS) (2010). Maps were created in ArcGIS Pro 2.3.2 using data from Esri, DigitalGlobe, GeoEye, Earthstar Geographics, CNES/Airbus DS, USDA, USGS, AeroGRID, IGN, and the GIS User Community.

Fig. B2. Individual maps of each updated isochrone in this study (36 PDF maps) overlain with the original isochrones of Dyke et al. (2003) for the same interval. No radiocarbon dates are shown on this series of maps. See Fig. B1 for additional information about data sources.

Appendix C

Zip file containing shapefiles of the updated ice margins (144 total files consisting of: 36 SHP files; 36 SHX files; 36 PRJ files; 36 DBF files)

References

Allard, M., Seguin, M.K., 1985. La deglaciation d'une partie du versant hudsonien Québécois: bassins des rivières Nastapoca, Sheldrake et à l'Eau-Claire. Géographie physique et Quaternaire 34, 13-24.

Anderson, T.W., 2012. Evidence from Nipawin Bay in Frobisher Lake, Saskatchewan, for three highstand and three lowstand lake phases between 9 and 10 (10.1 and 11.5 cal) ka BP. Quaternary International 260, 66-75.

Atkinson, N., 2003. Late Wisconsinan glaciation of Amund and Ellef Ringnes islands, Nunavut: evidence for the configuration, dynamics, and deglacial chronology of the northwest sector of the Innuitian Ice Sheet. Canadian Journal of Earth Sciences 40, 351-363.

Atkinson, N., Pawley, S., Utting, D.J., 2016. Flow-pattern evolution of the Laurentide and Cordilleran ice sheets across west-central Alberta, Canada: implications for ice sheet growth, retreat and dynamics during the last glacial cycle. Journal of Quaternary Science 31, 753-768.

Atkinson, N., Utting, D.J., Pawley, S.M., 2014. Landform signature of the Laurentide and Cordilleran ice sheets across Alberta during the last glaciation. Canadian Journal of Earth Sciences 51, 1067-1083.

Atkinson, N., Utting, D.J., Pawley, S.M., 2018. An update to the glacial landforms map of Alberta, Alberta Geological Survey Open File Report 2018-08. Alberta Geological Survey, Edmonton, Canada.

Attig, J.W., Hanson, P.R., Rawling, J.E., Young, A.R., Carson, E.C., 2011. Optical ages indicate the southwestern margin of the Green Bay Lobe in Wisconsin, USA, was at its maximum extent until about 18,500 years ago. Geomorphology 130, 384-390.

Baltzer, A., Cochonat, P., Piper, D.J.W., 1994. In situ geotechnical characterization of sediments on the Nova Scotian Slope, eastern Canadian continental margin. Marine Geology 120, 291-308.

Barber, D.C., Dyke, A., Hillaire-Marcel, C., Jennings, A.E., Andrews, J.T., Kerwin, M.W., Bilodeau, G., McNeely, R., Southon, J., Morehead, M.D., Gagnon, J.M., 1999.

Forcing of the cold event of 8,200 years ago by catastrophic drainage of Laurentide lakes. Nature 400, 344-348.

Barnett, P.J., 1992. Chapter 21: Quaternary Geology of Ontario. Ontario Geological Survey, Special Volume 4; pt. 2, pp. 1011-1088.

Barnett, P.J., Yeung, K.H., 2012. Field investigations for remote predictive terrain mapping in the far north of Ontario. Summary of Field Work and Other Activities 2012: Ontario Geological Survey, Open File Report 6280, 24-21 to 24-25.

Barth, A.M., Marcott, S.A., Licciardi, J.M., Shakun, J.D., 2019. Deglacial thinning of the Laurentide Ice Sheet in the Adirondack Mountains, New York, USA revealed by 36Cl exposure dating. Paleoceanography and Paleoclimatology 34, 946-953.

Batchelor, C.L., Dowdeswell, J.A., Pietras, J.T., 2014. Evidence for multiple Quaternary ice advances and fan development from the Amundsen Gulf cross-shelf trough and slope, Canadian Beaufort Sea margin. Marine and Petroleum Geology 52, 125-143.

Batchelor, C.L., Margold, M., Krapp, M., Murton, D.K., Dalton, A.S., Gibbard, P.L., Stokes, C.R., Murton, J.B., Manica, A., 2019. The configuration of Northern Hemisphere ice sheets through the Quaternary. Nature communications 10, 3713.

Bennett, R., Campbell, D.C., Furze, M.F.A., 2013. The shallow stratigraphy and geohazards of the northern Baffin Island shelf: studies to 2012. Geological Survey of Canada Open File 7355, 42 p.

Bennike, O., 2002. Late Quaternary history of Washington Land, North Greenland. Boreas 31, 260-272.

Bettis, E.A., Hoyer, B.E., 1986. Late Wisconsinan and Holocene landscape evolution and alluvial stratigraphy in the Saylorvile Lake area, central Des Moines River Valley, Iowa. Iowa Geological Survey Open File Report 86-1, 71 p.

Böhm, E., Lippold, J., Gutjahr, M., Frank, M., Blaser, P., Antz, B., Fohlmeister, J., Frank, N., Andersen, M.B., Deininger, M., 2015. Strong and deep Atlantic meridional overturning circulation during the last glacial cycle. Nature 517, 73-76.

Borns, H.W., Jr., Doner, L.A., Dorion, C.C., Jacobson, G.L., Jr., Kaplan, M.R., Kreutz, K.J., Lowell, T.V., Thompson, W.B., Weddle, T.K., 2004. The deglaciation of Maine, U.S.A., in: Ehlers, J., Gibbard, P.L. (Eds.), Quaternary Glaciations – Extent and Chronology, Part II: North America. Elsevier, Amsterdam, pp. 89-109.

Breckenridge, A., 2013. An analysis of the late glacial lake levels within the western Lake Superior basin based on digital elevation models. Quaternary Research 80, 383-395.

Breckenridge, A., 2015. The Tintah-Campbell gap and implications for glacial Lake Agassiz drainage during the Younger Dryas cold interval. Quaternary Science Reviews 117, 124-134.

Breckenridge, A., Johnson, T.C., Beske-Diehl, S., Mothersill, J.S., 2004. The timing of regional Lateglacial events and post-glacial sedimentation rates from Lake Superior. Quaternary Science Reviews 23, 2355–2367.

Briner, J.P., Bini, A.C., Anderson, R.S., 2009. Rapid early Holocene retreat of a Laurentide outlet glacier through an Arctic fjord. Nature Geoscience 2, 496-499.

Briner, J.P., Kaufman, D.S., 2008. Late Pleistocene mountain glaciation in Alaska: key chronologies. Journal of Quaternary Science 23, 659-670.

Briner, J.P., Miller, G.H., Davis, P.T., Finkel, R.C., 2005. Cosmogenic exposure dating in arctic glacial landscapes: implications for the glacial history of northeastern Baffin Island, Arctic Canada. Canadian Journal of Earth Sciences 42, 67-84.

Briner, J.P., Miller, G.H., Davis, P.T., Finkel, R.C., 2006. Cosmogenic radionuclides from fiord landscapes support differential erosion by overriding ice sheets. Geological Society of America Bulletin 118, 406-420.

Brouard, E., Lajeunesse, P., 2017. Maximum extent and decay of the Laurentide Ice Sheet in Western Baffin Bay during the Last glacial episode. Scientific Reports 7, 10711.

Brouard, E., Lajeunesse, P., 2019. Glacial to postglacial submarine landform assemblages in fiords of northeastern Baffin Island. Geomorphology 330, 40-56.

Bryson, R.A., Wendland, W.M., Ives, J.D., Andrews, J.T., 1969. Radiocarbon isochrones on the distintegration of the Laurentide Ice Sheet. Arctic and Alpine Research 1, 1-14.

Campbell, J.E., Little, E.C., Utting, D., McMartin, I., 2013. Surficial geology, Nanuraqtalik Lake, Nunavut; CGM-P60; Geological Survey of Canada; 1: 50 000 scale.

Campbell, J.E., McMartin, I., Normandeau, P.X., Godbout, P.-M., 2019. Report of 2018 activities for the GEM-2 Rae project glacial history activity in the eastern Northwest Territories and the Kitikmeot and Kivalliq Regions, Nunavut. Geological Survey of Canada, Open File 8586, 18 p.

Carlson, A.E., Clark, P.U., 2012. Ice sheet sources of sea level rise and freshwater discharge during the last deglaciation. Reviews of Geophysics 50, RG4007.

Chapdelaine, C., Richard, P.J.H., 2017. Middle and Late Paleoindian Adaptation to the Landscapes of Southeastern Québec. PaleoAmerica, 299-312.

Charman, D.J., Amesbury, M.J., Hinchliffe, W., Hughes, P.D.M., Mallon, G., Blake, W.H., Daley, T.J., Gallego-Sala, A.V., Mauquoy, D., 2015. Drivers of Holocene peatland carbon accumulation across a climate gradient in northeastern North America. Quaternary Science Reviews 121, 110-119.

Clark, C.D., Ely, J.C., Greenwood, S.L., Hughes, A.L.C., Meehan, R., Barr, I.D., Bateman, M.D., Bradwell, T., Doole, J., Evans, D.J.A., Jordan, C.J., Monteys, X., Pellicer, X.M., Sheehy, M., 2018. BRITICE Glacial Map, version 2: a map and GIS database of glacial landforms of the last British–Irish Ice Sheet. Boreas 47, 11-27.

Clark, C.D., Knight, J.K., T. Gray, J., 2000. Geomorphological reconstruction of the Labrador Sector of the Laurentide Ice Sheet. Quaternary Science Reviews 19, 1343-1366.

Clark, P.U., Dyke, A.S., Shakun, J.D., Carlson, A.E., Clark, J., Wohlfarth, B., Mitrovica, J.X., Hostetler, S.W., McCabe, A.M., 2009. The Last Glacial Maximum. Science 325, 710-714.

Clayton, L., 1966. Notes on Pleistocene stratigraphy of North Dakota. North Dakota Geological Survey Report of Investigations no. 44, 26 p.

Clayton, L., Moran, S.R., 1982. Chronology of Late Wisconsinan Glaciation in Middle North America. Quaternary Science Reviews 1, 55-82.

Colgan, P.M., Mickelson, D.M., Cutler, P.M., 2003. Ice-marginal terrestrial landsystems: southern Laurentide ice sheet margin, in: Evans, D.J.A. (Ed.), Glacial Landsystems. Routledge, London, pp. 111-142.

Cooper, W.S., 1935. The history of the upper Mississippi River in late Wisconsin and postglacial time. Minnesota Geological Survey Bulletin 26, 116 p.

Corbett, L.B., Bierman, P.R., Rood, D.H., Caffee, M.W., Lifton, N.A., Woodruff, T.E., 2017a. Cosmogenic 26Al/10Be surface production ratio in Greenland. Geophysical Research Letters 44, 1350-1359.

Corbett, L.B., Bierman, P.R., Stone, B.D., Caffee, M.W., Larsen, P.L., 2017b. Cosmogenic nuclide age estimate for Laurentide Ice Sheet recession from the terminal moraine, New Jersey, USA, and constraints on latest Pleistocene ice sheet history. Quaternary Research 87, 482-498.

Corbett, L.B., Bierman, P.R., Wright, S.F., Shakun, J.D., Davis, P.T., Goehring, B.M., Halsted, C.T., Koester, A.J., Caffee, M.W., Zimmerman, S.R., 2019. Analysis of multiple cosmogenic nuclides constrains Laurentide Ice Sheet history and process on Mt. Mansfield, Vermont's highest peak. Quaternary Science Reviews 205, 234-246.

Coulthard, R.D., Furze, M.F.A., Pieńkowski, A.J., Nixon, F.C., England, J.H., 2010. New marine ΔR values for Arctic Canada. Quaternary Geochronology 5, 419-434.

Cronin, T.M., Rayburn, J.A., Guilbault, J.P., Thunell, R., Franzi, D.A., 2012. Stable isotope evidence for glacial lake drainage through the St. Lawrence Estuary, eastern Canada, ~13.1–12.9 ka. Quaternary International 260, 55-65.

Curry, B., Petras, J., 2011. Chronological framework for the deglaciation of the Lake Michigan lobe of the Laurentide Ice Sheet from ice-walled lake deposits. Journal of Quaternary Science 26, 402-410.

Curry, B.B., Hajic, E.R., Clark, J.A., Befus, K.M., Carrell, J.E., Brown, S.E., 2014. The Kankakee Torrent and other large meltwater flooding events during the last deglaciation, Illinois, USA. Quaternary Science Reviews 90, 22-36.

Curry, B.B., Lowell, T.V., Wang, H., Anderson, A.C., 2018. Revised time-distance diagram for the Lake Michigan Lobe, Michigan Subepisode, Wisconsin Episode, Illinois, USA, in: Kehew, A.E., Curry, B.B. (Eds.), Quaternary Glaciation of the Great Lakes Region: Process, Landforms, Sediments, and Chronology: Geological Society of America Special Paper 530, pp. 69–101.

Daigneault, R., Bouchard, M.A., 2004. Les écoulements et le transport glaciaires dans la partie septentrionale du Nunavik (Québec). Canadian Journal of Earth Sciences 41, 919-938.

Daigneault, R.A., 2008. Géologie du Quaternaire du nord de la péninsule d'Ungava, Québec. Commission géologique du Canada, Bulletin no. 533, 116 p.

Daubois, V., Roy, M., Veillette, J.J., Ménard, M., 2015. The drainage of Lake Ojibway in glaciolacustrine sediments of northern Ontario and Quebec, Canada. Boreas 44, 305-318.

De Angelis, H., Kleman, J., 2007. Palaeo-ice streams in the Foxe/Baffin sector of the Laurentide Ice Sheet. Quaternary Science Reviews 26, 1313-1331.

Dieffenbacher-Krall, A.C., Borns, H.W., Nurse, A.M., Langley, G.E.C., Birkel, S., Cwynar, L.C., Doner, L.A., Dorion, C.C., Fastook, J., Jr, G.L.J., Sayles, C., 2016. Younger Dryas Paleoenvironments and Ice Dynamics in Northern Maine: A Multi-Proxy, Case History. Northeastern Naturalist 23, 67-87.

Dredge, L.A., Kerr, D.E., 2013. Reconnaissance Surficial Geology, Overby Lake, Nunavut, NTS 76-I, scale 1:125,000, Geological Survey of Canada CGM Map 143.

Dredge, L.A., McMartin, I., 2007. Surficial geology, Wager Bay, Nunavut, scale 1:100 000, Geological Survey of Canada, A Series Map 2111A.

Dubé-Loubert, H., Daubois, V., Roy, M., 2015. Géologie des dépôts de surface de la région du lac Henrietta; RP 2014-06 (inclus 1 carte des dépôts de surface – 24H; 1:250K). Ministère des Ressources Naturelles du Québec, p. 31.

Dubé-Loubert, H., Daubois, V., Roy, M., 2016. Géologie des dépôts de surface de la région du lac Brisson (incl. 1 map of surfical deposits - 24A; 1:250K). Ministère des Ressources Naturelles du Québec, p. 32.

Dubé-Loubert, H., Hébert, S., Roy, M., 2018a. Géologie des dépôts de surface de la région de la Rivière Arnaud (SNRC 25D et 24M), Rapport (inclus une carte 1 :250,000) Ministère de l'Énergie et des Ressources naturelles – Québec, p. 35.

Dubé-Loubert, H., Roy, M., 2014. Glacial landforms of the southern Ungava Bay region (Canada): implications for the late-glacial dynamics and the damming of glacial Lake Naskaupi, Poster Presentation EGU General Assembly (Vienna, Austria).

Dubé-Loubert, H., Roy, M., 2017. Development, evolution and drainage of glacial Lake Naskaupi during the deglaciation of north-central Quebec and Labrador. Journal of Quaternary Science 32, 1121-1137.

Dubé-Loubert, H., Roy, M., Schaefer, J.M., Clark, P.U., 2018b. ^{10}Be dating of former glacial Lake Naskaupi (Québec-Labrador) and timing of its discharges during the last deglaciation. Quaternary Science Reviews 191, 31-40.

Dyke, A.S., 2004. An outline of North American deglaciation with emphasis on central and northern Canada, in: Ehlers, J., Gibbard, P.L. (Eds.), Quaternary Glaciations - Extent and Chronology, Part II. Elsevier, pp. 373-424.

Dyke, A.S., Andrews, J.T., Clark, P.U., England, J.H., Miller, G.H., Shaw, J., Veillette, J.J., 2002. The Laurentide and Innuitian ice sheets during the Last Glacial Maximum. Quaternary Science Reviews 21, 9-31.

Dyke, A.S., Moore, A., Robertson, L., 2003. Deglaciation of North America: Thirty-two digital maps at 1:7,000,000 scale with accompanying digital chronological database and one poster (two sheets) with full map series. Geological Survey of Canada Open File 1574, https://doi.org/10.4095/214399.

Dyke, A.S., Prest, V.K., 1987. Late Wisconsinan and Holocene History of the Laurentide Ice Sheet. Géographie physique et Quaternaire 41, 237-263.

Dyke, A.S., Savelle, J.M., 2000. Major end moraines of Younger Dryas age on Wollaston Peninsula, Victoria Island, Canadian Arctic: implications for paleoclimate and for formation of hummocky moraine. Canadian Journal of Earth Sciences 37, 601-619.

Dyke, L.M., Hughes, A.L.C., Andresen, C.S., Murray, T., Hiemstra, J.F., Bjørk, A.A., Rodés, Á., 2018. The deglaciation of coastal areas of southeast Greenland. The Holocene 28, 1535-1544.

Easterbrook, D.J., 2015. Late Quaternary Glaciation of the Puget Lowland, North Cascade Range, and Columbia Plateau, Washington. University of Washington Press, 50 p.

England, J., Atkinson, N., Bednarski, J., Dyke, A.S., Hodgson, D.A., Ó Cofaigh, C., 2006. The Innuitian Ice Sheet: configuration, dynamics and chronology. Quaternary Science Reviews 25, 689-703.

England, J.H., Atkinson, N., Dyke, A.S., Evans, D.J.A., Zreda, M., 2004. Late Wisconsinan buildup and wastage of the Innuitian Ice Sheet across southern Ellesmere Island, Nunavut. Canadian Journal of Earth Sciences 41, 39-61.

England, J.H., Furze, M.F.A., Doupé, J.P., 2009. Revision of the NW Laurentide Ice Sheet: implications for paleoclimate, the northeast extremity of Beringia, and Arctic Ocean sedimentation. Quaternary Science Reviews 28, 1573-1596.

Evans, D.J.A., Clark, C.D., Rea, B.R., 2008. Landform and sediment imprints of fast glacier flow in the southwest Laurentide Ice Sheet. Journal of Quaternary Science 23, 249-272.

Evans, D.J.A., Hiemstra, J.F., Boston, C.M., Leighton, I., Ó Cofaigh, C., Rea, B.R., 2012. Till stratigraphy and sedimentology at the margins of terrestrially terminating ice streams: case study of the western Canadian prairies and high plains. Quaternary Science Reviews 46, 80-125.

Evans, D.J.A., Lemmen, D.S., Rea, B.R., 1999. Glacial landsystems of the southwest Laurentide Ice Sheet: modern Icelandic analogues. Journal of Quaternary Science 14, 673-691.

Evans, D.J.A., Young, N.J.P., Ó Cofaigh, C., 2014. Glacial geomorphology of terrestrial-terminating fast flow lobes/ice stream margins in the southwest Laurentide Ice Sheet. Geomorphology 204, 86-113.

Fisher, T.G., Waterson, N., Lowell, T.V., Hajdas, I., 2009. Deglaciation ages and meltwater routing in the Fort McMurray region, northeastern Alberta and northwestern Saskatchewan, Canada. Quaternary Science Reviews 28, 1608-1624.

Franzi, D.A., Ridge, J.C., Pair, D.L., Desimone, D., Rayburn, J.A., Barclay, D.J., 2016. Post-valley heads deglacation of the Adirondack Mountains and adjacent lowlands. Adirondack Journal of Environmental Studies 21, 119-146.

Fullerton, D.S., 1980. Preliminary correlation of post-Erie interstadial events: (16,000-10,000 radiocarbon years before present), central and eastern Great Lakes region, and Hudson, Champlain, and St. Lawrence Lowlands, United States and Canada, United States Geological Survey Professional Paper 1089, p. 52.

Funder, S., Kjeldsen, K.K., Kjær, K.H., Ó Cofaigh, C., 2011. Chapter 50 - The Greenland Ice Sheet During the Past 300,000 Years: A Review, in: Ehlers, J., Gibbard, P.L., Hughes, P.D. (Eds.), Developments in Quaternary Sciences. Elsevier, pp. 699-713.

Furze, M.F.A., Pieńkowski, A.J., McNeely, M.A., Bennett, R., Cage, A.G., 2018. Deglaciation and ice shelf development at the northeast margin of the Laurentide Ice Sheet during the Younger Dryas chronozone. Boreas 47, 271-296.

Gauthier, M.S., 2016. Postglacial lacustrine and marine deposits, far northeastern Manitoba (parts of NTS 54E, L, M, 64I, P). Manitoba Mineral Resources Manitoba Geological Survey, Geological paper GP2015-1, 37 p. + 34 p. in appendices.

Gauthier, M.S., Hodder, T.J., Ross, M., Kelley, S.E., Rochester, A., McCausland, P., 2019. The subglacial mosaic of the Laurentide Ice Sheet; a study of the interior region of southwestern Hudson Bay. Quaternary Science Reviews 214, 1-27.

Gauthier, M.S., Kelley, S.E., Hodder, T.J., *in review*. Lake Agassiz drainage bracketed Holocene Hudson Bay Ice Saddle collapse. Earth and Planetary Science Letters.

Georgiadis, E., Giraudeau, J., Martinez, P., Lajeunesse, P., St-Onge, G., Schmidt, S., Massé, G., 2018. Deglacial to postglacial history of Nares Strait, Northwest Greenland: a marine perspective from Kane Basin. Climate of the Past 14, 1991-2010.

Giangioppi, M., Little, E.C., Ferby, T., Ozyer, C.A., Utting, D.J., 2003. Quaternary glaciomarine environments west of Committee Bay, central mainland Nunavut. Geological Survey of Canada, Current Research 2003-C5, 12 p.

Glover, K.C., Lowell, T.V., Wiles, G.C., Pair, D., Applegate, P., Hajdas, I., 2011. Deglaciation, basin formation and post-glacial climate change from a regional network of sediment core sites in Ohio and eastern Indiana. Quaternary Research 76, 401-410.

Godbout, P.-M., Roy, M., Veillette, J.J., 2019. High-resolution varve sequences record one major late-glacial ice readvance and two drainage events in the eastern Lake Agassiz-Ojibway basin. Quaternary Science Reviews 223, 105942.

Goebel, T., Waters, M.R., O'Rourke, D.H., 2008. The Late Pleistocene Dispersal of Modern Humans in the Americas. Science 319, 1497-1502.

Gray, J., Lauriol, B., Bruneau, D., Ricard, J., 1993. Postglacial emergence of Ungava Peninsula, and its relationship to glacial history. Canadian Journal of Earth Sciences 30, 1676-1696.

Hallberg, G.R., Kemmis, T.J., 1986. Stratigraphy and correlation of the glacial deposits of the Des Moines and James lobes and adjacent areas in North Dakota, South Dakota, Minnesota, and Iowa. Quaternary Science Reviews 5, 65-68.

Hanson, M.A., 2003. Late Quaternary Glaciation, Relative Sea-level History and Recent Coastal Submergence of Northeast Melville Island, Nunavut (M.Sc thesis), University of Alberta, Edmonton, Canada.

Hardy, L., 1977. La déglaciation et les épisodes lacustre et marin sur le versant québécois des basses terres de la baie de James. Géographie physique et Quaternaire 31, 261-273.

Harris, K.L., 1998. Computer-assisted lithostratigraphy, in: Patterson, C.J., Wright, H.E.J. (Eds.), Contributions to Quaternary studies in Minnesota: Minnesota Geological Survey Report of Investigations 49, pp. 179-191.

Heath, S.L., Loope, H.M., Curry, B.B., Lowell, T.V., 2018. Pattern of southern Laurentide Ice Sheet margin position changes during Heinrich Stadials 2 and 1. Quaternary Science Reviews 201, 362-379.

Heaton, T.H., Grady, F., 2003. The Late Wisconsin vertebrate history of Prince of Wales Island, Southeast Alaska, Ice Cave Faunas of North America. Indiana University Press, pp. 17-53.

Heisinger, B., Lal, D., Jull, A.J.T., Kubik, P., Ivy-Ochs, S., Neumaier, S., Knie, K., Lazarev, V., Nolte, E., 2002. Production of selected cosmogenic radionuclides by muons: 1. Fast muons. Earth and Planetary Science Letters 200, 345-355.

Hickin, A.S., Lian, O.B., Levson, V.M., Cui, Y., 2015. Pattern and chronology of glacial Lake Peace shorelines and implications for isostacy and ice-sheet configuration in northeastern British Columbia, Canada. Boreas 44, 288-304.

Hillaire-Marcel, C., Occhietti, S., Vincent, J.-S., 1981. Sakami moraine, Quebec: A 500-km-long moraine without climatic control. Geology 9, 210-214.

Hogan, K.A., Ó Cofaigh, C., Jennings, A.E., Dowdeswell, J.A., Hiemstra, J.F., 2016. Deglaciation of a major palaeo-ice stream in Disko Trough, West Greenland. Quaternary Science Reviews 147, 5-26.

Hughes, A.L.C., Gyllencreutz, R., Lohne, Ø.S., Mangerud, J., Svendsen, J.I., 2016. The last Eurasian ice sheets – a chronological database and time-slice reconstruction, DATED-1. Boreas 45, 1-45.

Hughes, O.L., 1965. Surficial Geology of Part of the Cochrane District, Ontario, Canada. The Geological Society of America Inc. Special Paper 84, 535-565.

Hundert, T., Piper, D.J.W., 2008. Late Quaternary sedimentation on the southwestern Scotian Slope, eastern Canada: relationship to glaciation. Canadian Journal of Earth Sciences 45, 267-285.

Hyodo, A., Longstaffe, F.J., 2011. The chronostratigraphy of Holocene sediments from four Lake Superior sub-basins. Canadian Journal of Earth Sciences 48, 1581-1599.

Jakobsson, M., Andreassen, K., Bjarnadóttir, L.R., Dove, D., Dowdeswell, J.A., England, J.H., Funder, S., Hogan, K., Ingólfsson, Ó., Jennings, A., Krog Larsen, N., Kirchner, N., Landvik, J.Y., Mayer, L., Mikkelsen, N., Möller, P., Niessen, F., Nilsson, J., O'Regan, M., Polyak, L., Nørgaard-Pedersen, N., Stein, R., 2014. Arctic Ocean glacial history. Quaternary Science Reviews 92, 40-67.

Jenner, K.A., Campbell, D.C., Piper, D.J.W., 2018. Along-slope variations in sediment lithofacies and depositional processes since the Last Glacial Maximum on the northeast Baffin margin, Canada. Marine Geology 405, 92-107.

Jennings, A., Andrews, J., Pearce, C., Wilson, L., Ólfasdótttir, S., 2015. Detrital carbonate peaks on the Labrador shelf, a 13–7ka template for freshwater forcing from the

Hudson Strait outlet of the Laurentide Ice Sheet into the subpolar gyre. Quaternary Science Reviews 107, 62-80.

Jennings, A.E., Manley, W.F., Maclean, B., Andrews, J.T., 1998. Marine evidence for the last glacial advance across eastern Hudson Strait, eastern Canadian Arctic. Journal of Quaternary Science 13, 501-514.

Jennings, A.E., Sheldon, C., Cronin, T.M., Francus, P., Stoner, J., Andrews, J.T., 2011a. The Holocene history of Nares Strait: Transition from glacial bay to Arctic-Atlantic throughflow. Oceanography 24, 26-41.

Jennings, C.E., Knaeble, A.R., Meyer, G.N., Lusardi, B.A., Bovee, T.L., Curry, B., Murphy, M., V., S., Wright, H.E., 2011b. A glacial record spanning the Pleistocene in southern Minnesota, in: Miller, J.D., Hudak, G.J., Wittkop, C., McLaughlin, P.I. (Eds.), Archean to Anthropocene: Field Guides to the Geology of the Mid-Continent of North America. GSA Field Guide 24, pp. 351-378.

Johnson, M.D., Hemstad, C., 1998. Glacial Lake Grantsburg: A short-lived lake recording the advance and retreat of the Grantsburg sublobe. ontributions to Quaternary studies in Minnesota: Minnesota Geological Survey Report of Investigations 49, 49-60.

Jones, R.S., Whitehouse, P.L., Bentley, M.J., Small, D., Dalton, A.S., 2019. Impact of glacial isostatic adjustment on cosmogenic surface-exposure dating. Quaternary Science Reviews 212, 206-212.

Josenhans, H.W., Zevenhuizen, J., Klassen, R.A., 1986. The Quaternary geology of the Labrador shelf. Canadian Journal of Earth Sciences 23, 1190-1213.

Kageyama, M., Braconnot, P., Harrison, S.P., Haywood, A.M., Jungclaus, J.H., Otto-Bliesner, B.L., Peterschmitt, J.Y., Abe-Ouchi, A., Albani, S., Bartlein, P.J., Brierley, C., Crucifix, M., Dolan, A., Fernandez-Donado, L., Fischer, H., Hopcroft, P.O., Ivanovic, R.F., Lambert, F., Lunt, D.J., Mahowald, N.M., Peltier, W.R., Phipps, S.J., Roche, D.M., Schmidt, G.A., Tarasov, L., Valdes, P.J., Zhang, Q., Zhou, T., 2018. The PMIP4 contribution to CMIP6 – Part 1: Overview and over-arching analysis plan. Geoscientific Model Development 11, 1033-1057.

Karrow, P.F., Dreimanis, A., Barnett, P.J., 2000. A Proposed Diachronic Revision of Late Quaternary Time-Stratigraphic Classification in the Eastern and Northern Great Lakes Area. Quaternary Research 54, 1-12.

Kaufman, D.S., Young, N.E., Briner, J.P., Manley, W.F., 2011. Alaska PaleoGlacier Atlas version 2, http://instaar.colorado.edu/groups/QGISL/ak_paleoglacier_atlas/downloads/index.html.

King, E.L., 2001. Atlantic shore of Nova Scotia are time transgressive. Geological Survey of Canada, Current Research 2001-D19, 23 p.

King, E.L., 2012. Mineral resource assessment of the shallowest bedrock and overburden, Laurentian Channel, Newfoundland: potential marine protected area. Geological Survey of Canada Open File 6969, 27 p.

King, E.L., 2015. Late glaciation in the eastern Beaufort Sea: contrasts in shallow depositional styles from Amundsen Gulf, Banks Island Shelf and M'Clure Strait, ArcticNet, 2015 Annual Scientific Meeting: oral presentation abstracts, Vancouver, Canada.

King, E.L., Duchesne, M.J., Keun Jin, Y., Dallimore, S., 2019. Shallow marine permafrost occurrence on the westernmost arctic Canadian shelf: A potential record of long-term subsea top-down thaw rates? [abstract], 25th International Symposium on Polar Sciences, May 13-15, Korea.

King, E.L., Lakeman, T.R., Blasco, S., 2014. The shallow geologic framework of the Banks Island Shelf, eastern Beaufort Sea: Evidence for glaciation of the entire shelf and multiple shelf edge geohazards [abstract], Arctic Change 2014, Ottawa, Canada.

King, L.H., 1996. Late Wisconsinan ice retreat from the Scotian Shelf. Geological Society of America Bulletin 108, 1056-1067.

Klassen, R.W., 1991. Surficial geology and drift thickness, Cypress Lake, Geological Survey of Canada, Map 1766A, scale 1:250 000.

Klassen, R.W., 1992. Surficial geology and drift thickness, Wood Mountain, SK. Geological Survey of Canada, Map 1802A., scale 1:250 000.

Klassen, R.W., 2002. Surficial geology of the Cypress Lake and Wood Mountain map areas, southwestern Saskatchewan. Geological Survey of Canada Bulletin 562, 60 p. +62 sheets.

Lacelle, D., Lauriol, B., Zazula, G., Ghaleb, B., Utting, N., Clark, I.D., 2013. Timing of advance and basal condition of the Laurentide Ice Sheet during the last glacial maximum in the Richardson Mountains, NWT. Quaternary Research 80, 274-283.

Lajeunesse, P., 2008. Early Holocene deglaciation of the eastern coast of Hudson Bay. Geomorphology 99, 341-352.

Lajeunesse, P., Allard, M., 2003. The Nastapoka drift belt, eastern Hudson Bay: implications of a stillstand of the Quebec Labrador ice margin in the Tyrrell Sea at 8 ka BP. Canadian Journal of Earth Sciences 40, 65-76.

Lakeman, T.R., England, J.H., 2012. Paleoglaciological insights from the age and morphology of the Jesse moraine belt, western Canadian Arctic. Quaternary Science Reviews 47, 82-100.

Lakeman, T.R., England, J.H., 2013. Late Wisconsinan glaciation and postglacial relative sea-level change on western Banks Island, Canadian Arctic Archipelago. Quaternary Research 80, 99-112.

Lakeman, T.R., Pieńkowski, A.J., Nixon, F.C., Furze, M.F.A., Blasco, S., Andrews, J.T., King, E.L., 2018. Collapse of a marine-based ice stream during the early Younger Dryas chronozone, western Canadian Arctic. Geology 46, 211-214.

Larsen, N.K., Funder, S., Kjær, K.H., Kjeldsen, K.K., Knudsen, M.F., Linge, H., 2014. Rapid early Holocene ice retreat in West Greenland. Quaternary Science Reviews 92, 310-323.

Larsen, N.K., Kjær, K.H., Funder, S., Möller, P., van der Meer, J.J.M., Schomacker, A., Linge, H., Darby, D.A., 2010. Late Quaternary glaciation history of northernmost Greenland – Evidence of shelf-based ice. Quaternary Science Reviews 29, 3399-3414.

Larsen, N.K., Strunk, A., Levy, L.B., Olsen, J., Bjørk, A., Lauridsen, T.L., Jeppesen, E., Davidson, T.A., 2017. Strong altitudinal control on the response of local glaciers to

Holocene climate change in southwest Greenland. Quaternary Science Reviews 168, 69-78.

Lauriol, B., Gray, J.T., 1987. The Decay and Disappearance of the Late Wisconsin Ice Sheet in the Ungava Peninsula, Northern Quebec, Canada. Arctic and Alpine Research 19, 109-126.

Lavoie, C., Allard, M., Duhamel, D., 2012. Deglaciation landforms and C-14 chronology of the Lac Guillaume-Delisle area, eastern Hudson Bay: A report on field evidence. Geomorphology 159-160, 142-155.

Ledu, D., Rochon, A., de Vernal, A., St-Onge, G., 2010. Holocene paleoceanography of the northwest passage, Canadian Arctic Archipelago. Quaternary Science Reviews 29, 3468-3488.

Lepper, K., Fisher, T.G., Hajdas, I., Lowell, T.V., 2007. Ages for the Big Stone Moraine and the oldest beaches of glacial Lake Agassiz: Implications for deglaciation chronology. Geology 35, 667-670.

Lesnek, A.J., Briner, J.P., Lindqvist, C., Baichtal, J.F., Heaton, T.H., 2018. Deglaciation of the Pacific coastal corridor directly preceded the human colonization of the Americas. Science Advances 4, eaar5040.

Lévesque, Y., St-Onge, G., Lajeunesse, P., Desiage, P.-A., Brouard, E., 2020. Defining the maximum extent of the Laurentide Ice Sheet in Home Bay (eastern Arctic Canada) during the Last Glacial episode. Boreas, 52-70.

Levson, V.M., Ferbey, T., Kerr, D.E., 2013. Reconnaissance surficial geology, Clarke River, NTS 65-M south half, Northwest Territories, scale 1:125 000, Geological Survey of Canada, Canadian Geoscience Map157, (preliminary).

Levy, L.B., Larsen, N.K., Davidson, T.A., Strunk, A., Olsen, J., Jeppesen, E., 2017. Contrasting evidence of Holocene ice margin retreat, south-western Greenland. Journal of Quaternary Science 32, 604-616.

Lewis, C.F.M., Anderson, T.W., 1990. Oscillations of levels and cool phases of the Laurentian Great Lakes caused by inflows from glacial Lakes Agassiz and Barlow-

Ojibway, in: Davis, R.B. (Ed.), Paleolimnology and the Reconstruction of Ancient Environments. Springer Netherlands, Dordrecht, pp. 59-106.

Leydet, D.J., Carlson, A.E., Teller, J.T., Breckenridge, A., Barth, A.M., Ullman, D.J., Sinclair, G., Milne, G.A., Cuzzone, J.K., Caffee, M.W., 2018. Opening of glacial Lake Agassiz’s eastern outlets by the start of the Younger Dryas cold period. Geology 46, 155-158.

Li, G., Piper, D.J.W., Campbell, D.C., 2011. The Quaternary Lancaster Sound trough-mouth fan, NW Baffin Bay. Journal of Quaternary Science 26, 511-522.

Little, E.C., 2006. Surficial geology, Ellice Hills (north), Nunavut. Geological Survey of Canada Open File 5016.

Lochte, A.A., Repschlager, J., Kienast, M., Garbe-Schonberg, D., Andersen, N., Hamann, C., Schneider, R., 2019. Labrador Sea freshening at 8.5 ka BP caused by Hudson Bay Ice Saddle collapse. Nature communications 10, 586.

Löfverström, M., Caballero, R., Nilsson, J., Kleman, J., 2014. Evolution of the large-scale atmospheric circulation in response to changing ice sheets over the last glacial cycle. Climate of the Past 10, 1453-1471.

Löfverström, M., Lora, J.M., 2017. Abrupt regime shifts in the North Atlantic atmospheric circulation over the last deglaciation. Geophysical Research Letters 44, 8047-8055.

Loope, H.M., Antinao, J.L., Monaghan, G.W., Autio, R.J., Curry, B.B., Grimley, D.A., Huot, S., Lowell, T.V., Nash, T.A., 2018. At the edge of the Laurentide Ice Sheet: Stratigraphy and chronology of glacial deposits in central Indiana, in: Florea, L.J. (Ed.), Ancient Oceans, Orogenic Uplifts, and Glacial Ice: Geologic Crossroads in America’s Heartland: Geological Society of America Field Guide 51, pp. 245-258.

Lowell, T.V., Fisher, T.G., Hajdas, I., Glover, K., Loope, H., Henry, T., 2009. Radiocarbon deglaciation chronology of the Thunder Bay, Ontario area and implications for ice sheet retreat patterns. Quaternary Science Reviews 28, 1597-1607.

Lundstrom, S., 2013. Aspects of the latest Pleistocene glacial geologic record of the James lobe of eastern South Dakota. GSA Abstracts with Programs 45, 413.

Lusardi, B.A., Jennings, C.E., Harris, K.L., 2011. Provenance of Des Moines lobe till records ice-stream catchment evolution during Laurentide deglaciation. Boreas 40, 585-597.

MacLean, B., Blasco, S., Bennett, R., Lakeman, T., Hughes-Clarke, J., Kuus, P., Patton, E., 2015. New marine evidence for a Late Wisconsinan ice stream in Amundsen Gulf, Arctic Canada. Quaternary Science Reviews 114, 149-166.

MacLean, B., Blasco, S., Bennett, R., Lakeman, T., Pieńkowski, A.J., Furze, M.F.A., Hughes Clarke, J., Patton, E., 2017. Seafloor features delineate Late Wisconsinan ice stream configurations in eastern Parry Channel, Canadian Arctic Archipelago. Quaternary Science Reviews 160, 67-84.

Manley, W.F., 1996. Late-glacial flow patterns, deglaciation, and postglacial emergence of the south-central Baffin Island and the north-central coast of Hudson Straight, eastern Canadian Arctic. Canadian Journal of Earth Sciences 33, 1499-1510.

Manley, W.F., Jennings, A.E., 1996. Radiocarbon Date List VIII: Eastern Canadian Arctic, Labrador, Northern Quebec, East Greenland Shelf, Iceland Shelf, and Antarctica, Occasional Paper No. 50. University of Colorado, Institute of Arctic and Alpine Research, p. 163.

Margold, M., Stokes, C.R., Clark, C.D., 2015. Ice streams in the Laurentide Ice Sheet: Identification, characteristics and comparison to modern ice sheets. Earth-Science Reviews 143, 117-146.

Margold, M., Stokes, C.R., Clark, C.D., 2018. Reconciling records of ice streaming and ice margin retreat to produce a palaeogeographic reconstruction of the deglaciation of the Laurentide Ice Sheet. Quaternary Science Reviews 189, 1-30.

Margreth, A., Gosse, J.C., Dyke, A.S., 2017. Wisconsinan and early Holocene glacial dynamics of Cumberland Peninsula, Baffin Island, Arctic Canada. Quaternary Science Reviews 168, 79-100.

Marsella, K.A., Bierman, P.R., Davis, P.T., Caffee, M.W., 2000. Cosmogenic 10Be and 26Al ages for the last glacial maximum, eastern Baffin Island, Arctic Canada. Geological Society of America Bulletin 112, 1296-1312.

McMartin, I., Campbell, J.E., Dredge, L.A., LeCheminant, A.N., McCurdy, M.W., Scromeda, N., 2015. Quaternary geology and till composition north of Wager Bay, Nunavut: results from the GEM Wager Bay Surficial Geology Project. Geological Survey of Canada Open File 7748.

McMartin, I., Campbell, J.E., Dredge, L.A., Robertson, L., 2012. Surficial Geology Map Compilation of the TGI-3 Flin Flon Project area, Manitoba and Saskatchewan. Geological Survey of Canada Open File 7089.

McMartin, I., Henderson, P.J., 2004. Evidence from Keewatin (Central Nunavut) for Paleo-Ice Divide Migration. Géographie physique et Quaternaire 58, 163-186.

Mickelson, D.M., Attig, J.W., 2017. Laurentide Ice Sheet: Ice-Margin Positions in Wisconsin. Wisconsin Geological and Natural History Survey Educational Series 56, 46 p.

Miller, G.H., Wolfe, A.P., Briner, J.P., Sauer, P.E., Nesje, A., 2005. Holocene glaciation and climate evolution of Baffin Island, Arctic Canada. Quaternary Science Reviews 24, 1703-1721.

Muhs, D.R., Bettis, E.A., III, Roberts, H.M., Harlan, S.S., Paces, J.B., Reynolds, R.L., 2013. Chronology and provenance of last-glacial (peoria) loess in western iowa and paleoclimatic implications. Quaternary Research 80, 468-481.

Munyikwa, K., Feathers, J.K., Rittenour, T.M., Shrimpton, H.K., 2011. Constraining the Late Wisconsinan retreat of the Laurentide ice sheet from western Canada using luminescence ages from postglacial aeolian dunes. Quaternary Geochronology 6, 407-422.

Narancic, B., Pienitz, R., Chapligin, B., Meyer, H., Francus, P., Guilbault, J.-P., 2016. Postglacial environmental succession of Nettilling Lake (Baffin Island, Canadian Arctic) inferred from biogeochemical and microfossil proxies. Quaternary Science Reviews 147, 391-405.

Nixon, F.C., England, J.H., 2014. Expanded Late Wisconsinan ice cap and ice sheet margins in the western Queen Elizabeth Islands, Arctic Canada. Quaternary Science Reviews 91, 146-164.

Norris, S.L., Evans, D.J.A., Ó Cofaigh, C., 2018. Geomorphology and till architecture of terrestrial palaeo-ice streams of the southwest Laurentide Ice Sheet: A borehole stratigraphic approach. Quaternary Science Reviews, 186-214.

Norris, S.L., Margold, M., Froese, D.G., 2017. Glacial landforms of northwest Saskatchewan. Journal of Maps 13, 600-607.

Ó Cofaigh, C., Evans, D.J.A., Smith, I.R., 2010. Large-scale reorganization and sedimentation of terrestrial ice streams during late Wisconsinan Laurentide Ice Sheet deglaciation. Geological Society of America Bulletin 122, 743-756.

Oakley, B.A., Boothroyd, J.C., 2012. Reconstructed topography of Southern New England prior to isostatic rebound with implications of total isostatic depression and relative sea level. Quaternary Research 78, 110-118.

Occhietti, S., 2007. The Saint-Narcisse morainic complex and early Younger Dryas events on the southeastern margin of the Laurentide Ice Sheet. Géographie physique et Quaternaire 61, 89-117.

Occhietti, S., Parent, M., Lajeunesse, P., Robert, F., Govare, É., 2011. Late Pleistocene–Early Holocene Decay of the Laurentide Ice Sheet in Québec–Labrador, in: van ver Meer, J. (Ed.), Developments in Quaternary Science, pp. 601-630.

Occhietti, S., Richard, P., 2003. Effet réservoir sur les âges 14C de la Mer de Champlain à la transition Pléistocène-Holocène : révision de la chronologie de la déglaciation au Québec méridional. Géographie physique et Quaternaire 57, 115-138.

Occhietti, S., Robitaille, D., Locat, P., Demers, D., 2015. Younger Dryas glacial readvance over the northern margin of Goldthwait Sea and mass movement implications on the coast downstream the Saguenay River, St. Lawrence Estuary, Québec, Geologial Society of America Northeastern Section - 50th Annual Meeting, Bretton Woods, New Hampshire, United States.

Parent, M., Occhietti, S., 1999. Late Wisconsinan deglaciation and glacial lake development in the Appalachians of southeastern Québec. Géographie physique et Quaternaire 53, 117-135.

Patterson, C.J., 1997. Surficial geology of southwestern Minnesota, in: Patterson, C.J. (Ed.), Contributions to the Quaternary geology of southwestern Minnesota: Minnesota Geological Survey Report of Investigations 47, p. 45.

Patterson, C.J., 1998. Laurentide glacial landscapes: The role of ice streams. Geology 26, 643-646.

Pieńkowski, A.J., England, J.H., Furze, M.F.A., Blasco, S., Mudie, P.J., MacLean, B., 2013. 11,000 yrs of environmental change in the Northwest Passage: A multiproxy core record from central Parry Channel, Canadian High Arctic. Marine Geology 341, 68-85.

Pieńkowski, A.J., England, J.H., Furze, M.F.A., MacLean, B., Blasco, S., 2014. The late Quaternary environmental evolution of marine Arctic Canada: Barrow Strait to Lancaster Sound. Quaternary Science Reviews 91, 184-203.

Pieńkowski, A.J., England, J.H., Furze, M.F.A., Marret, F., Eynaud, F., Vilks, G., Maclean, B., Blasco, S., Scourse, J.D., 2012. The deglacial to postglacial marine environments of SE Barrow Strait, Canadian Arctic Archipelago. Boreas 41, 141-179.

Piper, D., Macdonald, A., 2001. Timing and position of Late Wisconsinan ice-margins on the upper slope seaward of Laurentian Channel. Géographie physique et Quaternaire 55, 131-140.

Porreca, C., Briner, J.P., Kozlowski, A., 2018. Laurentide ice sheet meltwater routing along the Iro-Mohawk River, eastern New York, USA. Geomorphology 303, 155-161.

Potter, B.A., Baichtal, J.F., Beaudoin, A.B., Fehren-Schmitz, L., Haynes, C.V., Holliday, V.T., Holmes, C.E., Ives, J.W., Kelly, R.L., Llamas, B., Malhi, R.S., Miller, D.S., Reich, D., Reuther, J.D., Schiffels, S., Surovell, T.A., 2018. Current evidence allows multiple models for the peopling of the Americas. Science Advances 4, eaat5473.

Praeg, D., Maclean, B., Sonnichsen, G., 2007. Quaternary Geology of the Northeast Baffin Island Continental Shelf, Cape Aston to Buchan Gulf (70º to 72ºN). Geological Survey of Canada Open File 5409, 98 p.

Prest, V.K., 1969. Retreat of Wisconsin and Recent ice in North America, Geological Survey of Canada Map, 1257A, scale 1:5,000,000.

Rayburn, J.A., Knuepfer, P.L.K., Franzi, D.A., 2005. A series of large, Late Wisconsinan meltwater floods through the Champlain and Hudson Valleys, New York State, USA. Quaternary Science Reviews 24, 2410-2419.

Reimer, P.J., Bard, E., Bayliss, A., Beck, J.W., Blackwell, P.G., Bronk Ramsey, C., Buck, C.E., Cheng, H., Edwards, R.L., Friedrich, M., Grootes, P.M., Guilderson, T.P., Haflidason, H., Hajdas, I., Hatté, C., Heaton, T.J., Hoffmann, D.L., Hogg, A.G., Hughen, K.A., Kaiser, K.F., Kromer, B., Manning, S.W., Niu, M., Reimer, R.W., Richards, D.A., Scott, E.M., Southon, J.R., Staff, R.A., Turney, R.S.M., van der Plicht, J., 2013. IntCal13 and Marine13 Radiocarbon Age Calibration Curves 0–50,000 Years cal BP. Radiocarbon 55, 1869-1887.

Rémillard, A.M., St-Onge, G., Bernatchez, P., Hétu, B., Buylaert, J.-P., Murray, A.S., Vigneault, B., 2016. Chronology and stratigraphy of the Magdalen Islands archipelago from the last glaciation to the early Holocene: new insights into the glacial and sea-level history of eastern Canada. Boreas 45, 604-628.

Richard, P.J.H., Occhietti, S., 2005. ^{14}C chronology for ice retreat and inception of Champlain Sea in the St Lawrence Lowlands, Canada. Quaternary Research 63, 353-358.

Ridge, J.C., 2003. The last deglaciation of the northeastern United States: A combined varve, paleomagnetic, and calibrated ^{14}C chronology, in: Hart, J.P., Cremeens, D.L. (Eds.), Geoarchaeology of Landscapes in the Glaciated Northeast U.S.: New York State Museum Bulletin 497, pp. 15-45.

Ridge, J.C., 2004. The Quaternary glaciation of western New England with correlations to surrounding areas, in: Ehlers, J., Gibbard, P.L. (Eds.), Quaternary Glaciations – Extent and Chronology, Part II: North America. Developments in Quaternary Science, vol. 2b. Elsevier, Amsterdam, pp. 163-193.

Ridge, J.C., 2012. The North American Glacial Varve Project (http://eos.tufts.edu/varves/) sponsored by The U.S. National Science Foundation and The Department of Earth and Ocean Sciences of Tufts University, Medford, Massachusetts, USA.

Ridge, J.C., Balco, G., Bayless, R.L., Beck, C.C., Carter, L.B., Dean, J.L., Voytek, E.B., Wei, J.H., 2012. The new North American Varve Chronology: A precise record of southeastern Laurentide Ice Sheet deglaciation and climate, 18.2-12.5 kyr BP, and correlations with Greenland ice core records. American Journal of Science 312, 685-722.

Riedel, J.L., 2017. Deglaciation of the North Cascade Range, Washington and British Columbia, from the Last Glacial Maximum to the Holocene. Cuadernos de Investigación Geográfica 43, 467-496.

Robertson, L.S., 2018. The glacial and Holocene history of Notre Dame Trough, Northeast Newfoundland Shelf, Department of Geology (B.Sc thesis). Saint Mary’s University, Halifax, Nova Scotia, p. 82.

Roger, J., Saint-Ange, F., Lajeunesse, P., Duchesne, M.J., St-Onge, G., Trenhaile, A., 2013. Late Quaternary glacial history and meltwater discharges along the Northeastern Newfoundland Shelf. Canadian Journal of Earth Sciences 50, 1178-1194.

Ross, M., Campbell, J.E., Parent, M., Adams, R.S., 2009. Palaeo-ice streams and the subglacial landscape mosaic of the North American mid-continental prairies. Boreas 38, 421-439.

Ross, M., Parent, M., Benjumea, B., Hunter, J., 2006. The late Quaternary stratigraphic record northwest of Montréal: regional ice-sheet dynamics, ice-stream activity, and early deglacial events. Canadian Journal of Earth Sciences 43, 461-485.

Ross, M., Utting, D.J., Lajeunesse, P., Kosar, K.G.A., 2012. Early Holocene deglaciation of northern Hudson Bay and Foxe Channel constrained by new radiocarbon ages and marine reservoir correction. Quaternary Research 78, 82-94.

Roy, M., Dell’Oste, F., Veillette, J.J., de Vernal, A., Hélie, J.F., Parent, M., 2011. Insights on the events surrounding the final drainage of Lake Ojibway based on James Bay stratigraphic sequences. Quaternary Science Reviews 30, 682-692.

Shaw, J., Longva, O., 2017. Glacial geomorphology of the Northeast Newfoundland Shelf: ice-stream switching and widespread glaciotectonics. Boreas 46, 622-641.

Shaw, J., Piper, D.J.W., Fader, G.B.J., King, E.L., Todd, B.J., Bell, T., Batterson, M.J., Liverman, D.G.E., 2006. A conceptual model of the deglaciation of Atlantic Canada. Quaternary Science Reviews 25, 2059-2081.

Sinclair, G., Carlson, A.E., Mix, A.C., Lecavalier, B.S., Milne, G., Mathias, A., Buizert, C., DeConto, R., 2016. Diachronous retreat of the Greenland ice sheet during the last deglaciation. Quaternary Science Reviews 145, 243-258.

Small, D., Clark, C.D., Chiverrell, R.C., Smedley, R.K., Bateman, M.D., Duller, G.A.T., Ely, J.C., Fabel, D., Medialdea, A., Moreton, S.G., 2017. Devising quality assurance procedures for assessment of legacy geochronological data relating to deglaciation of the last British-Irish Ice Sheet. Earth-Science Reviews 164, 232-250.

Stea, R.R., Mott, R.J., 2005. Younger Dryas glacial advance in the southern Gulf of St. Lawrence, Canada: analogue for ice inception? Boreas 34, 345-362.

Stea, R.R., Seaman, A.A., Pronk, T., Parkhill, M.A., Allard, S., Utting, D., 2011. The Appalachian Glacier Complex in Maritime Canada, in: Ehlers, J., Gibbard, P.L., Hughes, P.D. (Eds.), Developments in Quaternary Science, Vol. 15, Amsterdam, pp. 631-659.

Stokes, C.R., 2017. Deglaciation of the Laurentide Ice Sheet from the Last Glacial Maximum. Cuadernos de Investigación Geográfica 43, 377-428.

Stokes, C.R., Margold, M., Clark, C.D., Tarasov, L., 2016. Ice stream activity scaled to ice sheet volume during Laurentide Ice Sheet deglaciation. Nature 530, 322-326.

Stokes, C.R., Tarasov, L., Blomdin, R., Cronin, T.M., Fisher, T.G., Gyllencreutz, R., Hättestrand, C., Heyman, J., Hindmarsh, R.C.A., Hughes, A.L.C., Jakobsson, M., Kirchner, N., Livingstone, S.J., Margold, M., Murton, J.B., Noormets, R., Peltier, W.R., Peteet, D.M., Piper, D.J.W., Preusser, F., Renssen, H., Roberts, D.H., Roche, D.M., Saint-Ange, F., Stroeven, A.P., Teller, J.T., 2015. On the reconstruction of palaeo-ice sheets: Recent advances and future challenges. Quaternary Science Reviews 125, 15-49.

Stone, J.R., Schafer, J.P., London, E.H., DiGiacomo-Cohen, M.L., Lewis, R.S., Thompson, W.B., 2005. Quaternary geologic map of Connecticut and Long Island Sound Basin, scale 1:100,000. United States Geological Survey.

Stuiver, M., Polach, H.A., 1977. Discussion: reporting of ^{14}C data. Radiocarbon 19, 355-363.

Tarasov, L., Dyke, A.S., Neal, R.M., Peltier, W.R., 2012. A data-calibrated distribution of deglacial chronologies for the North American ice complex from glaciological modeling. Earth and Planetary Science Letters 315-316, 30-40.

Teller, J.T., 2013. Lake Agassiz during the Younger Dryas. Quaternary Research 80, 361-369.

Teller, J.T., Boyd, M., Yang, Z., Kor, P.S.G., Mokhtari Fard, A., 2005. Alternative routing of Lake Agassiz overflow during the Younger Dryas: new dates, paleotopography, and a re-evaluation. Quaternary Science Reviews 24, 1890-1905.

Teller, J.T., Leverington, D.W., 2004. Glacial Lake Agassiz: A 5000 yr history of change and its relationship to the δ18O record of Greenland. GSA Bulletin 116, 729-742.

Thompson, W., Fowler, B., Dorion, C., 1999. Deglaciation of the northwestern White Mountains, New Hampshire. Géographie physique et Quaternaire 53, 59-77.

Thompson, W.B., Dorion, C.C., Ridge, J.C., Balco, G., Fowler, B.K., Svendsen, K.M., 2017. Deglaciation and late-glacial climate change in the White Mountains, New Hampshire, USA. Quaternary Research 87, 96-120.

Thompson, W.B., Griggs, C.B., Miller, N.G., Nelson, R.E., Weddle, T.K., Kilian, T.M., 2011. Associated terrestrial and marine fossils in the late-glacial Presumpscot Formation, southern Maine, USA, and the marine reservoir effect on radiocarbon ages. Quaternary Research 75, 552-565.

Todd, B.J., Shaw, J., 2012. Laurentide Ice Sheet dynamics in the Bay of Fundy, Canada, revealed through multibeam sonar mapping of glacial landsystems. Quaternary Science Reviews 58, 83-103.

Todd, B.J., Valentine, P.C., Longva, O., Shaw, J., 2007. Glacial landforms on German Bank, Scotian Shelf: evidence for Late Wisconsinan ice-sheet dynamics and implications for the formation of De Geer moraines. Boreas 36, 148-169.

Trommelen, M.S., Ross, M., Campbell, J.E., 2012. Glacial terrain zone analysis of a fragmented paleoglaciologic record, southeast Keewatin sector of the Laurentide Ice Sheet. Quaternary Science Reviews 40, 1-20.

Ullman, D.J., Carlson, A.E., Hostetler, S.W., Clark, P.U., Cuzzone, J., Milne, G.A., Winsor, K., Caffee, M., 2016. Final Laurentide ice-sheet deglaciation and Holocene climate-sea level change. Quaternary Science Reviews 152, 49-59.

Ullman, D.J., Carlson, A.E., LeGrande, A.N., Anslow, F.S., Moore, A.K., Caffee, M., Syverson, K.M., Licciardi, J.M., 2015. Southern Laurentide ice-sheet retreat synchronous with rising boreal summer insolation. Geology 43, 23-26.

United States Geological Survey's Center for Earth Resources Observation and Science (EROS), 2010. 30 arc-second DEM of North America, https://databasin.org/datasets/d2198be9d2264de19cb93fe6a380b69c.

Utting, D.J., Atkinson, N., Pawley, S., Livingstone, S.J., 2016a. Reconstructing the confluence zone between Laurentide and Cordilleran ice sheets along the Rocky Mountain Foothills, south-west Alberta. Journal of Quaternary Science 31, 769-787.

Utting, D.J., Gosse, J.C., Kelley, S.E., Vickers, K.J., Ward, B.C., Trommelen, M.S., 2016b. Advance, deglacial and sea-level chronology for Foxe Peninsula, Baffin Island, Nunavut. Boreas 45, 439-454.

Veillette, J.J., Roy, M., Paulen, R.C., Ménard, M., St-Jacques, G., 2017. Uncovering the hidden part of a large ice stream of the Laurentide Ice Sheet, northern Ontario, Canada. Quaternary Science Reviews 155, 136-158.

Ward, B.C., Thomson, B., 2004. Late Pleistocene stratigraphy and chronology of lower Chehalis River valley, southwestern British Columbia: evidence for a restricted Coquitlam Stade. Canadian Journal of Earth Sciences 41, 881-895.

Ward, B.C., Wilson, M.C., Nagorsen, D.W., Nelson, D.E., Driver, J.C., Wigen, R.J., 2003. Port Eliza cave: North American West Coast interstadial environment and implications for human migrations. Quaternary Science Reviews 22, 1383-1388.

Waters, M.R., 2019. Late Pleistocene exploration and settlement of the Americas by modern humans. Science 365, eaat5447.

Waters, M.R., Stafford, T.W., Jr., Kooyman, B., Hills, L.V., 2015. Late Pleistocene horse and camel hunting at the southern margin of the ice-free corridor: reassessing the age of

Wally's Beach, Canada. Proceedings of the National Academy of Sciences 112, 4263-4267.

Wayne, W.J., 1965. The Crawfordsville and Knightstown Moraines in Indiana. Indiana Geological Survey Report of Progress 28, 15 p.

Winsor, K., Carlson, A.E., Caffee, M.W., Rood, D.H., 2015. Rapid last-deglacial thinning and retreat of the marine-terminating southwestern Greenland ice sheet. Earth and Planetary Science Letters 426, 1-12.

Wolfe, S., Huntley, D., Ollerhead, J., 2004. Relict Late Wisconsinan Dune Fields of the Northern Great Plains, Canada. Géographie physique et Quaternaire 58, 323-336.

Wright, H.E., Matsch, C.L., Cushing, E.J., 1973. The Superior and Des Moines Lobes. Geological Society of America Memoir 136, 153-188.

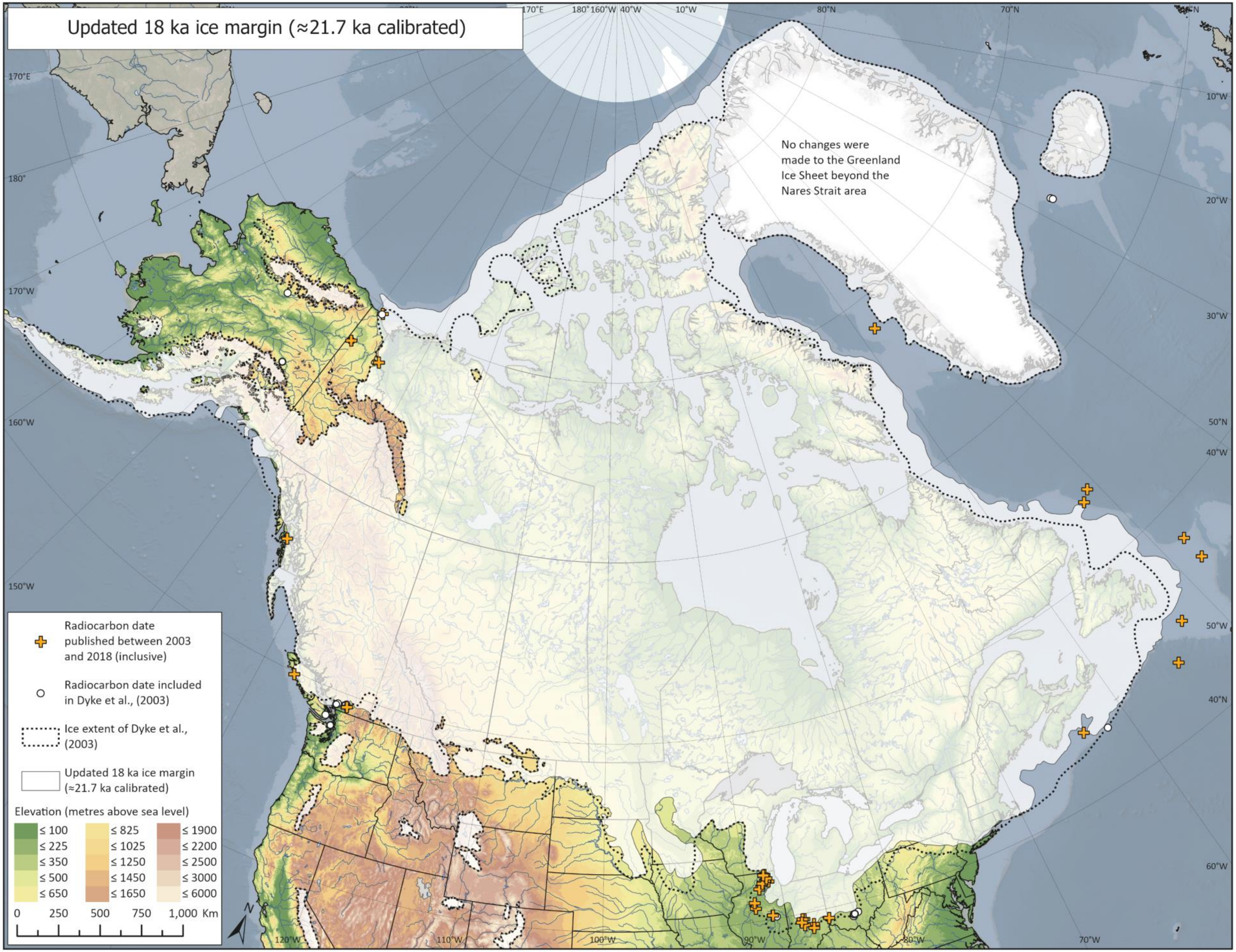
Updated 18 ka ice margin (≈21.7 ka calibrated)
No changes were made to the Greenland Ice Sheet beyond the Nares Strait area
Radiocarbon date published between 2003 and 2018 (inclusive)
Radiocarbon date included in Dyke et al., (2003)
Ice extent of Dyke et al., (2003)
Updated 18 ka ice margin (≈21.7 ka calibrated)
Elevation (metres above sea level)
≤ 100
≤ 225
≤ 350
≤ 500
≤ 650
≤ 825
≤ 1025
≤ 1250
≤ 1450
≤ 1650
≤ 1900
≤ 2200
≤ 2500
≤ 3000
≤ 6000
0 250 500 750 1,000 Km
N

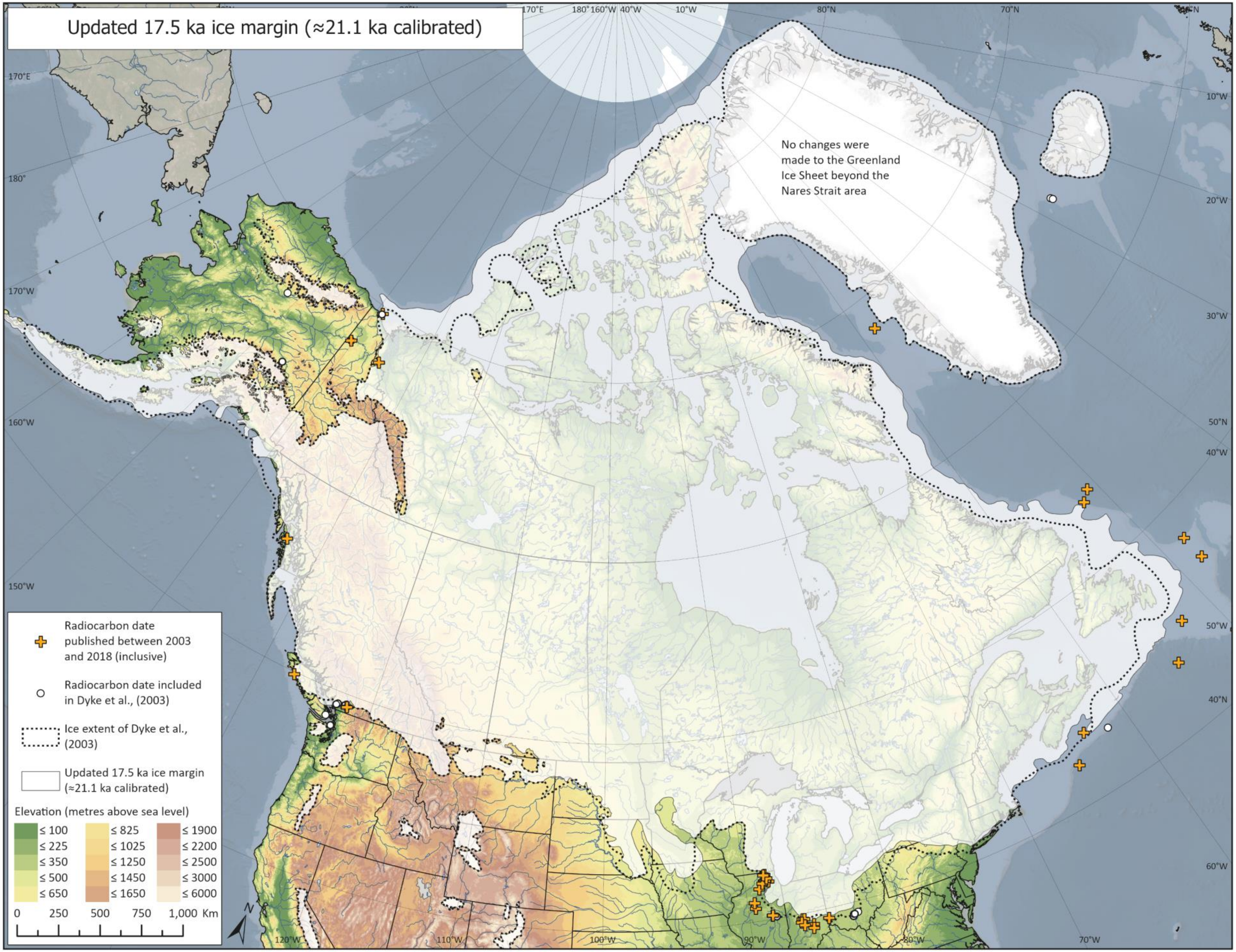

Updated 17.5 ka ice margin (≈21.1 ka calibrated)
No changes were made to the Greenland Ice Sheet beyond the Nares Strait area
Radiocarbon date published between 2003 and 2018 (inclusive)
Radiocarbon date included in Dyke et al., (2003)
Ice extent of Dyke et al., (2003)
Updated 17.5 ka ice margin (≈21.1 ka calibrated)
Elevation (metres above sea level)
≤ 100
≤ 225
≤ 350
≤ 500
≤ 650
≤ 825
≤ 1025
≤ 1250
≤ 1450
≤ 1650
≤ 1900
≤ 2200
≤ 2500
≤ 3000
≤ 6000
0 250 500 750 1,000 Km
N
170°E
180°
170°W
160°W
150°W
120°W
110°W
100°W
90°W
80°W
70°W
60°W
40°N
50°N
10°W
20°W
30°W
40°W
70°N
80°N

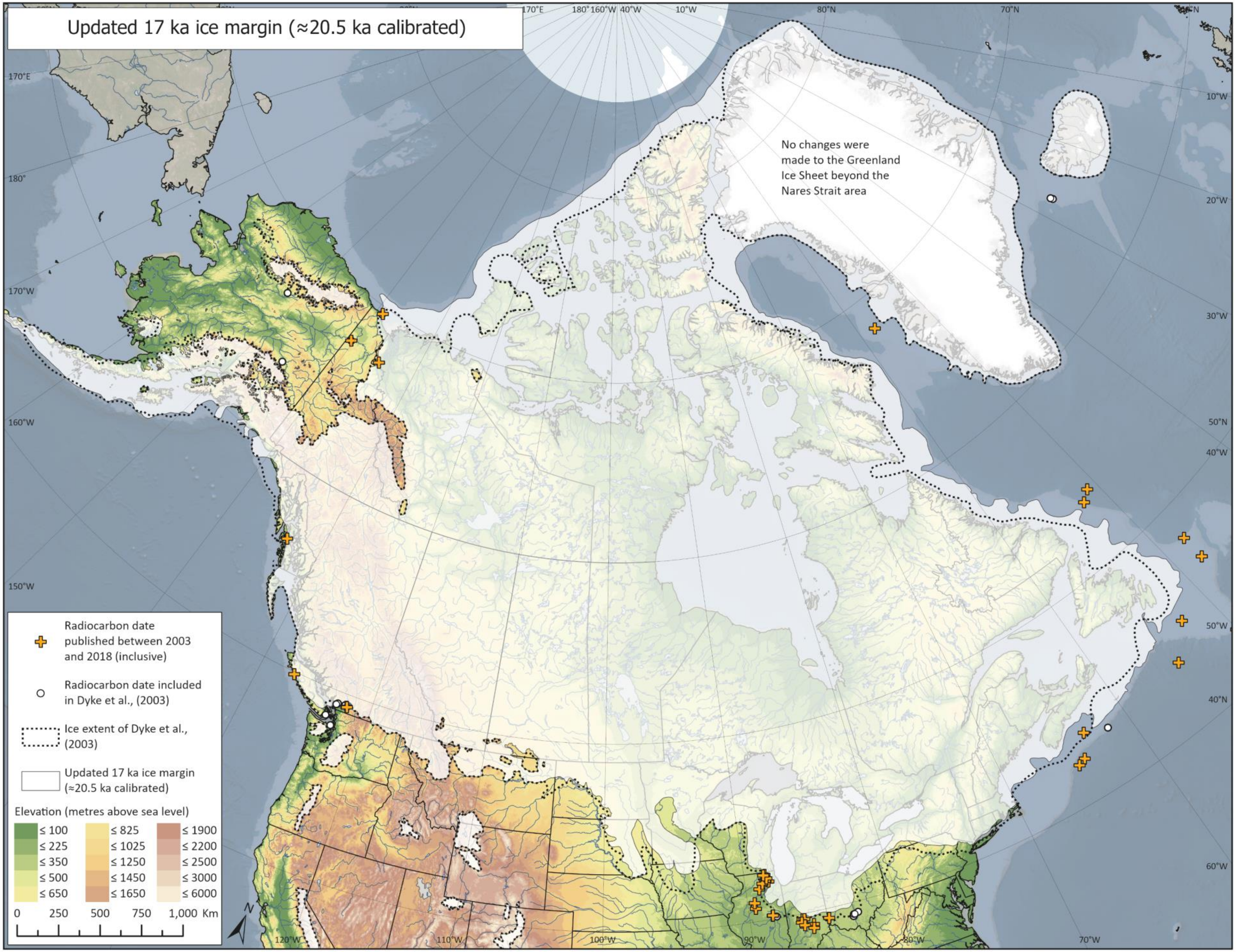

Updated 17 ka ice margin (≈20.5 ka calibrated)
No changes were made to the Greenland Ice Sheet beyond the Nares Strait area
Radiocarbon date published between 2003 and 2018 (inclusive)
Radiocarbon date included in Dyke et al., (2003)
Ice extent of Dyke et al., (2003)
Updated 17 ka ice margin (≈20.5 ka calibrated)
Elevation (metres above sea level)
≤ 100
≤ 225
≤ 350
≤ 500
≤ 650
≤ 825
≤ 1025
≤ 1250
≤ 1450
≤ 1650
≤ 1900
≤ 2200
≤ 2500
≤ 3000
≤ 6000
0 250 500 750 1,000 Km
N
170°E
180°
170°W
160°W
150°W
120°W
110°W
100°W
90°W
80°W
70°W
60°W
50°W
40°W
30°W
20°W
10°W
80°N
70°N
50°N
40°N

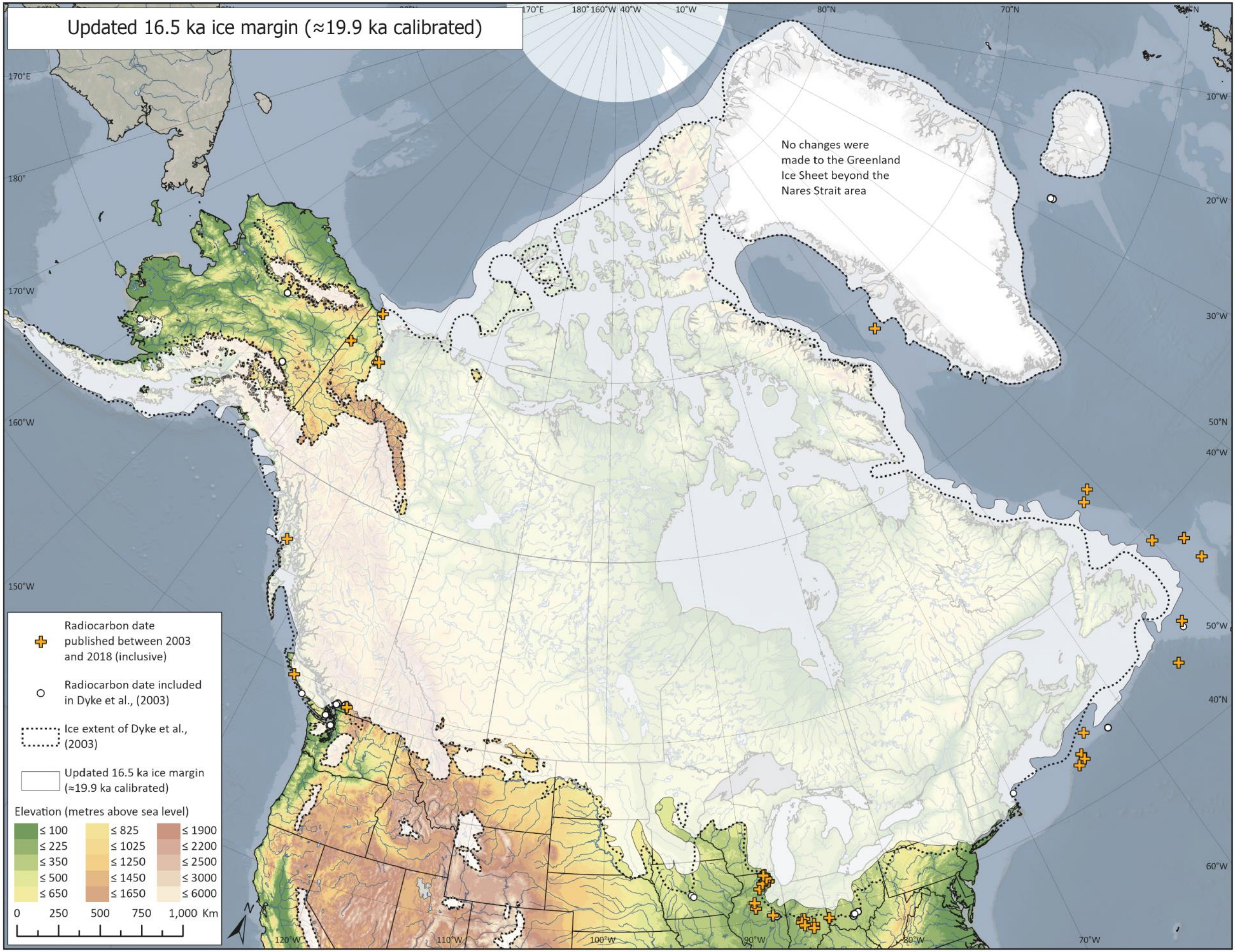

Updated 16.5 ka ice margin (≈19.9 ka calibrated)
No changes were made to the Greenland Ice Sheet beyond the Nares Strait area
Radiocarbon date published between 2003 and 2018 (inclusive)
Radiocarbon date included in Dyke et al., (2003)
Ice extent of Dyke et al., (2003)
Updated 16.5 ka ice margin (≈19.9 ka calibrated)
Elevation (metres above sea level)
≤ 100
≤ 225
≤ 350
≤ 500
≤ 650
≤ 825
≤ 1025
≤ 1250
≤ 1450
≤ 1650
≤ 1900
≤ 2200
≤ 2500
≤ 3000
≤ 6000
0 250 500 750 1,000 Km
N

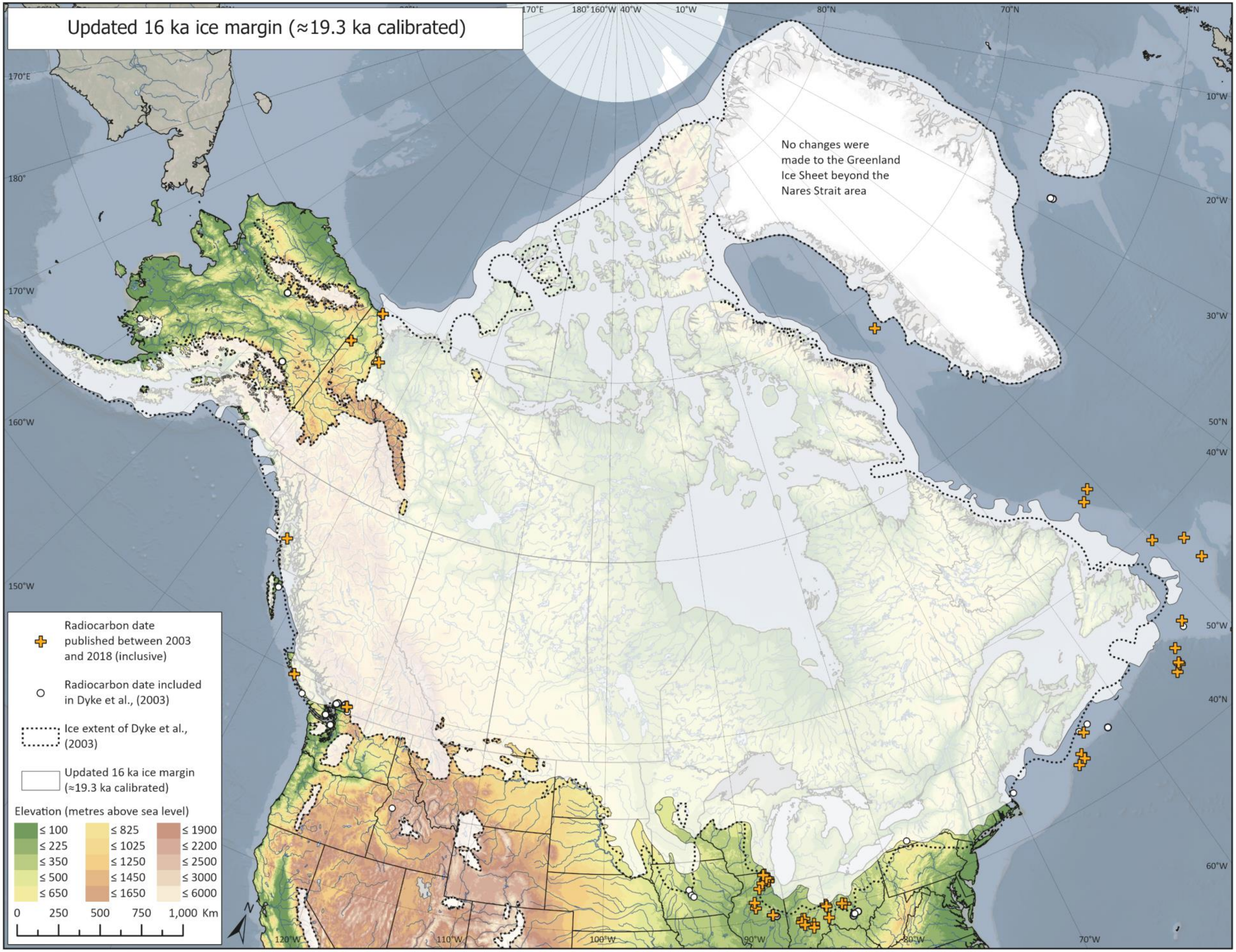
Updated 16 ka ice margin (≈19.3 ka calibrated)
No changes were made to the Greenland Ice Sheet beyond the Nares Strait area
Radiocarbon date published between 2003 and 2018 (inclusive)
Radiocarbon date included in Dyke et al., (2003)
Ice extent of Dyke et al., (2003)
Updated 16 ka ice margin (≈19.3 ka calibrated)
Elevation (metres above sea level)
≤ 100
≤ 225
≤ 350
≤ 500
≤ 650
≤ 825
≤ 1025
≤ 1250
≤ 1450
≤ 1650
≤ 1900
≤ 2200
≤ 2500
≤ 3000
≤ 6000
0 250 500 750 1,000 Km
N
170°E
180° 160°W 40°W
10°W
80°N
70°N
170°E
10°W
180°
20°W
170°W
30°W
160°W
50°N
40°W
150°W
50°W
40°N
60°W
120°W
110°W
100°W
90°W
80°W
70°W

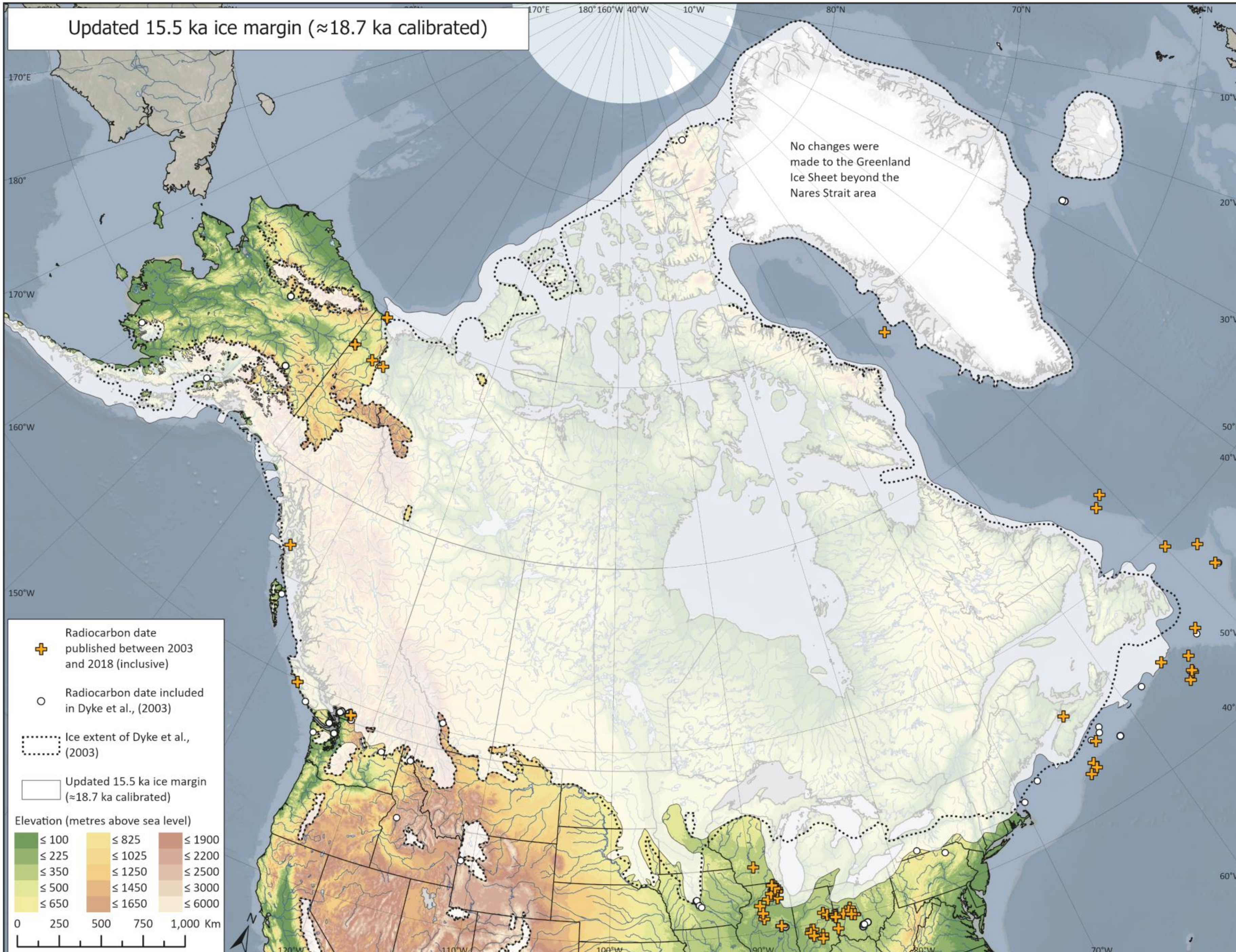

Updated 15.5 ka ice margin (≈18.7 ka calibrated)
No changes were made to the Greenland Ice Sheet beyond the Nares Strait area
Radiocarbon date published between 2003 and 2018 (inclusive)
Radiocarbon date included in Dyke et al., (2003)
Ice extent of Dyke et al., (2003)
Updated 15.5 ka ice margin (≈18.7 ka calibrated)
Elevation (metres above sea level)
≤ 100
≤ 225
≤ 350
≤ 500
≤ 650
≤ 825
≤ 1025
≤ 1250
≤ 1450
≤ 1650
≤ 1900
≤ 2200
≤ 2500
≤ 3000
≤ 6000
0 250 500 750 1,000 Km
N
170°E
180°
170°W
160°W
150°W
120°W
110°W
100°W
90°W
80°W
70°W
60°W
50°N
40°N
40°W
30°W
20°W
10°W
80°N
70°N
180° 160°W 40°W
10°W

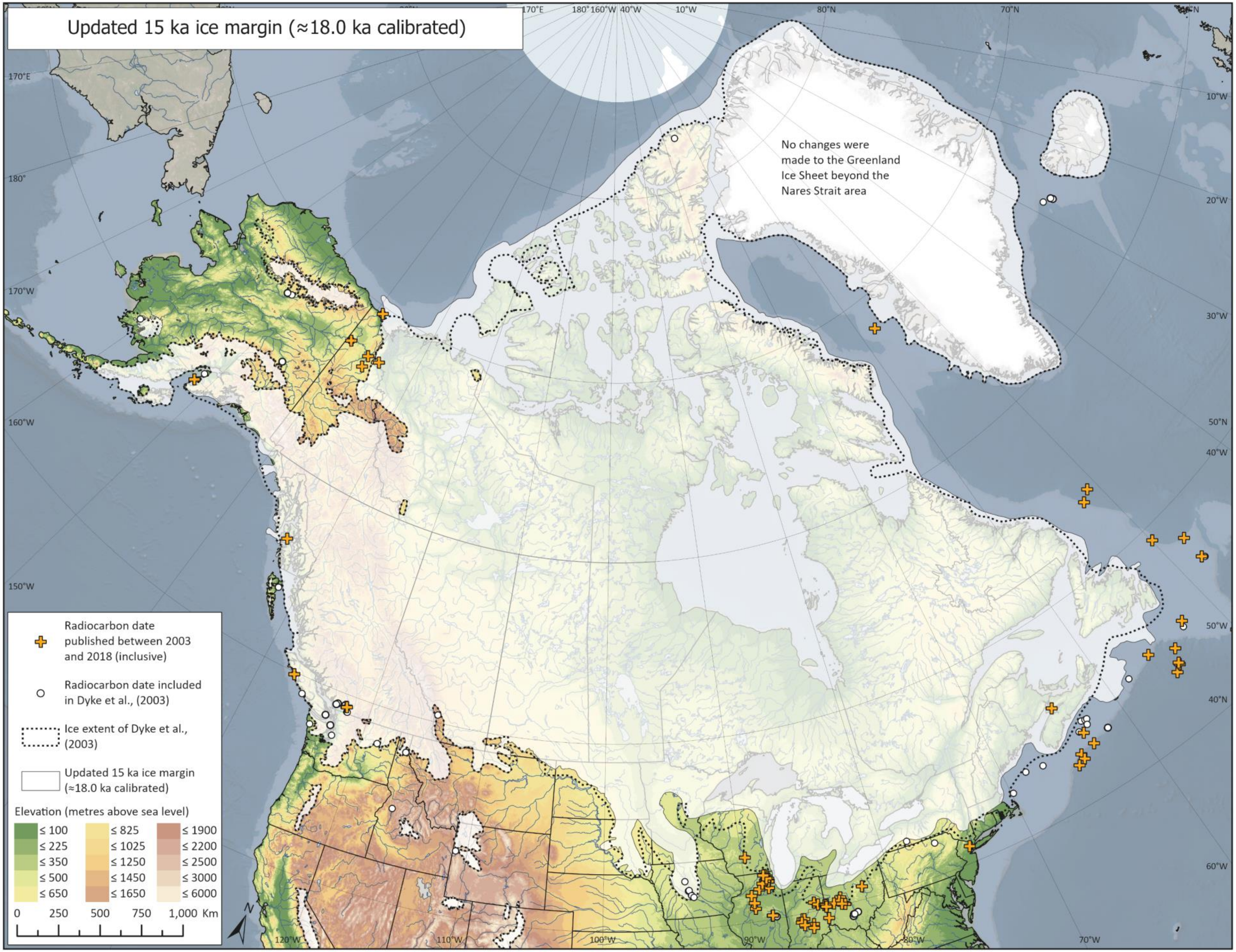
Updated 15 ka ice margin (≈18.0 ka calibrated)
No changes were made to the Greenland Ice Sheet beyond the Nares Strait area
Radiocarbon date published between 2003 and 2018 (inclusive)
Radiocarbon date included in Dyke et al., (2003)
Ice extent of Dyke et al., (2003)
Updated 15 ka ice margin (≈18.0 ka calibrated)
Elevation (metres above sea level)
≤ 100
≤ 225
≤ 350
≤ 500
≤ 650
≤ 825
≤ 1025
≤ 1250
≤ 1450
≤ 1650
≤ 1900
≤ 2200
≤ 2500
≤ 3000
≤ 6000
0 250 500 750 1,000 Km
N
170°E
180°
170°W
160°W
150°W
120°W
110°W
100°W
90°W
80°W
70°W
60°W
50°W
40°N
40°W
50°N
30°W
20°W
10°W
80°N
70°N
180° 160°W 40°W
10°W

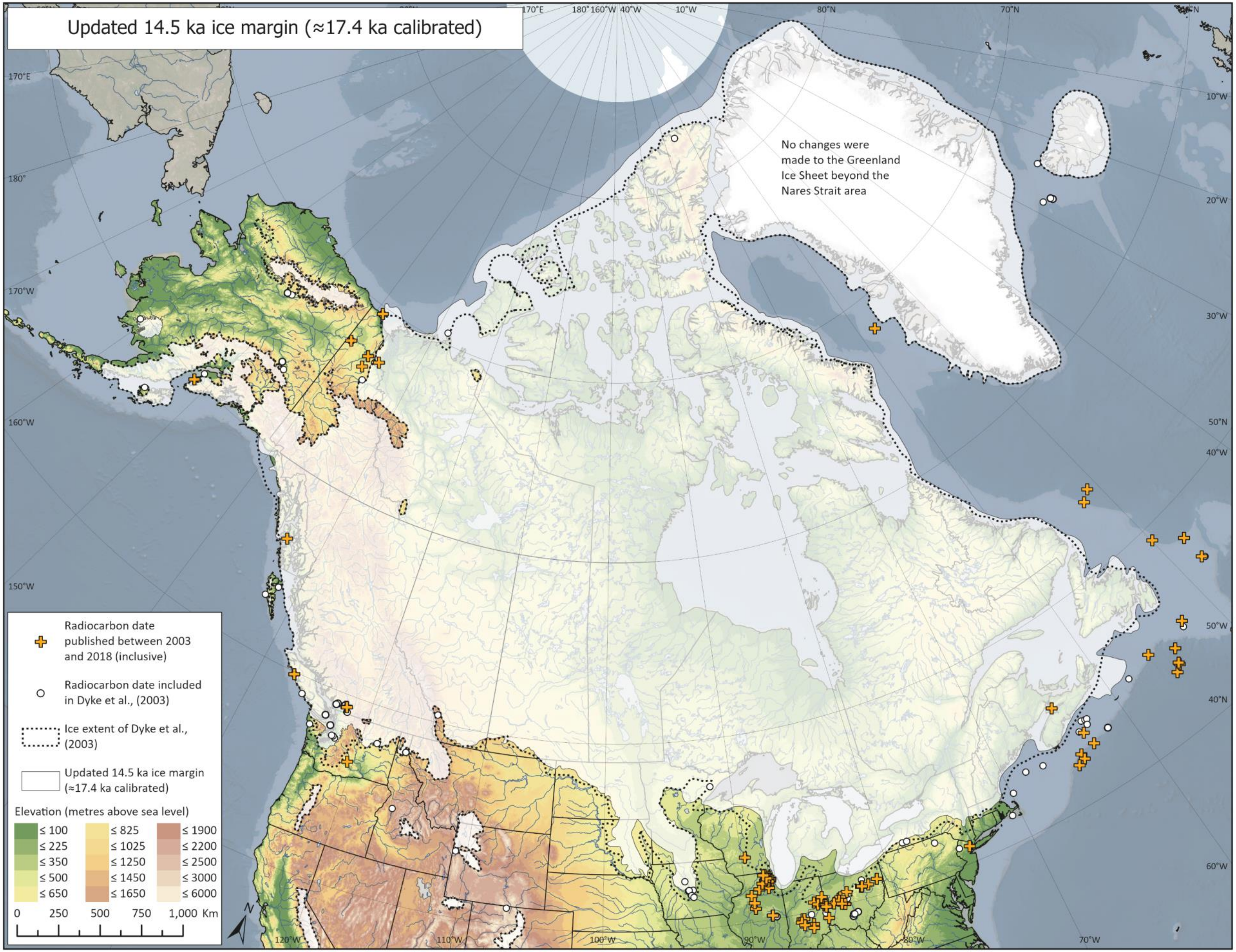
Updated 14.5 ka ice margin (≈17.4 ka calibrated)
No changes were made to the Greenland Ice Sheet beyond the Nares Strait area
Radiocarbon date published between 2003 and 2018 (inclusive)
Radiocarbon date included in Dyke et al., (2003)
Ice extent of Dyke et al., (2003)
Updated 14.5 ka ice margin (≈17.4 ka calibrated)
Elevation (metres above sea level)
≤ 100
≤ 225
≤ 350
≤ 500
≤ 650
≤ 825
≤ 1025
≤ 1250
≤ 1450
≤ 1650
≤ 1900
≤ 2200
≤ 2500
≤ 3000
≤ 6000
0 250 500 750 1,000 Km
N
170°E
180°
170°W
160°W
150°W
120°W
110°W
100°W
90°W
80°W
70°W
60°W
40°N
50°N
10°W
20°W
30°W
40°W
80°N
70°N

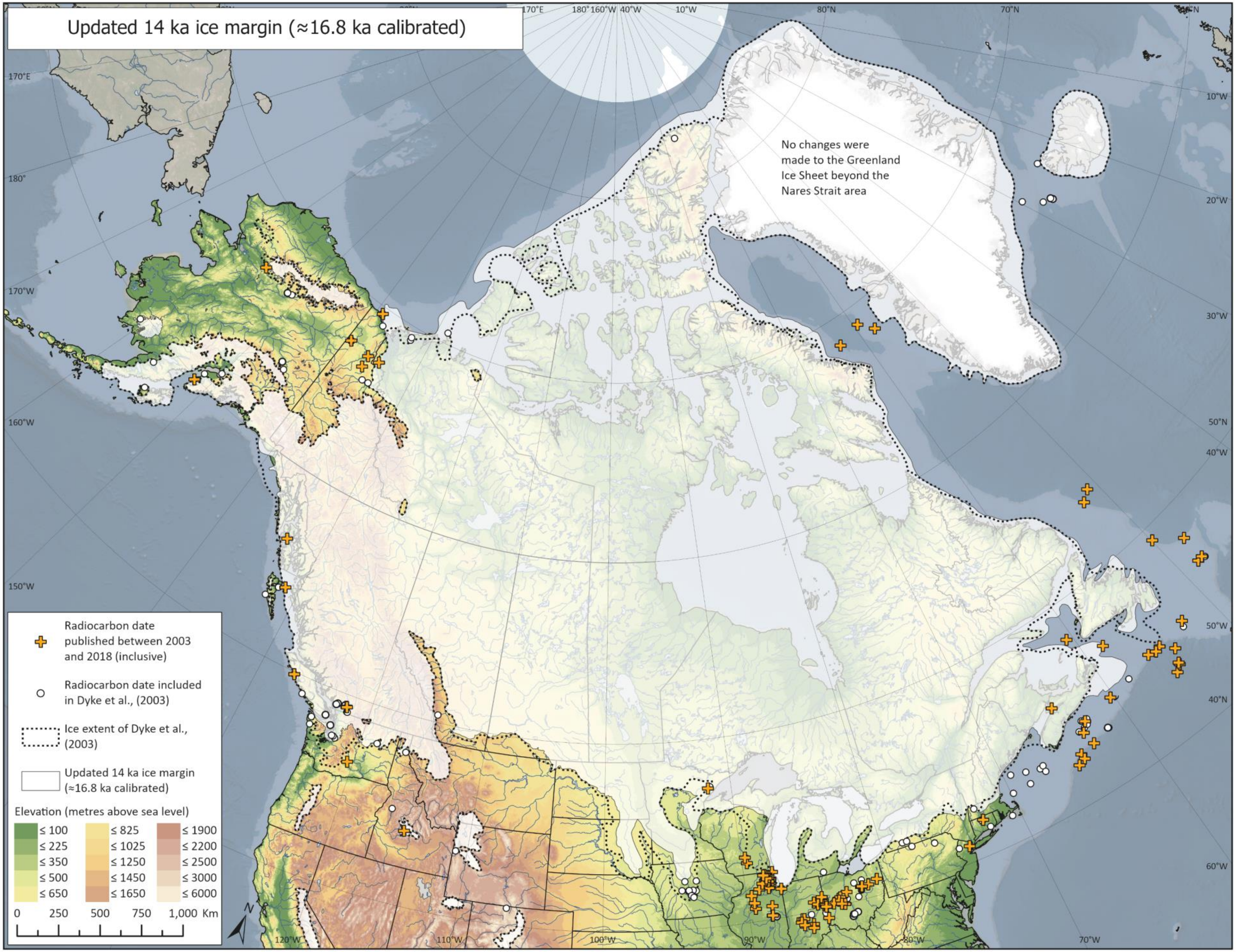

Updated 14 ka ice margin (≈16.8 ka calibrated)
No changes were made to the Greenland Ice Sheet beyond the Nares Strait area
Radiocarbon date published between 2003 and 2018 (inclusive)
Radiocarbon date included in Dyke et al., (2003)
Ice extent of Dyke et al., (2003)
Updated 14 ka ice margin (≈16.8 ka calibrated)
Elevation (metres above sea level)
≤ 100
≤ 225
≤ 350
≤ 500
≤ 650
≤ 825
≤ 1025
≤ 1250
≤ 1450
≤ 1650
≤ 1900
≤ 2200
≤ 2500
≤ 3000
≤ 6000
0 250 500 750 1,000 Km
N
170°E
180°
170°W
160°W
150°W
120°W
110°W
100°W
90°W
80°W
70°W
60°W
50°N
40°N
10°W
20°W
30°W
40°W
80°N
70°N
180° 160°W 40°W

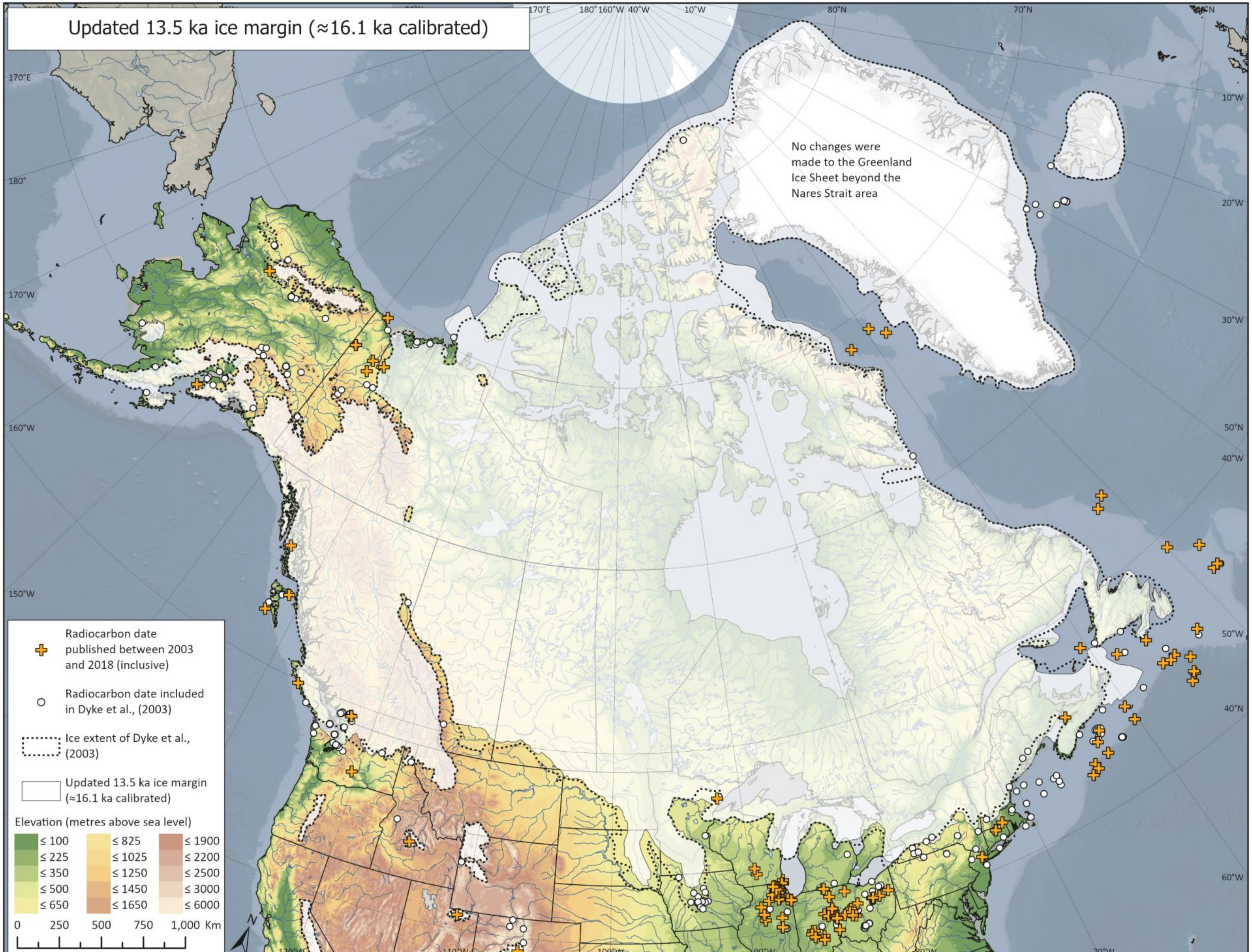

Updated 13.5 ka ice margin (≈16.1 ka calibrated)
No changes were made to the Greenland Ice Sheet beyond the Nares Strait area
Radiocarbon date published between 2003 and 2018 (inclusive)
Radiocarbon date included in Dyke et al., (2003)
Ice extent of Dyke et al., (2003)
Updated 13.5 ka ice margin (≈16.1 ka calibrated)
Elevation (metres above sea level)
≤ 100
≤ 225
≤ 350
≤ 500
≤ 650
≤ 825
≤ 1025
≤ 1250
≤ 1450
≤ 1650
≤ 1900
≤ 2200
≤ 2500
≤ 3000
≤ 6000
0 250 500 750 1,000 Km
N
170°E
180°
170°W
160°W
150°W
120°W
110°W
100°W
90°W
80°W
70°W
60°W
50°W
40°W
30°W
20°W
10°W
80°N
70°N
60°N
50°N
40°N
180° 160°W 40°W
10°W

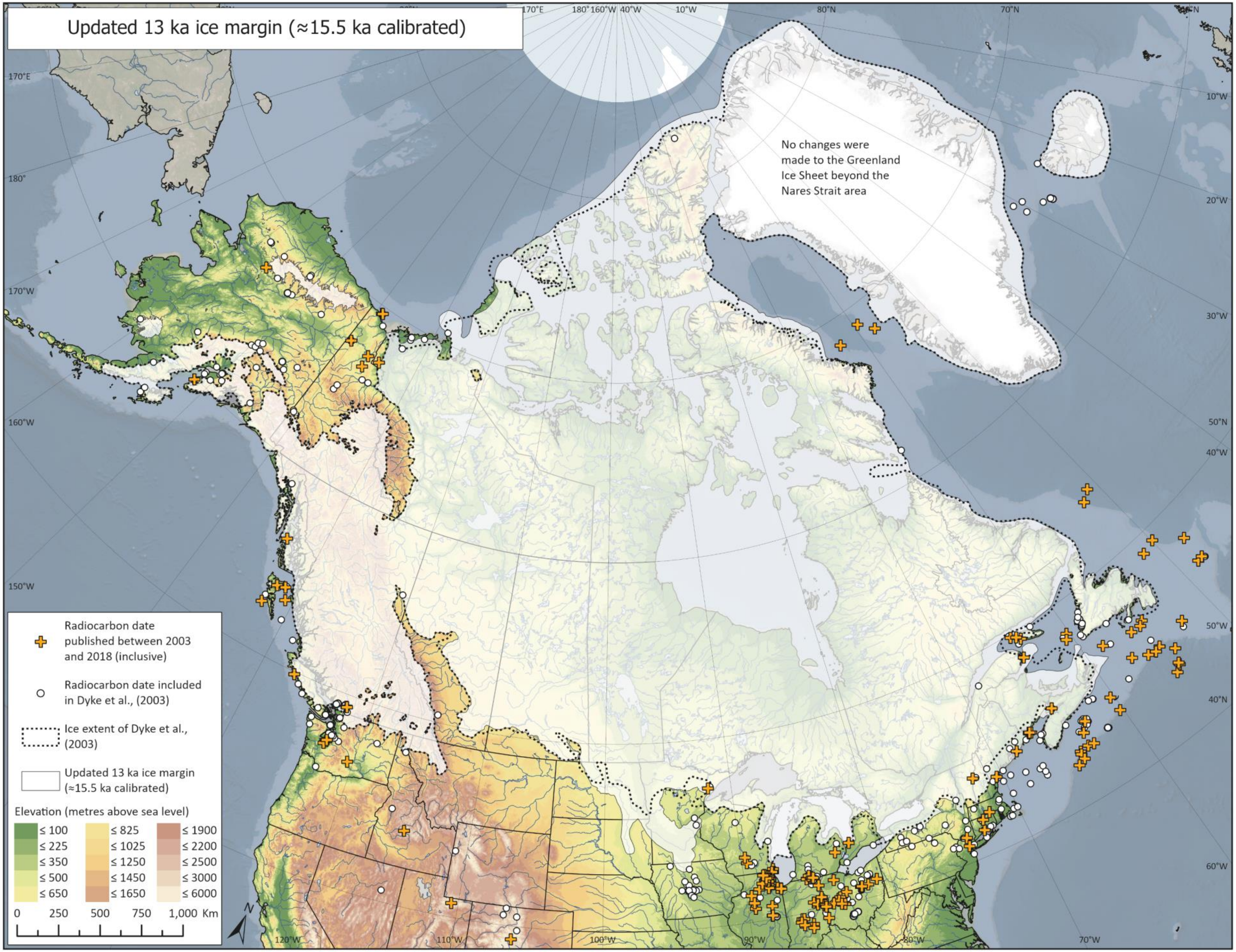
Updated 13 ka ice margin (≈15.5 ka calibrated)
No changes were made to the Greenland Ice Sheet beyond the Nares Strait area
Radiocarbon date published between 2003 and 2018 (inclusive)
Radiocarbon date included in Dyke et al., (2003)
Ice extent of Dyke et al., (2003)
Updated 13 ka ice margin (≈15.5 ka calibrated)
Elevation (metres above sea level)
≤ 100
≤ 225
≤ 350
≤ 500
≤ 650
≤ 825
≤ 1025
≤ 1250
≤ 1450
≤ 1650
≤ 1900
≤ 2200
≤ 2500
≤ 3000
≤ 6000
0 250 500 750 1,000 Km
N
170°E
180°
170°W
160°W
150°W
120°W
110°W
100°W
90°W
80°W
70°W
60°N
50°N
40°N
30°N
20°W
10°W

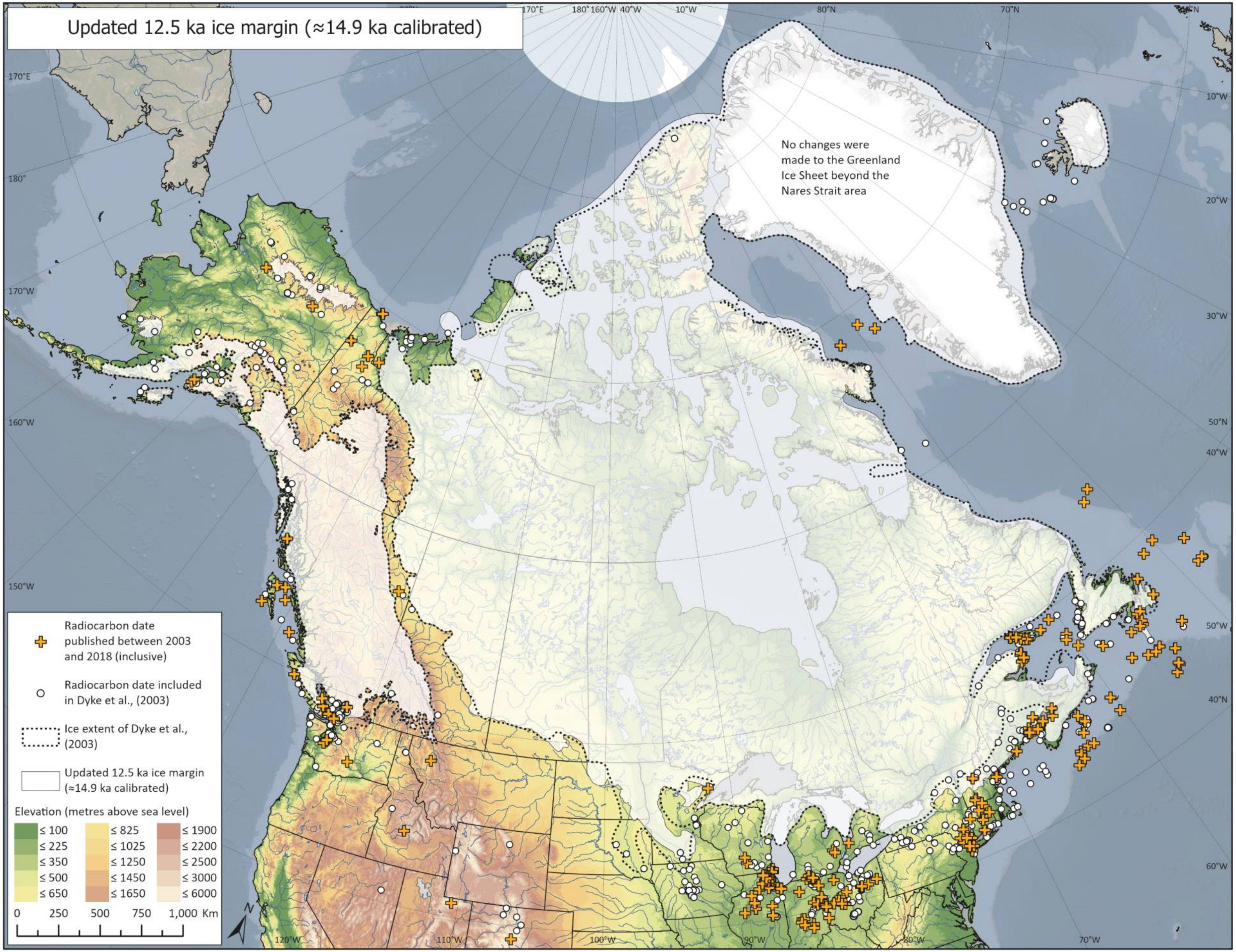

Updated 12.5 ka ice margin (≈14.9 ka calibrated)
No changes were made to the Greenland Ice Sheet beyond the Nares Strait area
Radiocarbon date published between 2003 and 2018 (inclusive)
Radiocarbon date included in Dyke et al., (2003)
Ice extent of Dyke et al., (2003)
Updated 12.5 ka ice margin (≈14.9 ka calibrated)
Elevation (metres above sea level)
≤ 100
≤ 225
≤ 350
≤ 500
≤ 650
≤ 825
≤ 1025
≤ 1250
≤ 1450
≤ 1650
≤ 1900
≤ 2200
≤ 2500
≤ 3000
≤ 6000
0 250 500 750 1,000 Km
N
170°E
180°
170°W
160°W
150°W
120°W
110°W
100°W
90°W
80°W
70°W
60°W
50°N
40°N
10°W
20°W
30°W
40°W
80°N
70°N

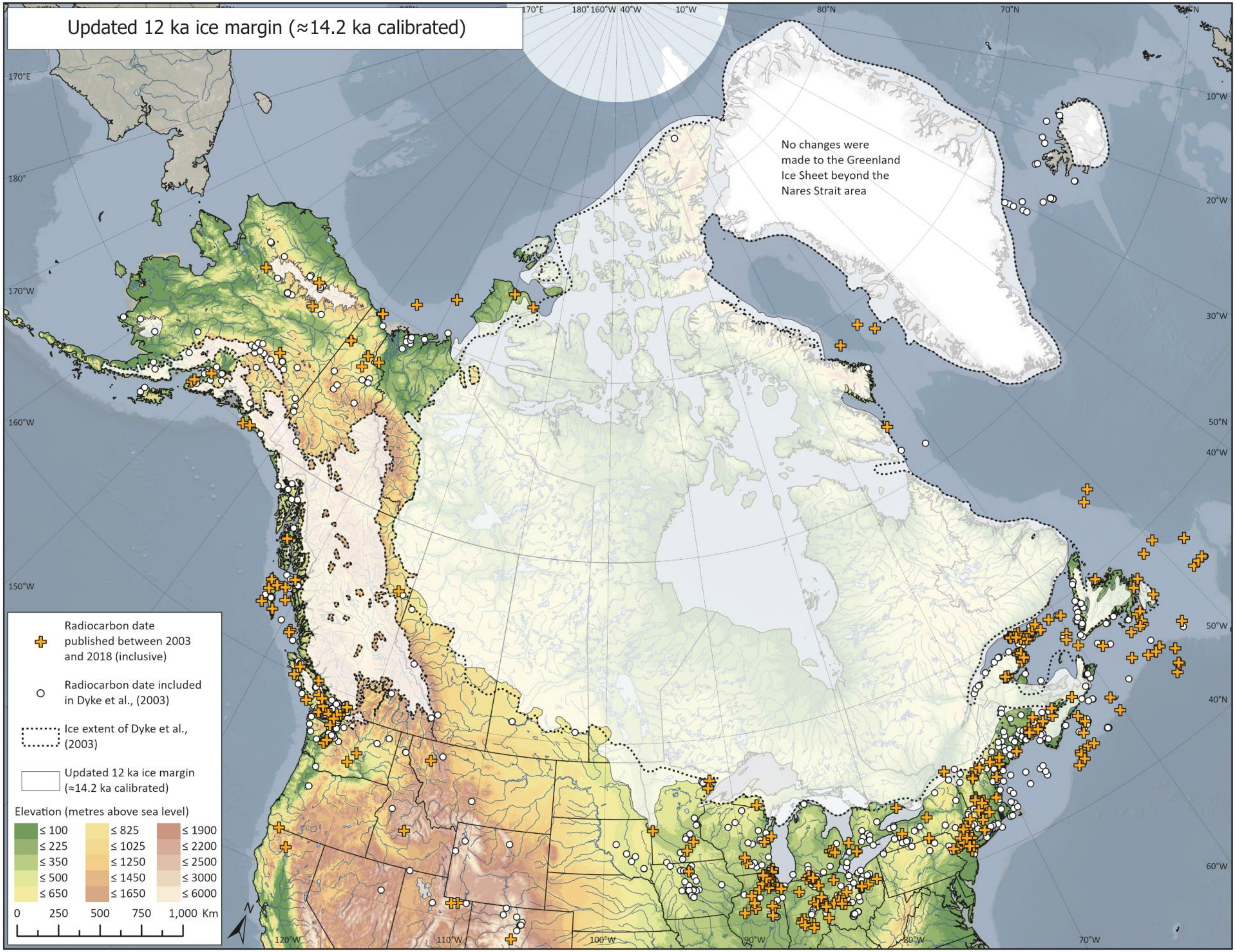
Updated 12 ka ice margin (≈14.2 ka calibrated)
No changes were made to the Greenland Ice Sheet beyond the Nares Strait area
Radiocarbon date published between 2003 and 2018 (inclusive)
Radiocarbon date included in Dyke et al., (2003)
Ice extent of Dyke et al., (2003)
Updated 12 ka ice margin (≈14.2 ka calibrated)
Elevation (metres above sea level)
≤ 100
≤ 225
≤ 350
≤ 500
≤ 650
≤ 825
≤ 1025
≤ 1250
≤ 1450
≤ 1650
≤ 1900
≤ 2200
≤ 2500
≤ 3000
≤ 6000
0 250 500 750 1,000 Km
N
170°E
180°
170°W
160°W
150°W
120°W
110°W
100°W
90°W
80°W
70°W
80°N
70°N
10°W
20°W
30°W
40°W
50°N
40°N
60°N

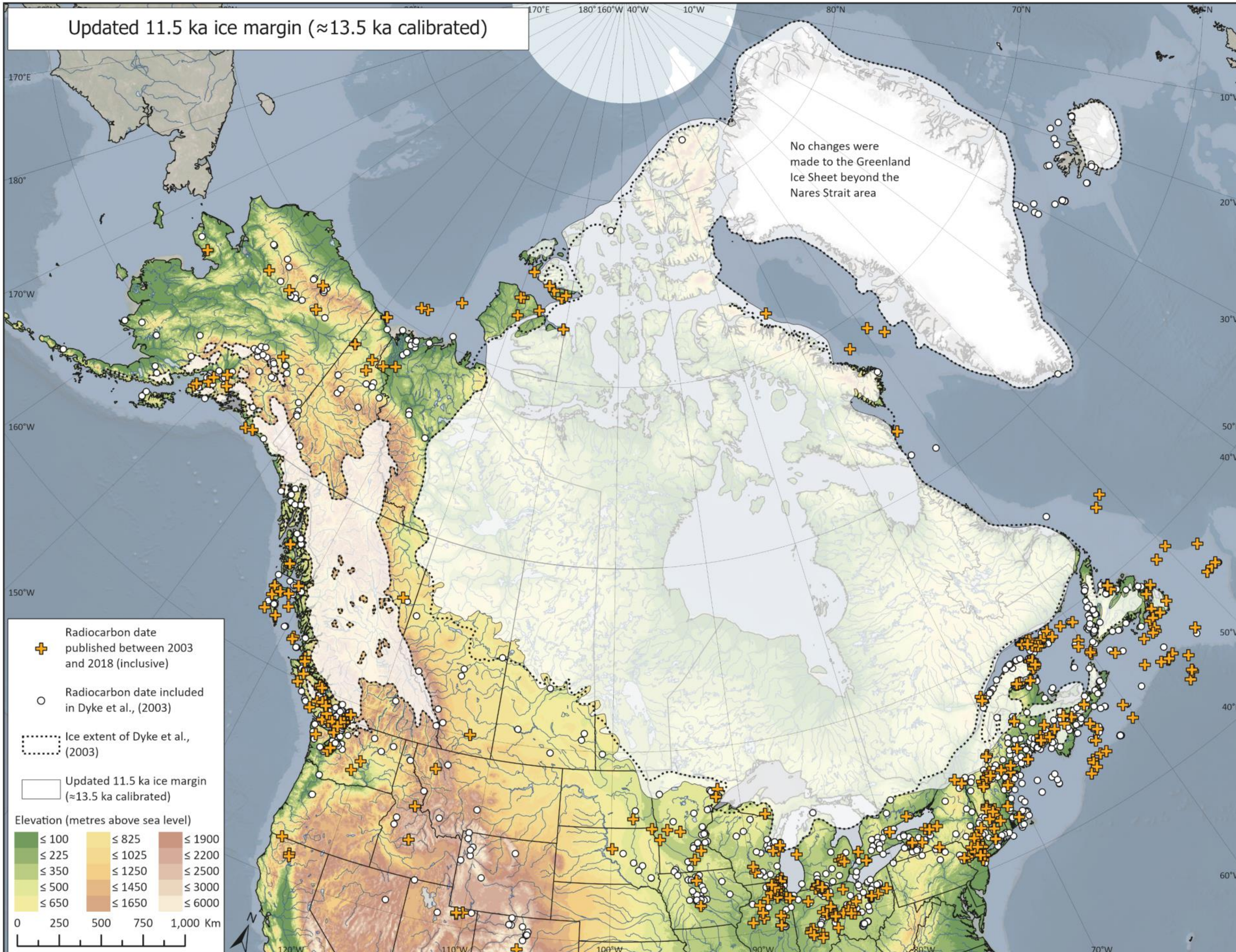

Updated 11.5 ka ice margin (≈13.5 ka calibrated)
No changes were made to the Greenland Ice Sheet beyond the Nares Strait area
Radiocarbon date published between 2003 and 2018 (inclusive)
Radiocarbon date included in Dyke et al., (2003)
Ice extent of Dyke et al., (2003)
Updated 11.5 ka ice margin (≈13.5 ka calibrated)
Elevation (metres above sea level)
≤ 100
≤ 225
≤ 350
≤ 500
≤ 650
≤ 825
≤ 1025
≤ 1250
≤ 1450
≤ 1650
≤ 1900
≤ 2200
≤ 2500
≤ 3000
≤ 6000
0 250 500 750 1,000 Km
N
170°E
180°
170°W
160°W
150°W
120°W
110°W
100°W
90°W
80°W
70°W
60°W
50°N
40°N
30°W
20°W
10°W
80°N
70°N

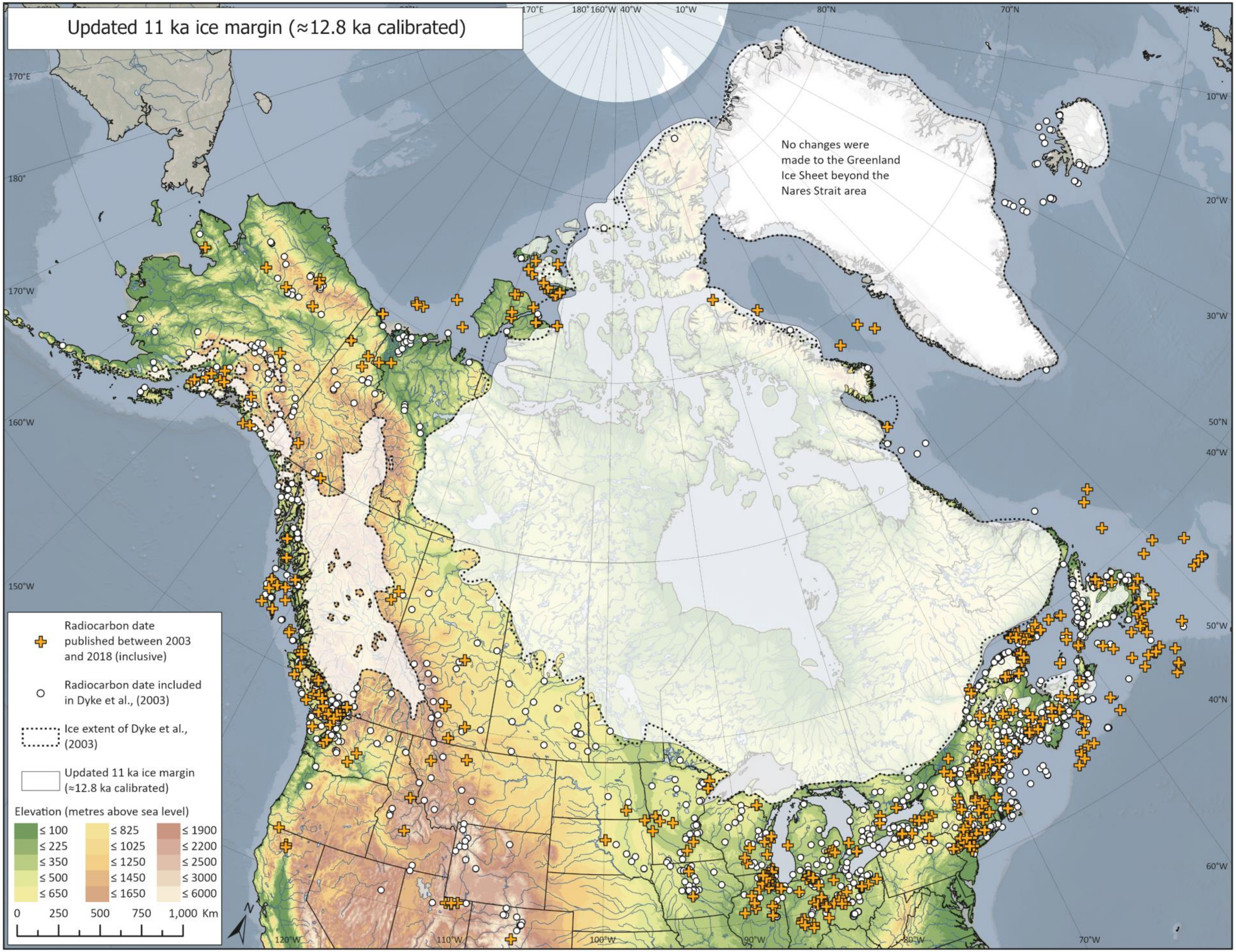

Updated 11 ka ice margin (≈12.8 ka calibrated)
No changes were made to the Greenland Ice Sheet beyond the Nares Strait area
Radiocarbon date published between 2003 and 2018 (inclusive)
Radiocarbon date included in Dyke et al., (2003)
Ice extent of Dyke et al., (2003)
Updated 11 ka ice margin (≈12.8 ka calibrated)
Elevation (metres above sea level)
≤ 100
≤ 225
≤ 350
≤ 500
≤ 650
≤ 825
≤ 1025
≤ 1250
≤ 1450
≤ 1650
≤ 1900
≤ 2200
≤ 2500
≤ 3000
≤ 6000
0 250 500 750 1,000 Km
N

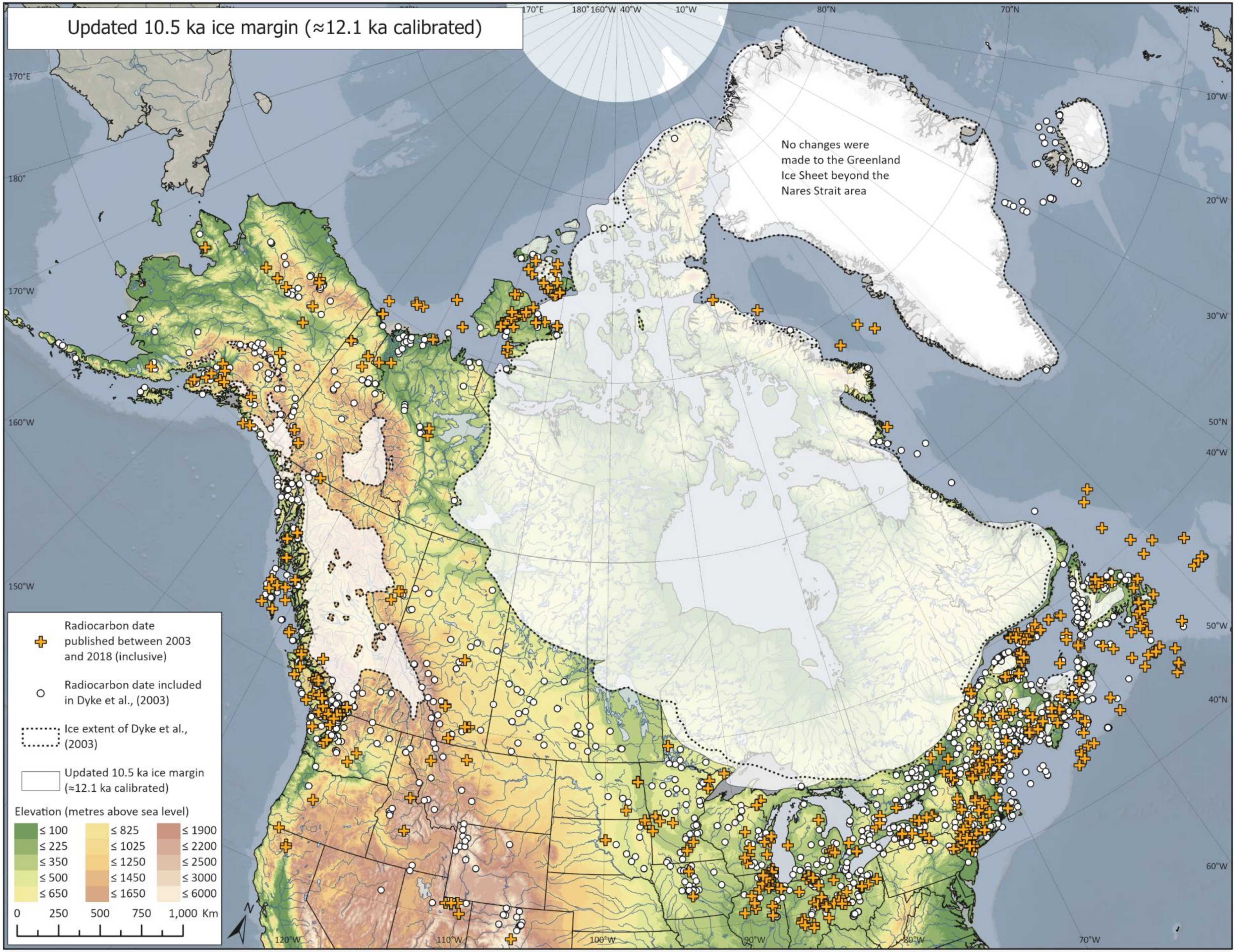

Updated 10.5 ka ice margin (≈12.1 ka calibrated)
No changes were made to the Greenland Ice Sheet beyond the Nares Strait area
Radiocarbon date published between 2003 and 2018 (inclusive)
Radiocarbon date included in Dyke et al., (2003)
Ice extent of Dyke et al., (2003)
Updated 10.5 ka ice margin (≈12.1 ka calibrated)
Elevation (metres above sea level)
≤ 100
≤ 225
≤ 350
≤ 500
≤ 650
≤ 825
≤ 1025
≤ 1250
≤ 1450
≤ 1650
≤ 1900
≤ 2200
≤ 2500
≤ 3000
≤ 6000
0 250 500 750 1,000 Km
N

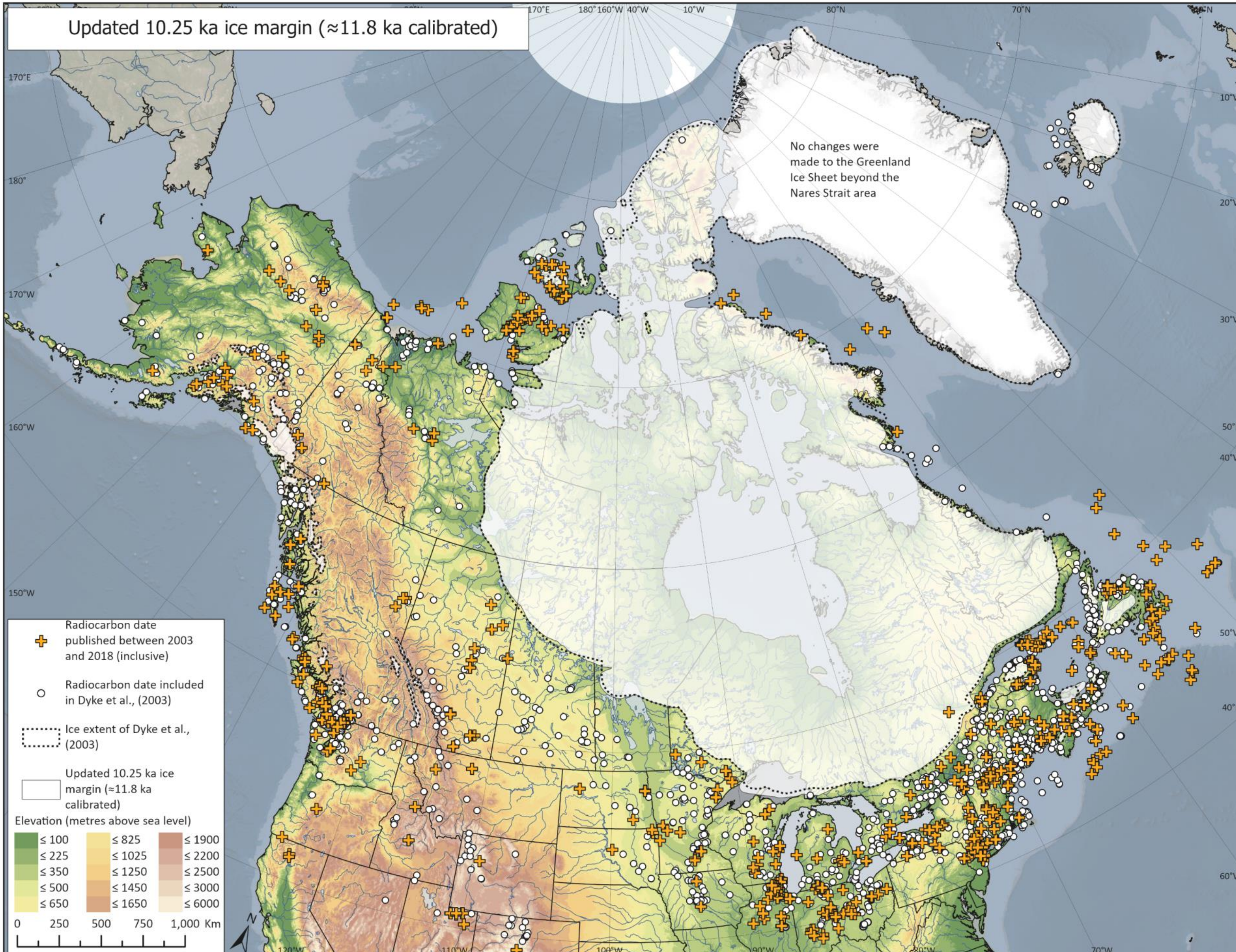

Updated 10.25 ka ice margin (≈11.8 ka calibrated)
No changes were made to the Greenland Ice Sheet beyond the Nares Strait area
Radiocarbon date published between 2003 and 2018 (inclusive)
Radiocarbon date included in Dyke et al., (2003)
Ice extent of Dyke et al., (2003)
Updated 10.25 ka ice margin (≈11.8 ka calibrated)
Elevation (metres above sea level)
≤ 100
≤ 225
≤ 350
≤ 500
≤ 650
≤ 825
≤ 1025
≤ 1250
≤ 1450
≤ 1650
≤ 1900
≤ 2200
≤ 2500
≤ 3000
≤ 6000
0 250 500 750 1,000 Km
N

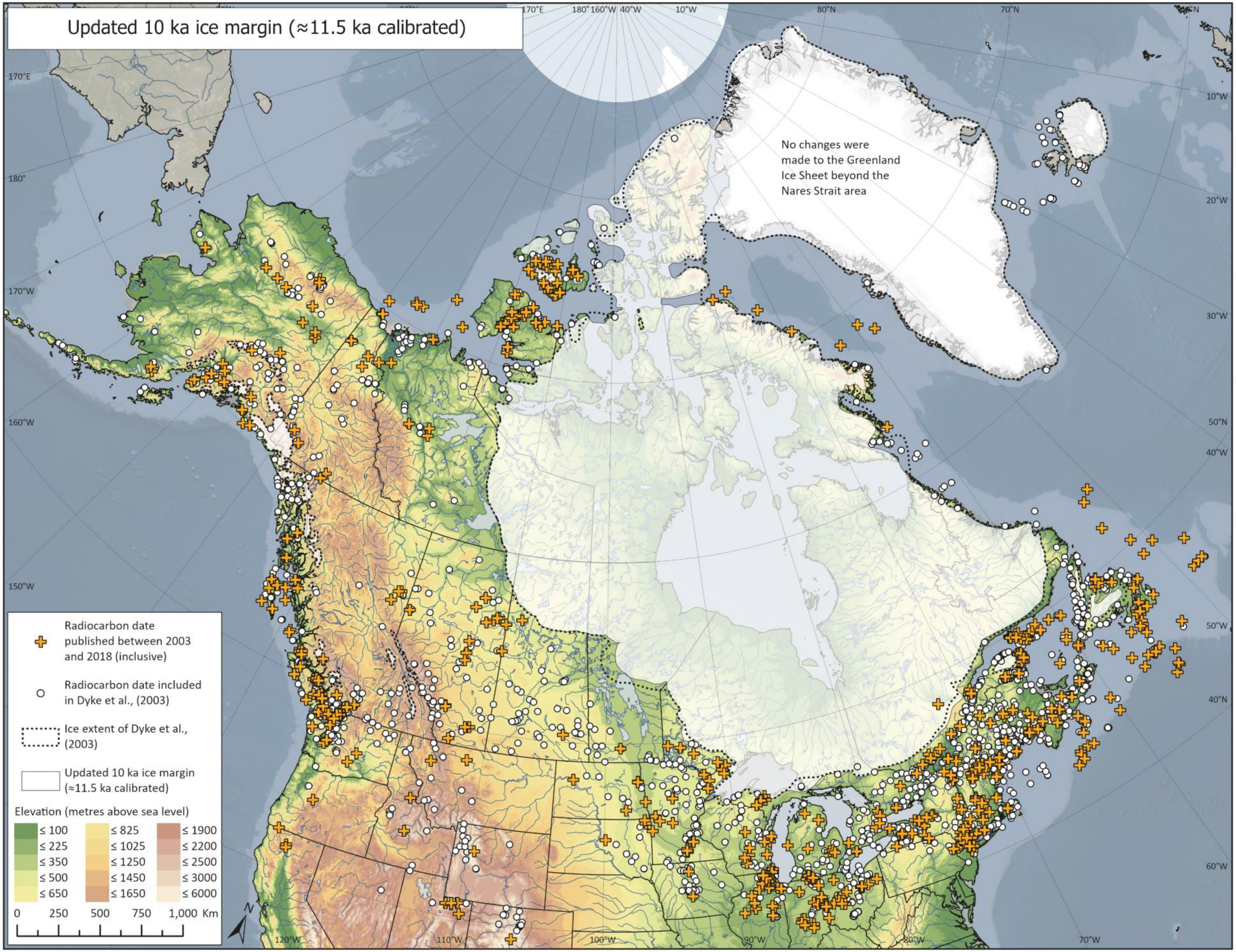

Updated 10 ka ice margin (≈11.5 ka calibrated)
No changes were made to the Greenland Ice Sheet beyond the Nares Strait area
Radiocarbon date published between 2003 and 2018 (inclusive)
Radiocarbon date included in Dyke et al., (2003)
Ice extent of Dyke et al., (2003)
Updated 10 ka ice margin (≈11.5 ka calibrated)
Elevation (metres above sea level)
≤ 100
≤ 225
≤ 350
≤ 500
≤ 650
≤ 825
≤ 1025
≤ 1250
≤ 1450
≤ 1650
≤ 1900
≤ 2200
≤ 2500
≤ 3000
≤ 6000
0 250 500 750 1,000 Km
N
170°E
180°
170°W
160°W
150°W
120°W
110°W
100°W
90°W
80°W
70°W
80°N
70°N
10°W
20°W
30°W
40°W
50°W
60°W
50°N
40°N
180° 160°W 40°W
10°W

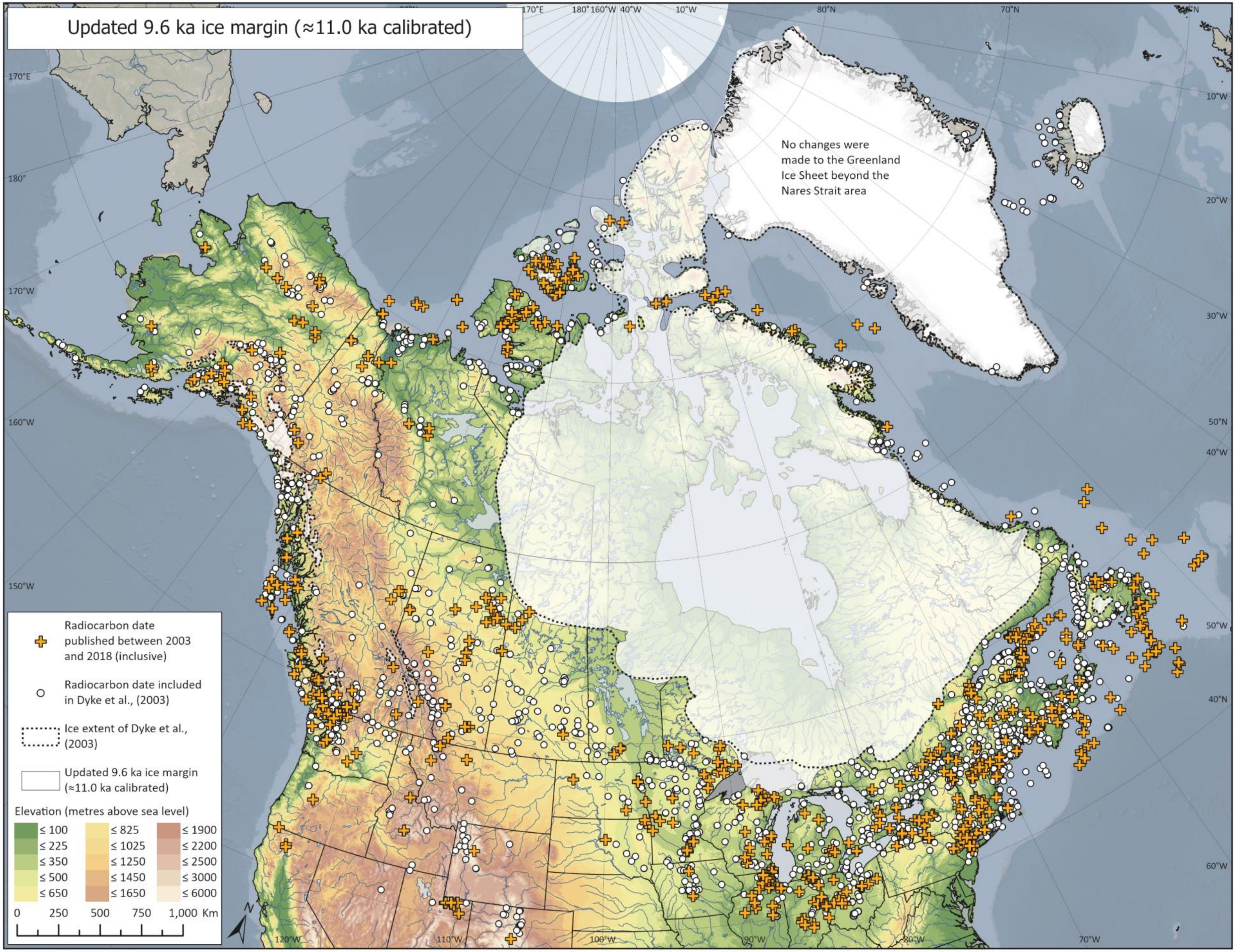

Updated 9.6 ka ice margin (≈11.0 ka calibrated)
No changes were made to the Greenland Ice Sheet beyond the Nares Strait area
Radiocarbon date published between 2003 and 2018 (inclusive)
Radiocarbon date included in Dyke et al., (2003)
Ice extent of Dyke et al., (2003)
Updated 9.6 ka ice margin (≈11.0 ka calibrated)
Elevation (metres above sea level)
≤ 100
≤ 225
≤ 350
≤ 500
≤ 650
≤ 825
≤ 1025
≤ 1250
≤ 1450
≤ 1650
≤ 1900
≤ 2200
≤ 2500
≤ 3000
≤ 6000
0 250 500 750 1,000 Km
N

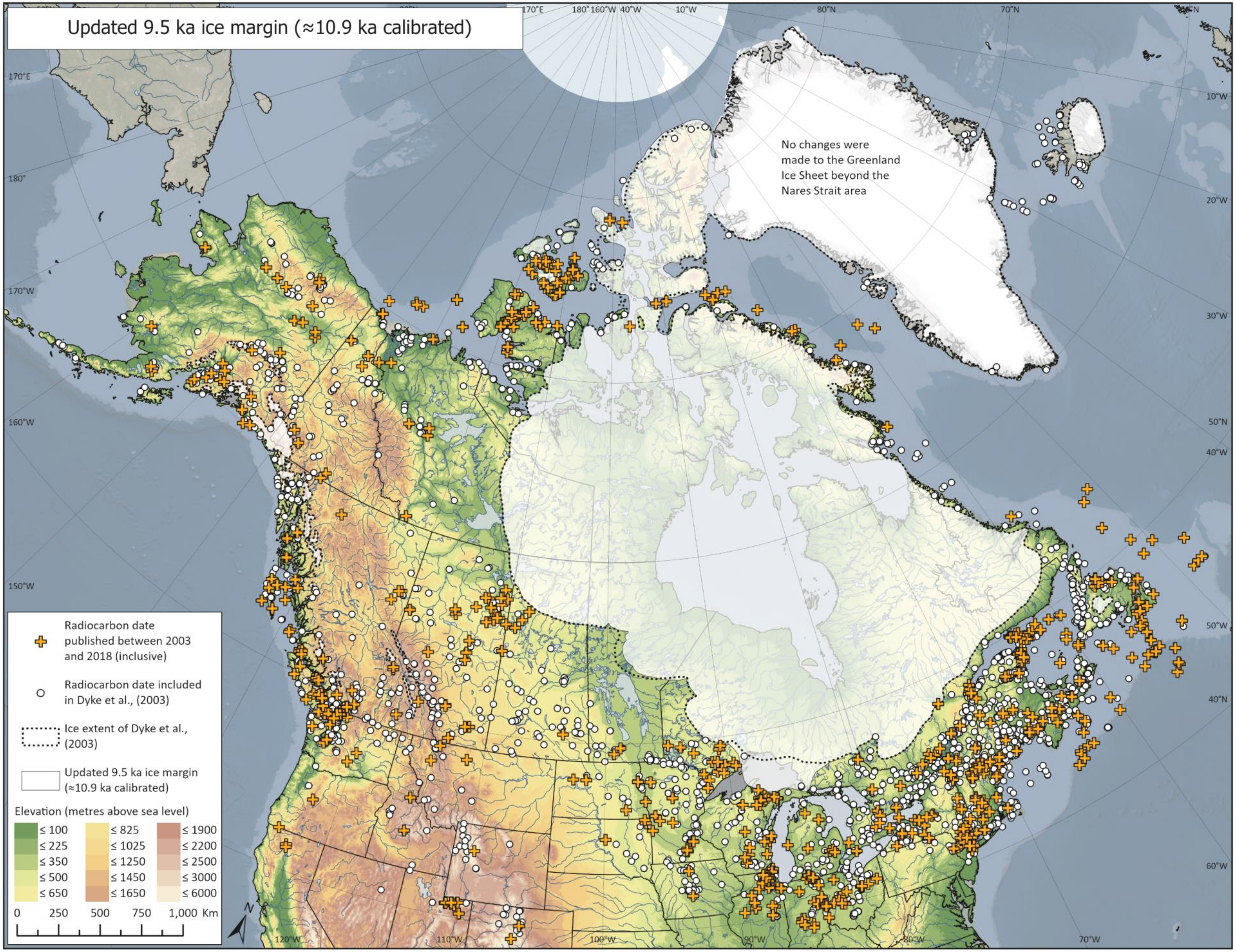

Updated 9.5 ka ice margin (≈10.9 ka calibrated)
No changes were made to the Greenland Ice Sheet beyond the Nares Strait area
Radiocarbon date published between 2003 and 2018 (inclusive)
Radiocarbon date included in Dyke et al., (2003)
Ice extent of Dyke et al., (2003)
Updated 9.5 ka ice margin (≈10.9 ka calibrated)
Elevation (metres above sea level)
≤ 100
≤ 225
≤ 350
≤ 500
≤ 650
≤ 825
≤ 1025
≤ 1250
≤ 1450
≤ 1650
≤ 1900
≤ 2200
≤ 2500
≤ 3000
≤ 6000
0 250 500 750 1,000 Km
N
170°E
180°
170°W
160°W
150°W
120°W
110°W
100°W
90°W
80°W
70°W
10°W
20°W
30°W
40°W
50°W
60°W
50°N
40°N
80°N
70°N

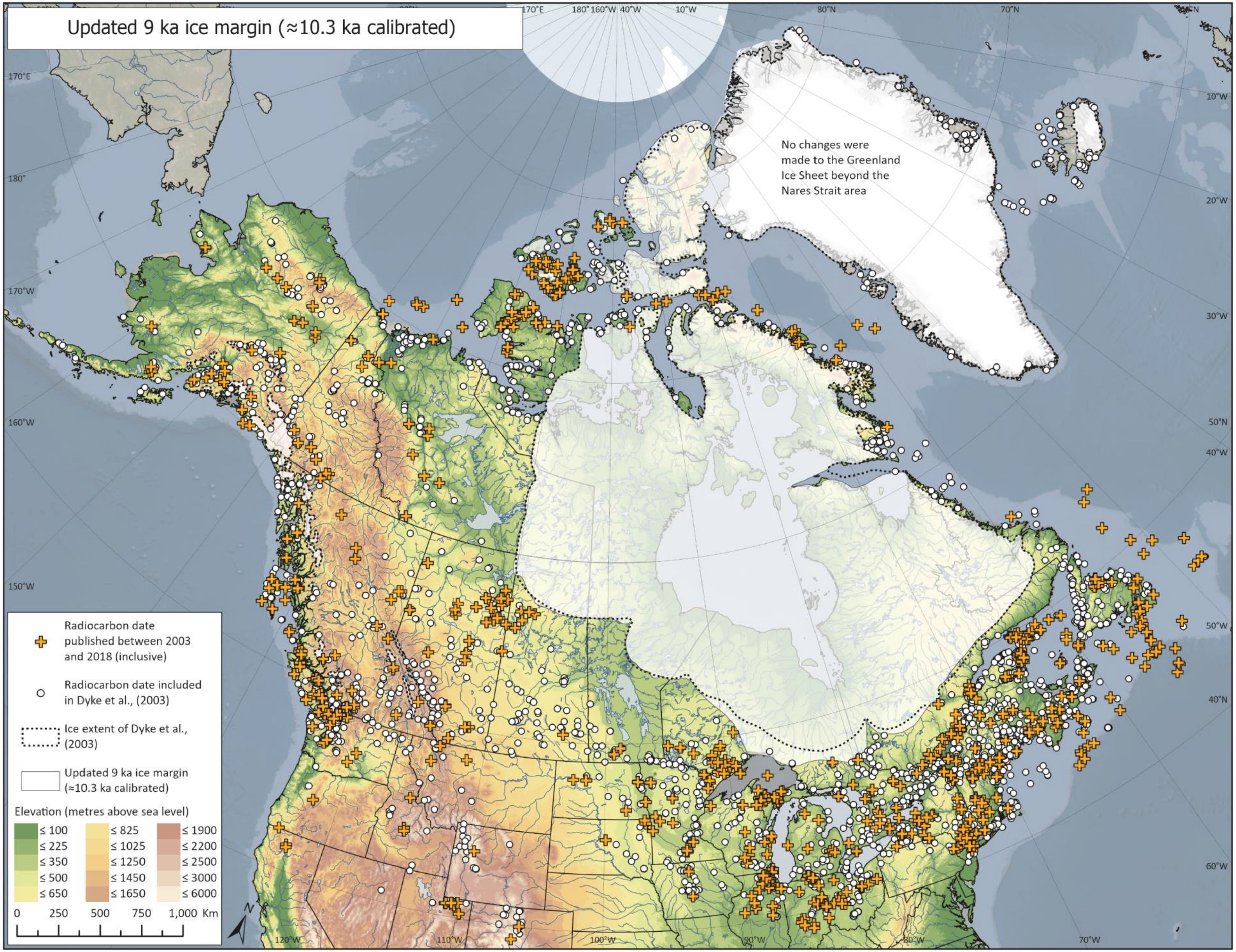

Updated 9 ka ice margin (≈10.3 ka calibrated)
No changes were made to the Greenland Ice Sheet beyond the Nares Strait area
Radiocarbon date published between 2003 and 2018 (inclusive)
Radiocarbon date included in Dyke et al., (2003)
Ice extent of Dyke et al., (2003)
Updated 9 ka ice margin (≈10.3 ka calibrated)
Elevation (metres above sea level)
≤ 100
≤ 225
≤ 350
≤ 500
≤ 650
≤ 825
≤ 1025
≤ 1250
≤ 1450
≤ 1650
≤ 1900
≤ 2200
≤ 2500
≤ 3000
≤ 6000
0 250 500 750 1,000 Km
N
170°E
180°
170°W
160°W
150°W
120°W
110°W
100°W
90°W
80°W
70°W
10°W
20°W
30°W
40°W
50°W
60°W
40°N
50°N
60°N
70°N
80°N

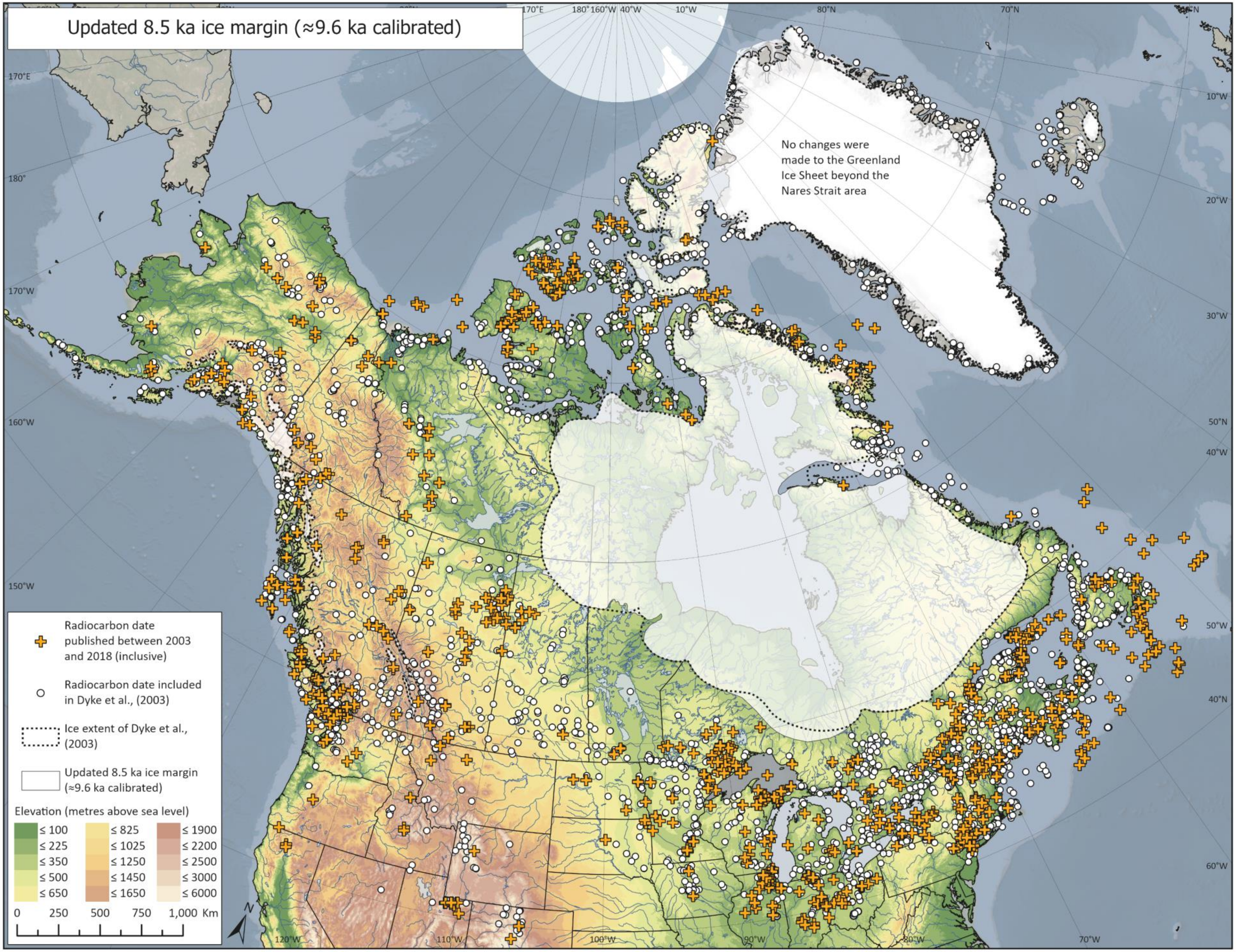

Updated 8.5 ka ice margin (≈9.6 ka calibrated)
No changes were made to the Greenland Ice Sheet beyond the Nares Strait area
Radiocarbon date published between 2003 and 2018 (inclusive)
Radiocarbon date included in Dyke et al., (2003)
Ice extent of Dyke et al., (2003)
Updated 8.5 ka ice margin (≈9.6 ka calibrated)
Elevation (metres above sea level)
≤ 100
≤ 225
≤ 350
≤ 500
≤ 650
≤ 825
≤ 1025
≤ 1250
≤ 1450
≤ 1650
≤ 1900
≤ 2200
≤ 2500
≤ 3000
≤ 6000
0 250 500 750 1,000 Km
N
170°E
180°
170°W
160°W
150°W
120°W
110°W
100°W
90°W
80°W
70°W
80°N
70°N
10°W
20°W
30°W
40°W
50°N
50°W
40°N
60°W

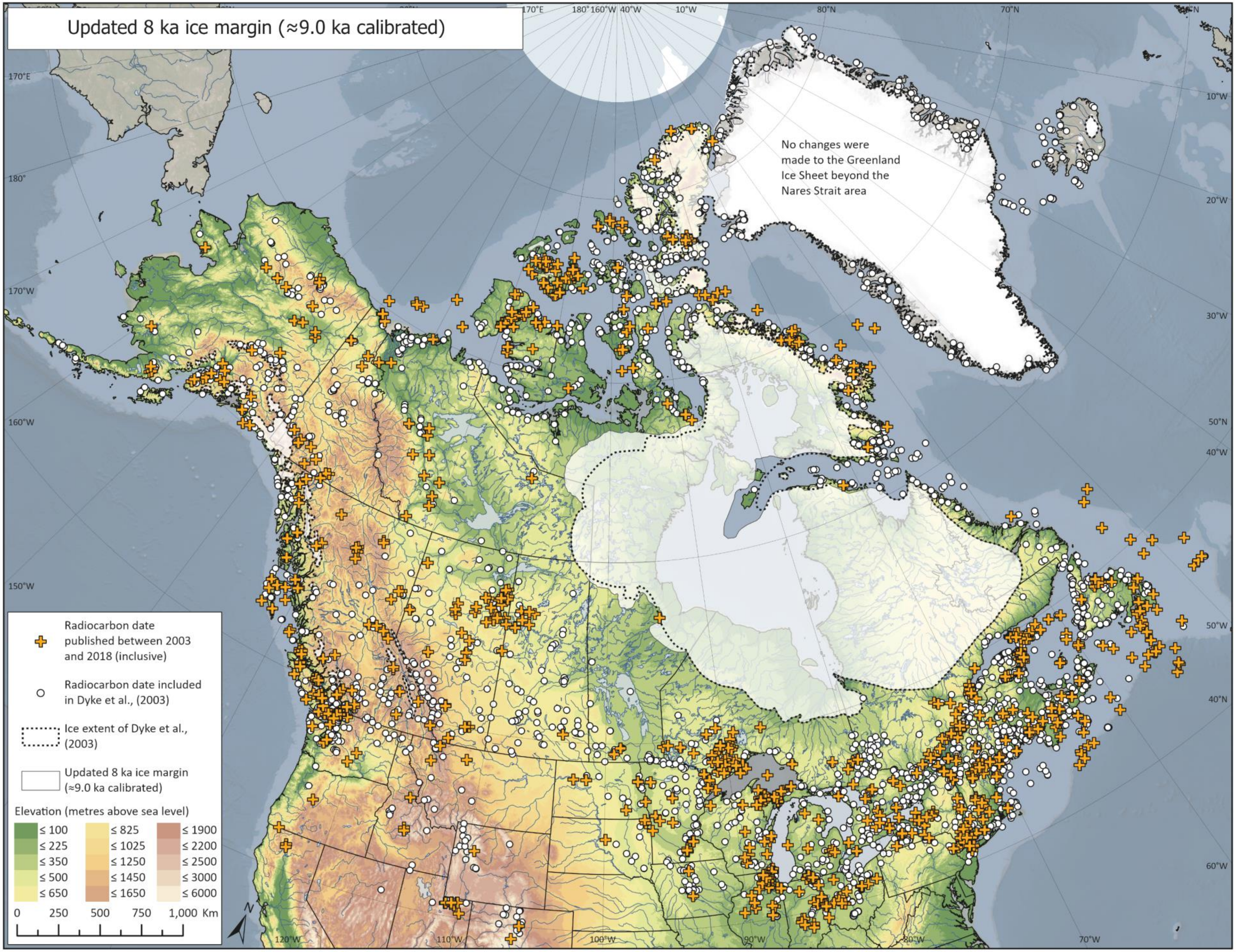

Updated 8 ka ice margin (≈9.0 ka calibrated)
No changes were made to the Greenland Ice Sheet beyond the Nares Strait area
Radiocarbon date published between 2003 and 2018 (inclusive)
Radiocarbon date included in Dyke et al., (2003)
Ice extent of Dyke et al., (2003)
Updated 8 ka ice margin (≈9.0 ka calibrated)
Elevation (metres above sea level)
≤ 100
≤ 225
≤ 350
≤ 500
≤ 650
≤ 825
≤ 1025
≤ 1250
≤ 1450
≤ 1650
≤ 1900
≤ 2200
≤ 2500
≤ 3000
≤ 6000
0 250 500 750 1,000 Km
N

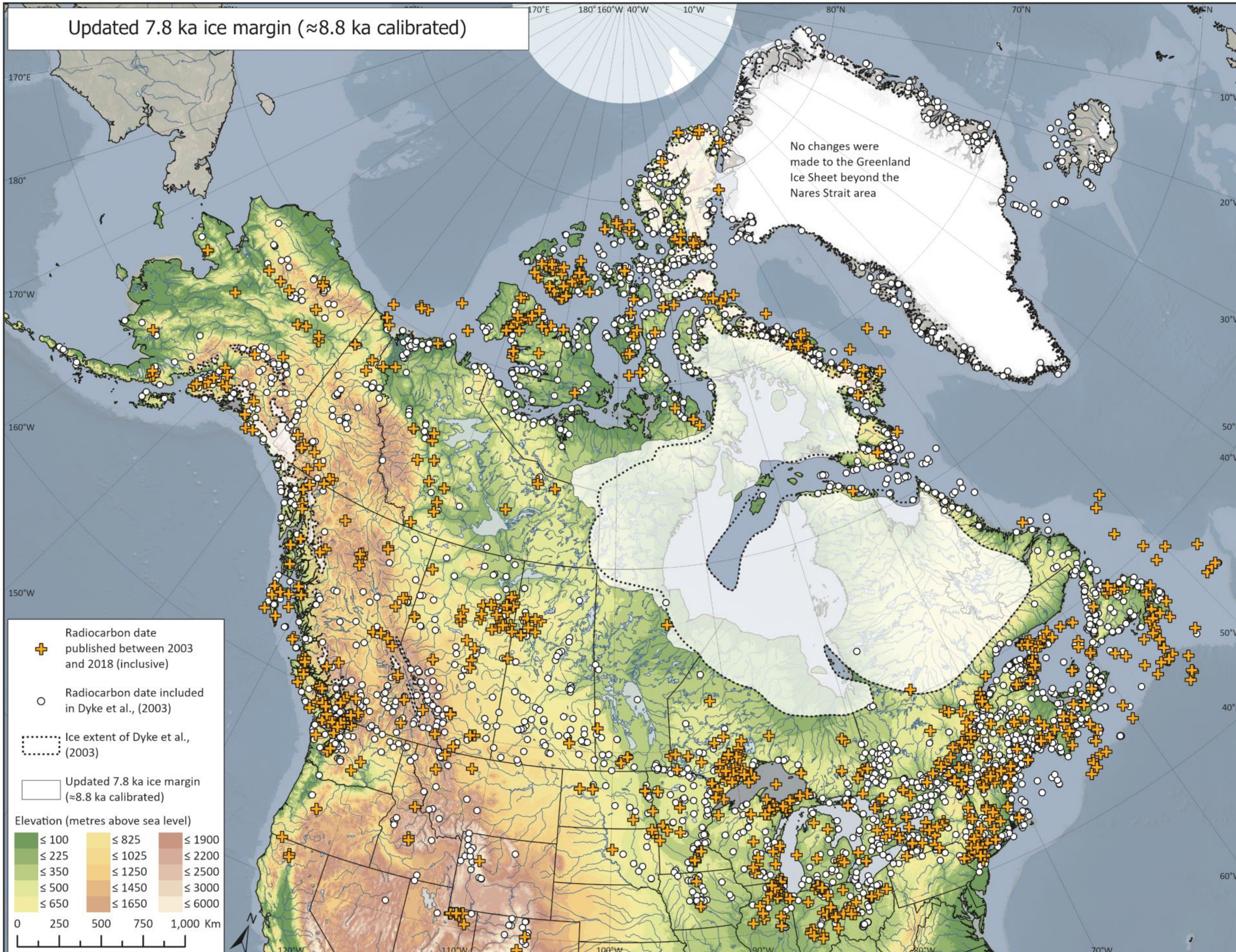

Updated 7.8 ka ice margin (≈8.8 ka calibrated)
No changes were made to the Greenland Ice Sheet beyond the Nares Strait area
Radiocarbon date published between 2003 and 2018 (inclusive)
Radiocarbon date included in Dyke et al., (2003)
Ice extent of Dyke et al., (2003)
Updated 7.8 ka ice margin (≈8.8 ka calibrated)
Elevation (metres above sea level)
≤ 100
≤ 225
≤ 350
≤ 500
≤ 650
≤ 825
≤ 1025
≤ 1250
≤ 1450
≤ 1650
≤ 1900
≤ 2200
≤ 2500
≤ 3000
≤ 6000
0 250 500 750 1,000 Km
N
170°E
180°
170°W
160°W
150°W
120°W
110°W
100°W
90°W
80°W
70°W
60°W
10°W
20°W
30°W
40°W
50°N
50°W
40°N
80°N
70°N

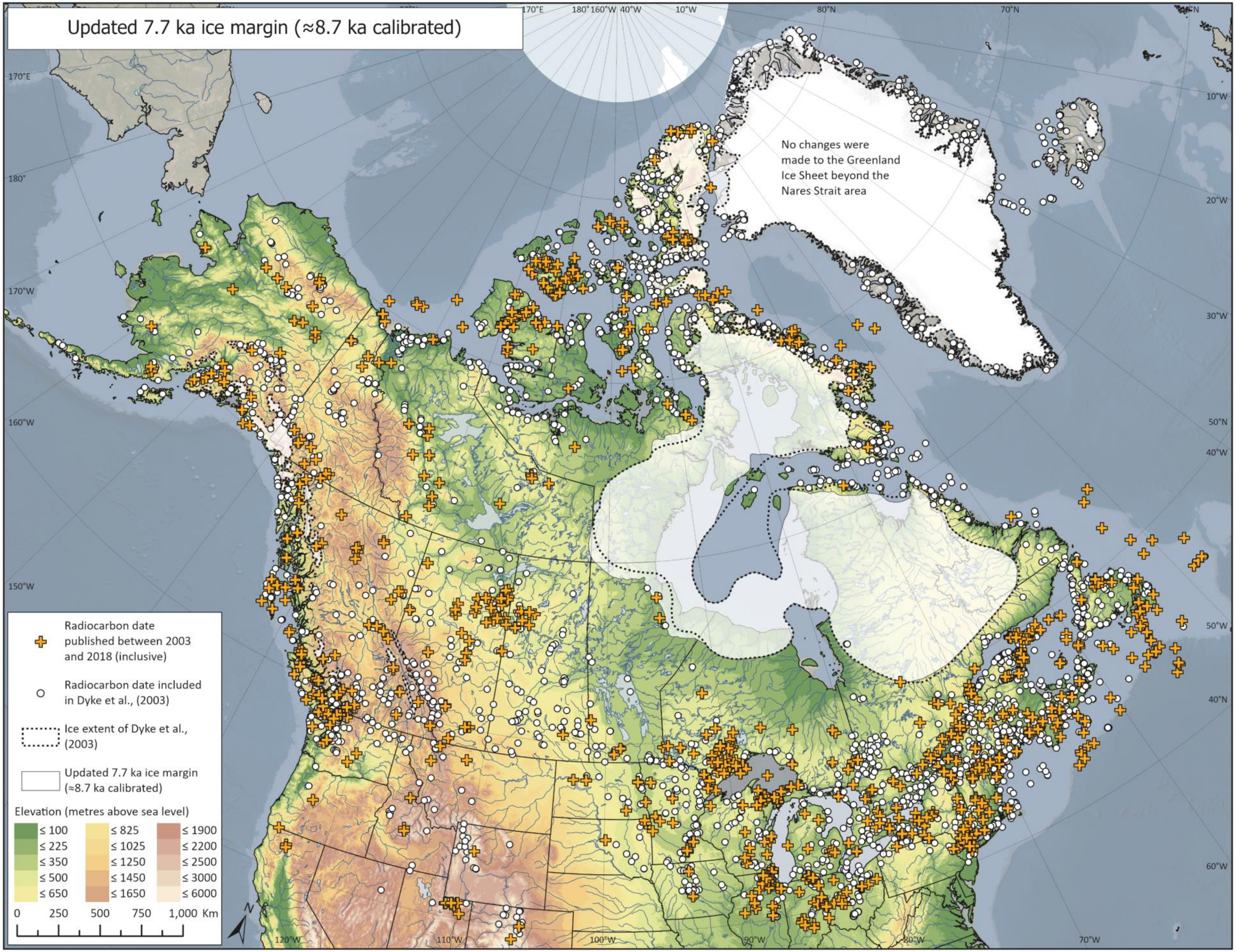

Updated 7.7 ka ice margin (≈8.7 ka calibrated)
No changes were made to the Greenland Ice Sheet beyond the Nares Strait area
Radiocarbon date published between 2003 and 2018 (inclusive)
Radiocarbon date included in Dyke et al., (2003)
Ice extent of Dyke et al., (2003)
Updated 7.7 ka ice margin (≈8.7 ka calibrated)
Elevation (metres above sea level)
≤ 100
≤ 225
≤ 350
≤ 500
≤ 650
≤ 825
≤ 1025
≤ 1250
≤ 1450
≤ 1650
≤ 1900
≤ 2200
≤ 2500
≤ 3000
≤ 6000
0 250 500 750 1,000 Km
N

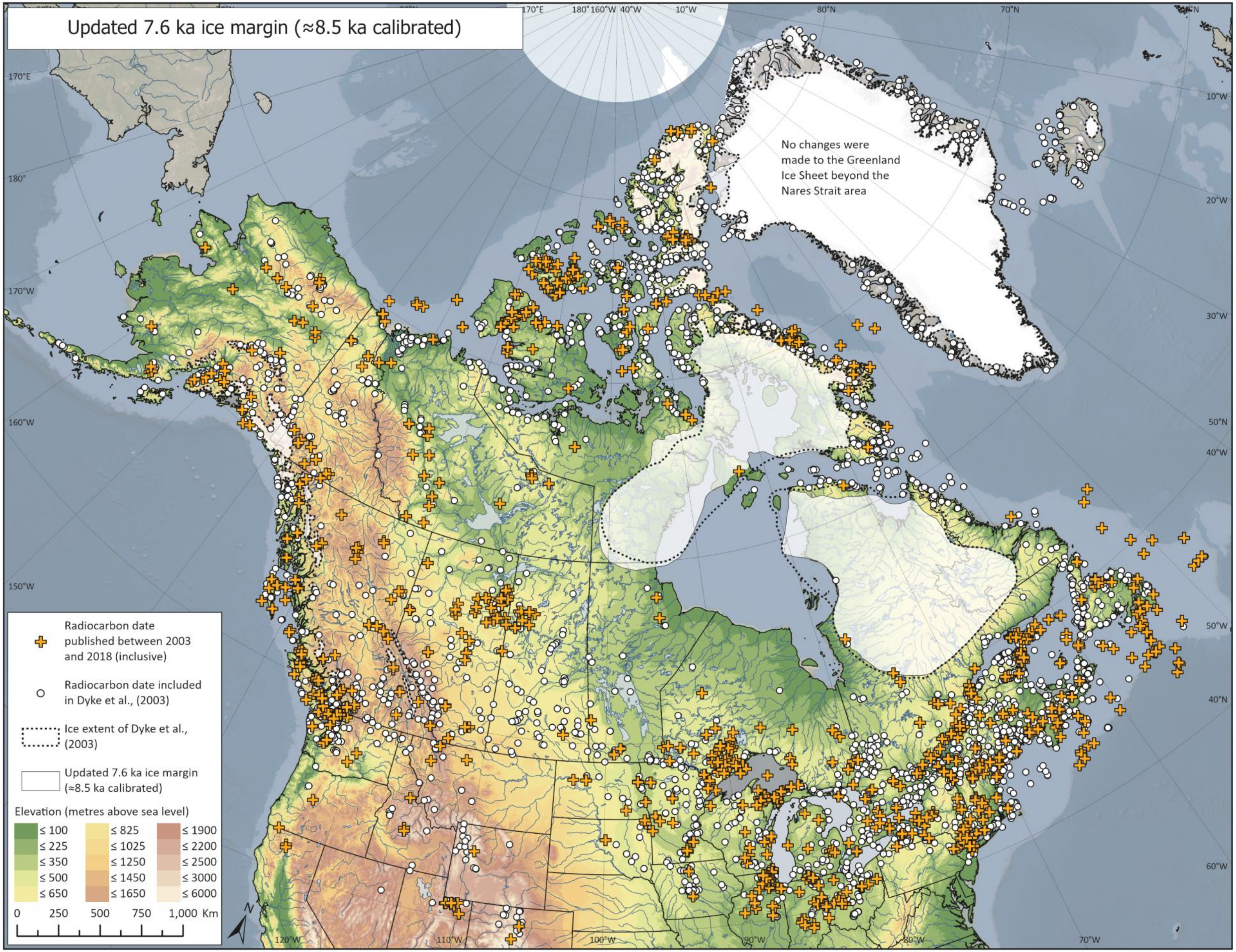

Updated 7.6 ka ice margin (≈8.5 ka calibrated)
No changes were made to the Greenland Ice Sheet beyond the Nares Strait area
Radiocarbon date published between 2003 and 2018 (inclusive)
Radiocarbon date included in Dyke et al., (2003)
Ice extent of Dyke et al., (2003)
Updated 7.6 ka ice margin (≈8.5 ka calibrated)
Elevation (metres above sea level)
≤ 100
≤ 225
≤ 350
≤ 500
≤ 650
≤ 825
≤ 1025
≤ 1250
≤ 1450
≤ 1650
≤ 1900
≤ 2200
≤ 2500
≤ 3000
≤ 6000
0 250 500 750 1,000 Km
N

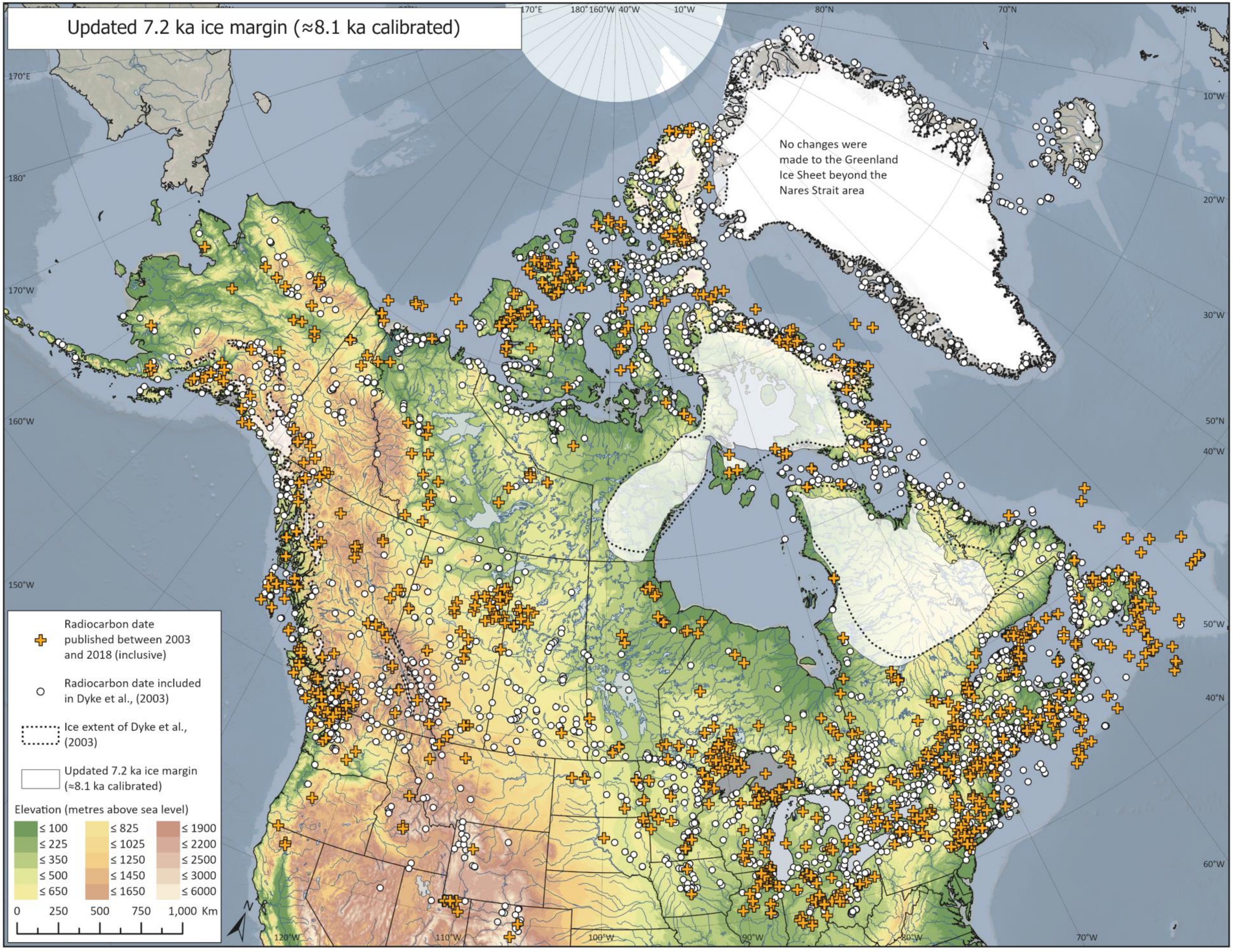
Updated 7.2 ka ice margin (≈8.1 ka calibrated)
No changes were made to the Greenland Ice Sheet beyond the Nares Strait area
Radiocarbon date published between 2003 and 2018 (inclusive)
Radiocarbon date included in Dyke et al., (2003)
Ice extent of Dyke et al., (2003)
Updated 7.2 ka ice margin (≈8.1 ka calibrated)
Elevation (metres above sea level)
≤ 100
≤ 225
≤ 350
≤ 500
≤ 650
≤ 825
≤ 1025
≤ 1250
≤ 1450
≤ 1650
≤ 1900
≤ 2200
≤ 2500
≤ 3000
≤ 6000
0 250 500 750 1,000 Km
N
170°E
180°
170°W
160°W
150°W
120°W
110°W
100°W
90°W
80°W
70°W
10°W
20°W
30°W
40°W
50°N
50°W
40°N
60°W
80°N
70°N

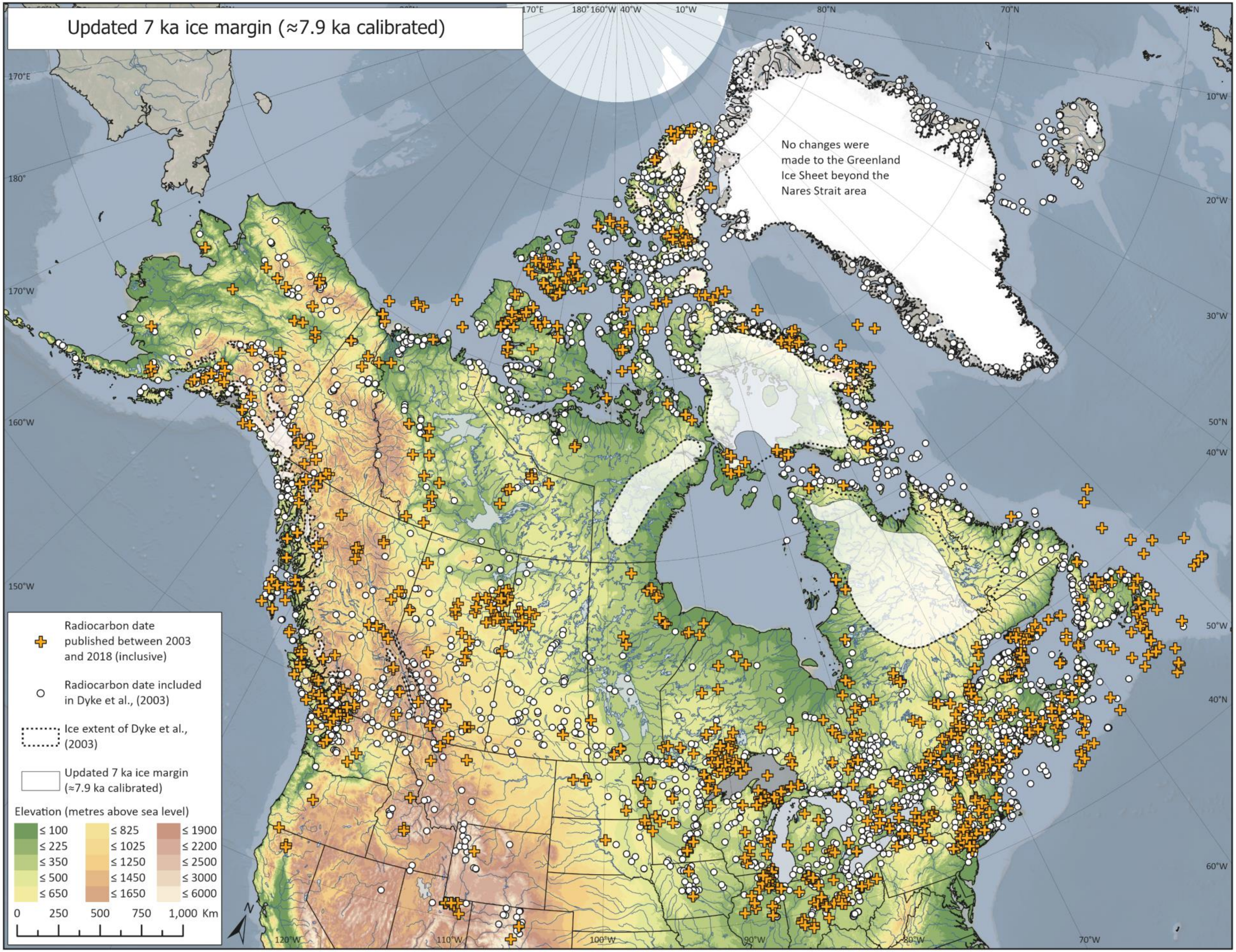

Updated 7 ka ice margin (≈7.9 ka calibrated)
No changes were made to the Greenland Ice Sheet beyond the Nares Strait area
Radiocarbon date published between 2003 and 2018 (inclusive)
Radiocarbon date included in Dyke et al., (2003)
Ice extent of Dyke et al., (2003)
Updated 7 ka ice margin (≈7.9 ka calibrated)
Elevation (metres above sea level)
≤ 100
≤ 225
≤ 350
≤ 500
≤ 650
≤ 825
≤ 1025
≤ 1250
≤ 1450
≤ 1650
≤ 1900
≤ 2200
≤ 2500
≤ 3000
≤ 6000
0 250 500 750 1,000 Km
N

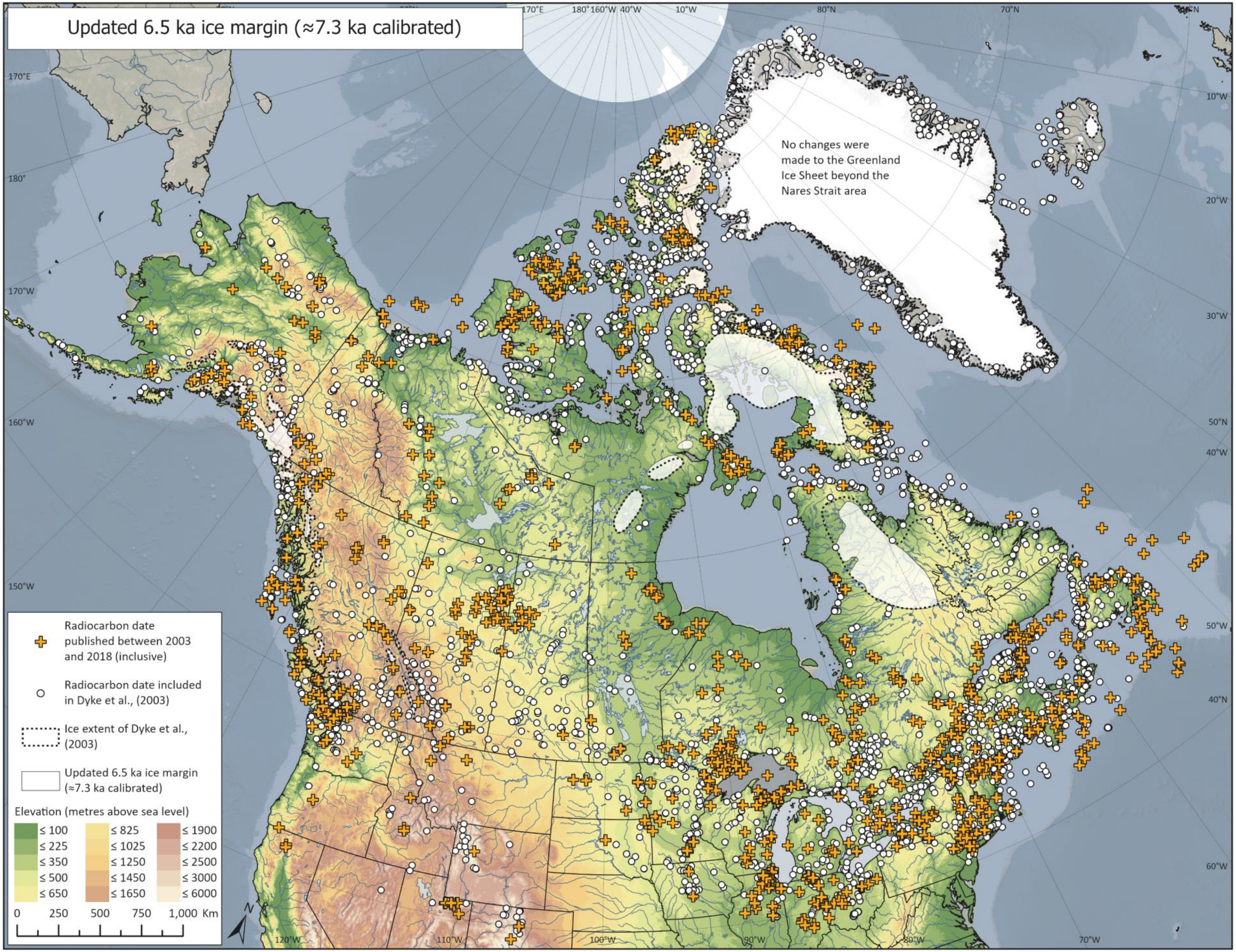
Updated 6.5 ka ice margin (≈7.3 ka calibrated)
No changes were made to the Greenland Ice Sheet beyond the Nares Strait area
Radiocarbon date published between 2003 and 2018 (inclusive)
Radiocarbon date included in Dyke et al., (2003)
Ice extent of Dyke et al., (2003)
Updated 6.5 ka ice margin (≈7.3 ka calibrated)
Elevation (metres above sea level)
≤ 100
≤ 225
≤ 350
≤ 500
≤ 650
≤ 825
≤ 1025
≤ 1250
≤ 1450
≤ 1650
≤ 1900
≤ 2200
≤ 2500
≤ 3000
≤ 6000
0 250 500 750 1,000 Km
N

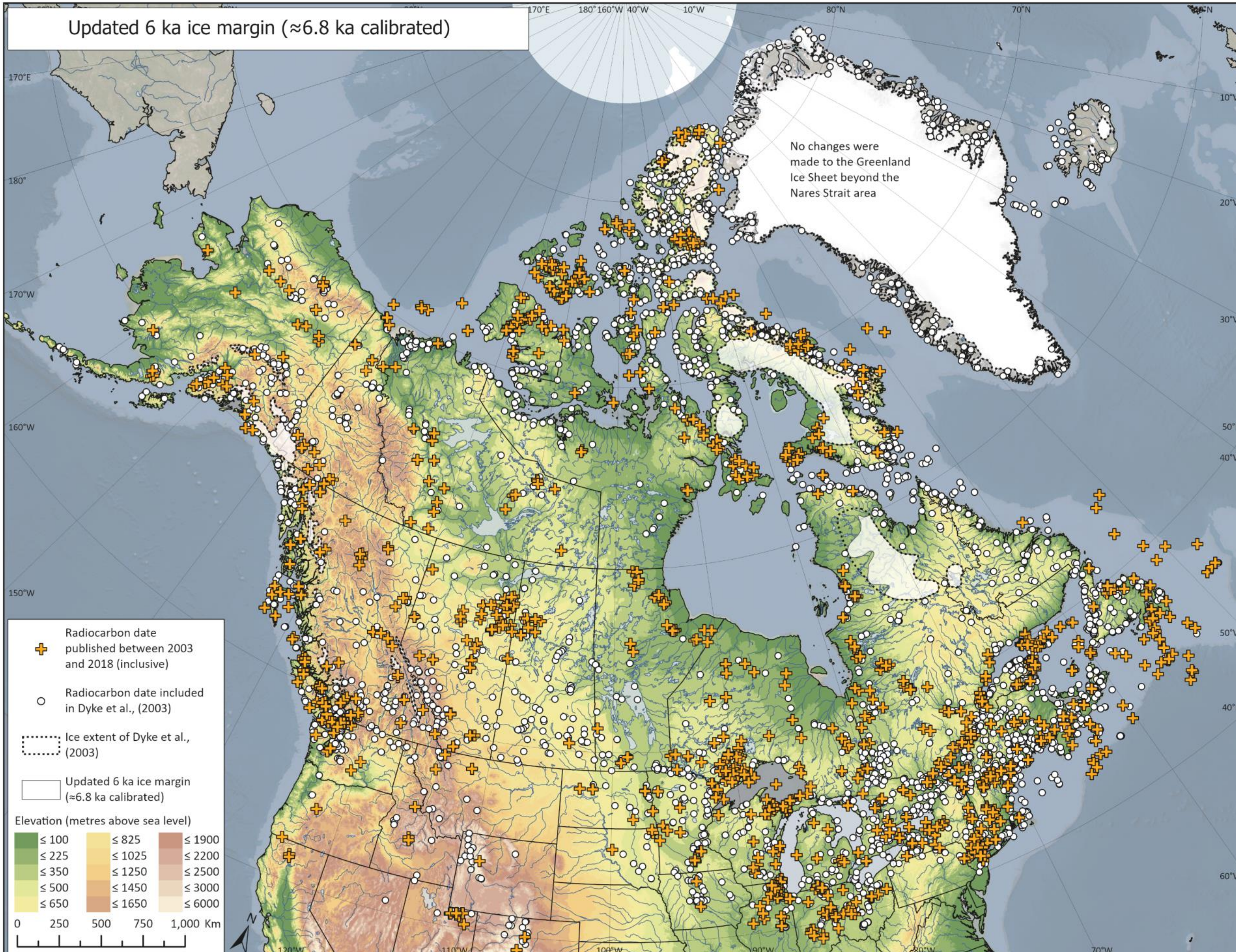

Updated 6 ka ice margin (≈6.8 ka calibrated)
No changes were made to the Greenland Ice Sheet beyond the Nares Strait area
Radiocarbon date published between 2003 and 2018 (inclusive)
Radiocarbon date included in Dyke et al., (2003)
Ice extent of Dyke et al., (2003)
Updated 6 ka ice margin (≈6.8 ka calibrated)
Elevation (metres above sea level)
≤ 100
≤ 225
≤ 350
≤ 500
≤ 650
≤ 825
≤ 1025
≤ 1250
≤ 1450
≤ 1650
≤ 1900
≤ 2200
≤ 2500
≤ 3000
≤ 6000
0 250 500 750 1,000 Km
N
170°E
180°
170°W
160°W
150°W
120°W
110°W
100°W
90°W
80°W
70°W
60°W
50°W
40°N
40°W
50°N
30°W
20°W
10°W
80°N
70°N
170°E
180° 160°W 40°W
10°W

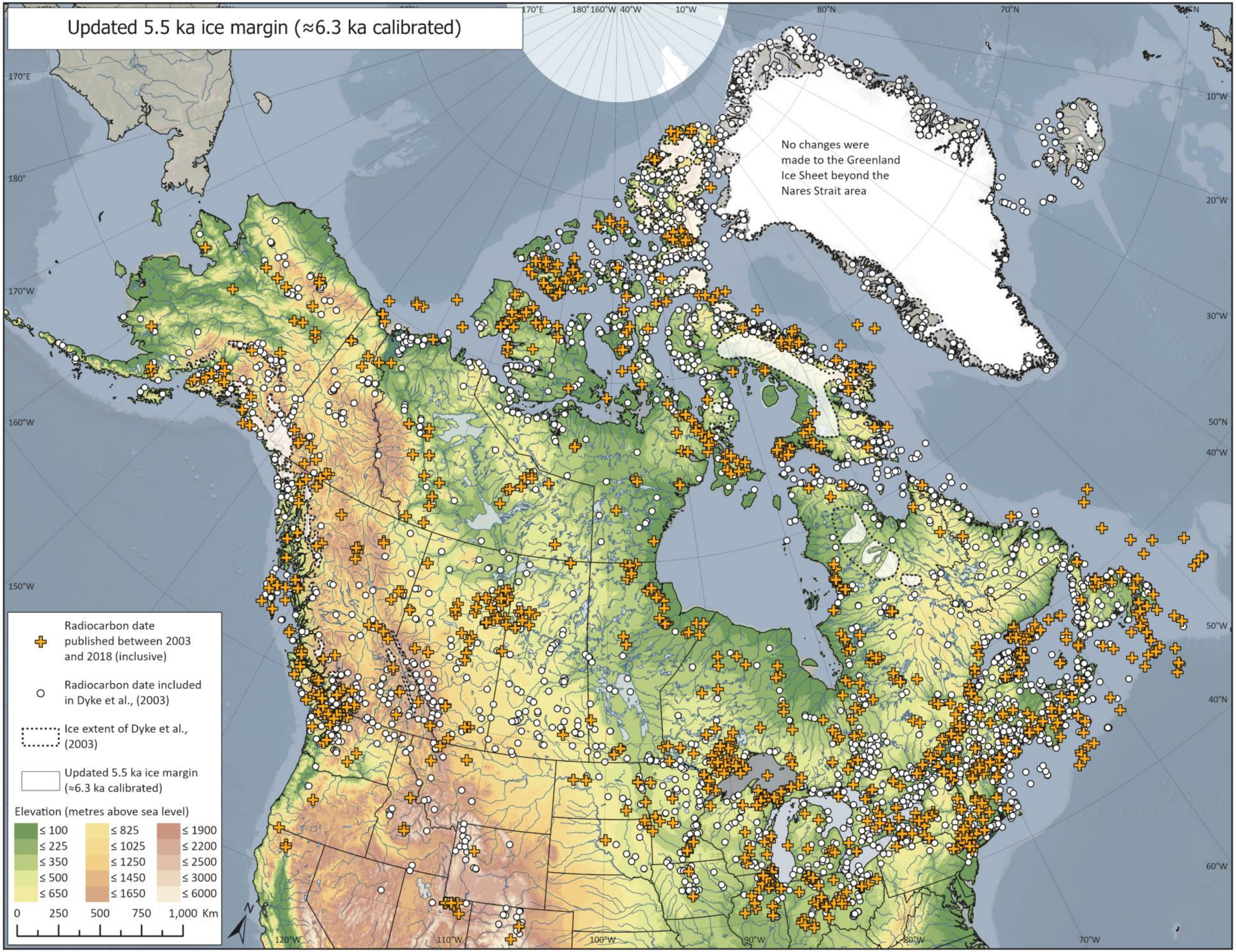
Updated 5.5 ka ice margin (≈6.3 ka calibrated)
No changes were made to the Greenland Ice Sheet beyond the Nares Strait area
Radiocarbon date published between 2003 and 2018 (inclusive)
Radiocarbon date included in Dyke et al., (2003)
Ice extent of Dyke et al., (2003)
Updated 5.5 ka ice margin (≈6.3 ka calibrated)
Elevation (metres above sea level)
≤ 100
≤ 225
≤ 350
≤ 500
≤ 650
≤ 825
≤ 1025
≤ 1250
≤ 1450
≤ 1650
≤ 1900
≤ 2200
≤ 2500
≤ 3000
≤ 6000
0 250 500 750 1,000 Km
N
170°E
180°
170°W
160°W
150°W
120°W
110°W
100°W
90°W
80°W
70°W
10°W
20°W
30°W
40°W
50°W
60°W
50°N
40°N
60°N
80°N
70°N
180°160°W 40°W
10°W

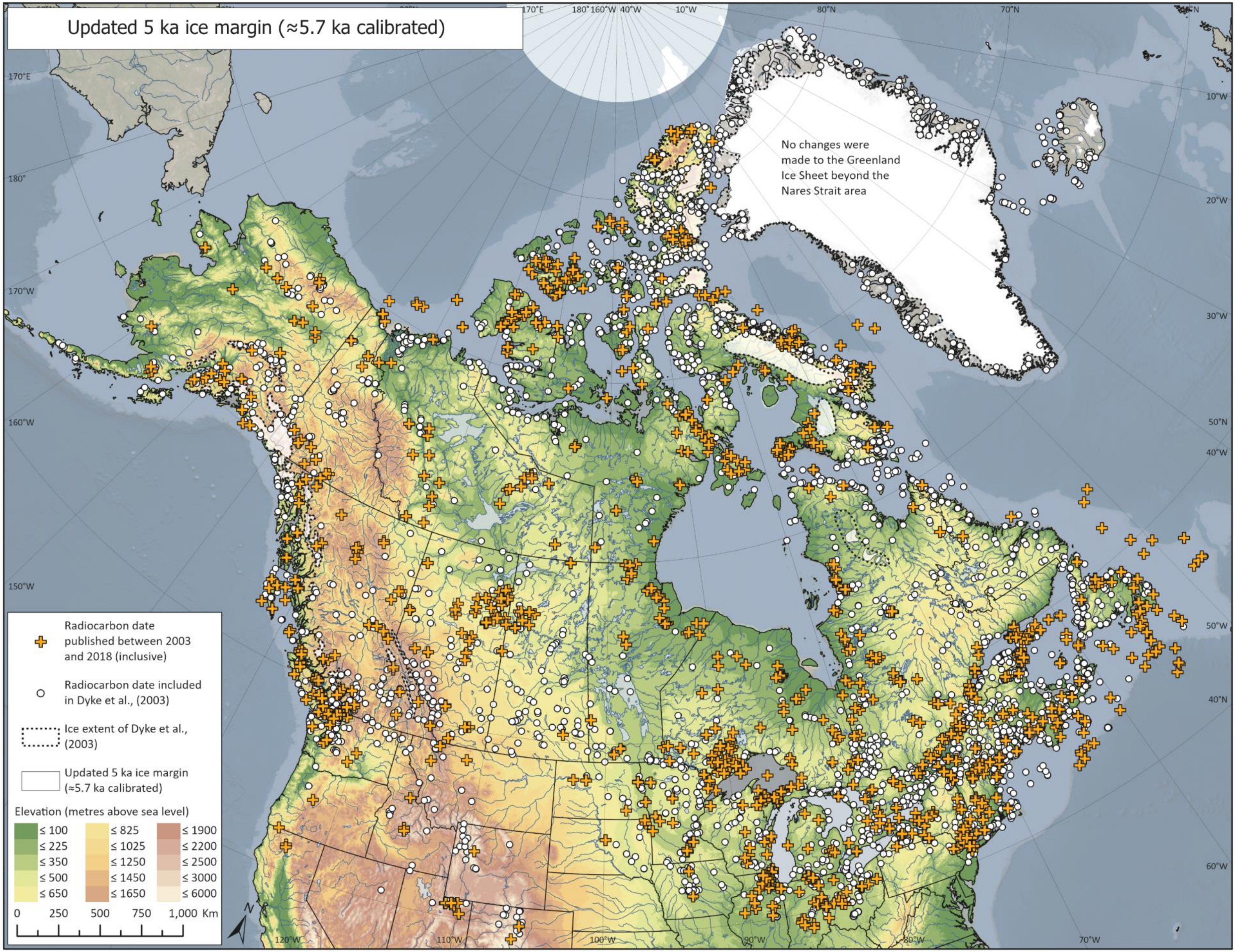
Updated 5 ka ice margin (≈5.7 ka calibrated)
No changes were made to the Greenland Ice Sheet beyond the Nares Strait area
Radiocarbon date published between 2003 and 2018 (inclusive)
Radiocarbon date included in Dyke et al., (2003)
Ice extent of Dyke et al., (2003)
Updated 5 ka ice margin (≈5.7 ka calibrated)
Elevation (metres above sea level)
≤ 100
≤ 225
≤ 350
≤ 500
≤ 650
≤ 825
≤ 1025
≤ 1250
≤ 1450
≤ 1650
≤ 1900
≤ 2200
≤ 2500
≤ 3000
≤ 6000
0 250 500 750 1,000 Km
N

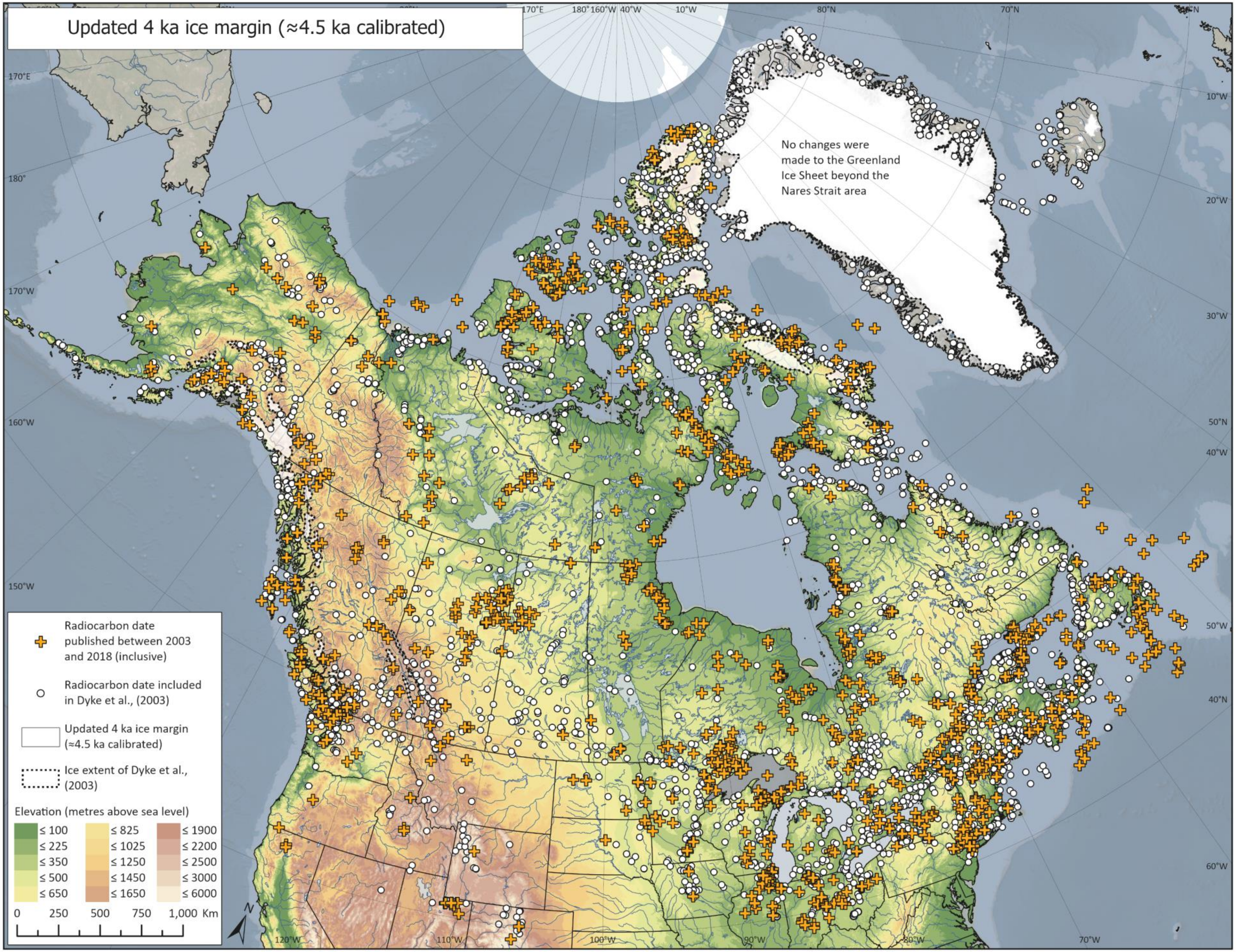
Updated 4 ka ice margin (≈4.5 ka calibrated)
No changes were made to the Greenland Ice Sheet beyond the Nares Strait area
Radiocarbon date published between 2003 and 2018 (inclusive)
Radiocarbon date included in Dyke et al., (2003)
Updated 4 ka ice margin (≈4.5 ka calibrated)
Ice extent of Dyke et al., (2003)
Elevation (metres above sea level)
≤ 100
≤ 225
≤ 350
≤ 500
≤ 650
≤ 825
≤ 1025
≤ 1250
≤ 1450
≤ 1650
≤ 1900
≤ 2200
≤ 2500
≤ 3000
≤ 6000
0 250 500 750 1,000 Km
N

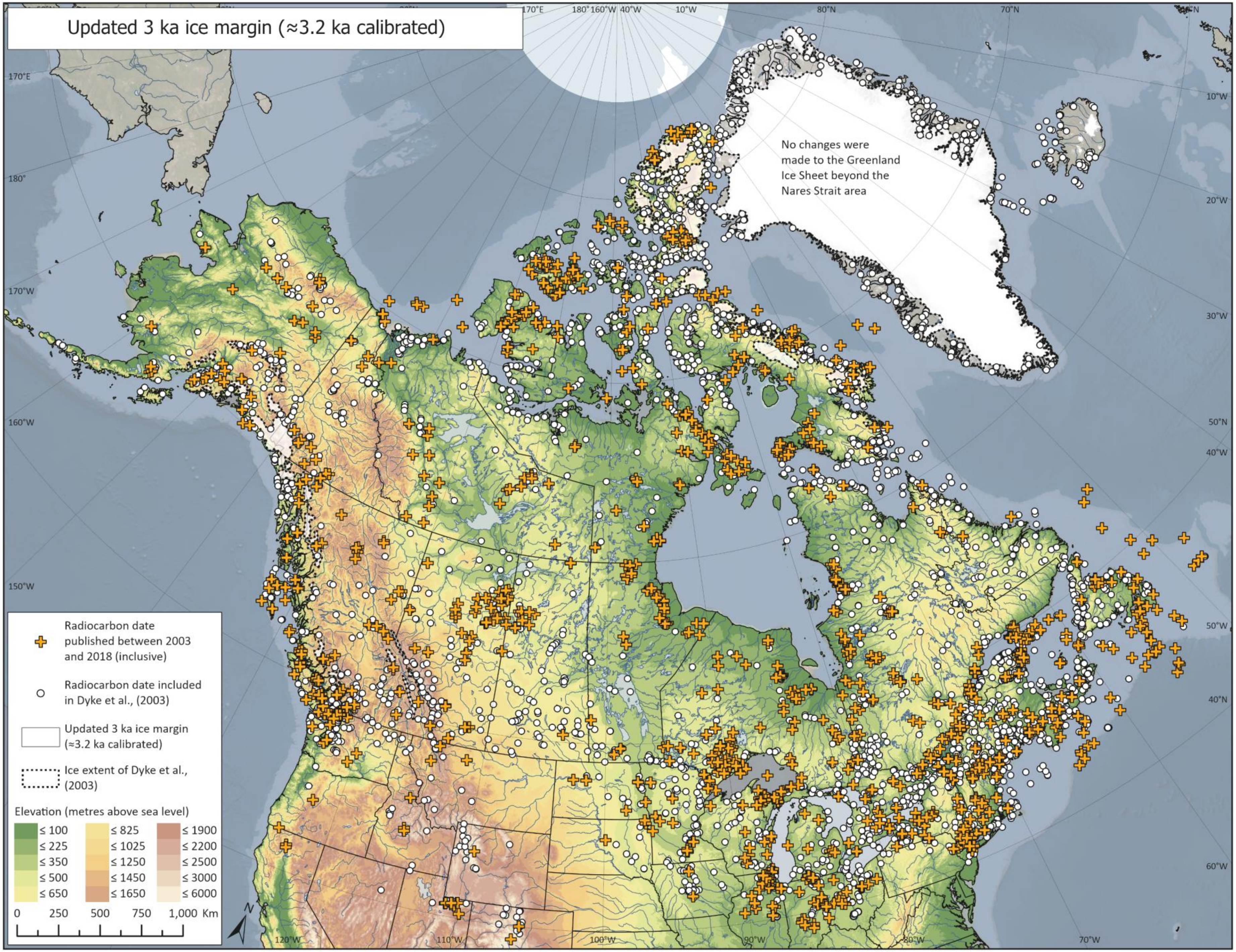

Updated 3 ka ice margin (≈3.2 ka calibrated)
No changes were made to the Greenland Ice Sheet beyond the Nares Strait area
Radiocarbon date published between 2003 and 2018 (inclusive)
Radiocarbon date included in Dyke et al., (2003)
Updated 3 ka ice margin (≈3.2 ka calibrated)
Ice extent of Dyke et al., (2003)
Elevation (metres above sea level)
≤ 100
≤ 225
≤ 350
≤ 500
≤ 650
≤ 825
≤ 1025
≤ 1250
≤ 1450
≤ 1650
≤ 1900
≤ 2200
≤ 2500
≤ 3000
≤ 6000
0
250
500
750
1,000 Km
N
170°E
180°
170°W
160°W
150°W
120°W
110°W
100°W
90°W
80°W
70°W
10°W
20°W
30°W
40°W
50°N
50°W
40°N
60°W
80°N
70°N

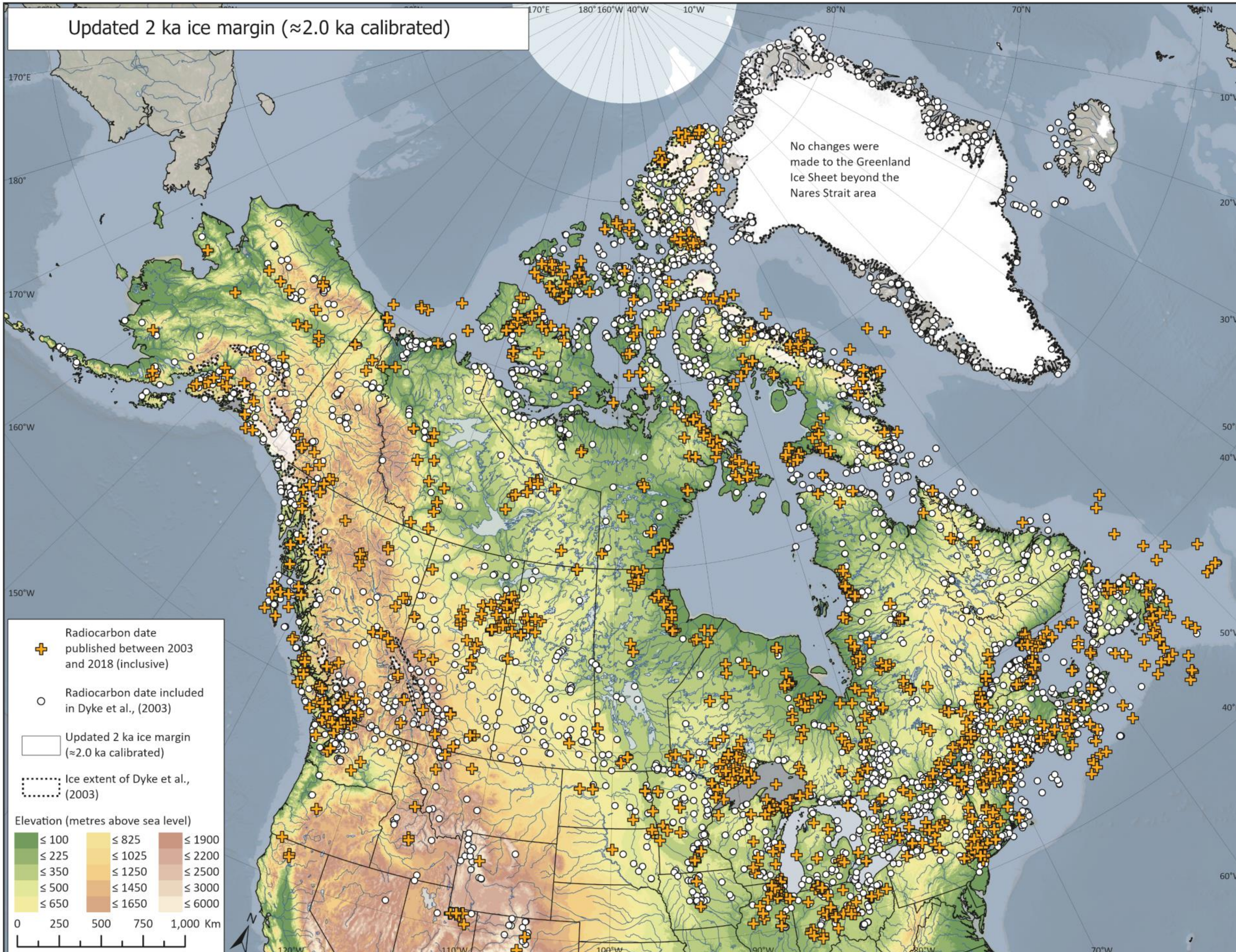

Updated 2 ka ice margin (≈2.0 ka calibrated)
No changes were made to the Greenland Ice Sheet beyond the Nares Strait area
Radiocarbon date published between 2003 and 2018 (inclusive)
Radiocarbon date included in Dyke et al., (2003)
Updated 2 ka ice margin (≈2.0 ka calibrated)
Ice extent of Dyke et al., (2003)
Elevation (metres above sea level)
≤ 100
≤ 225
≤ 350
≤ 500
≤ 650
≤ 825
≤ 1025
≤ 1250
≤ 1450
≤ 1650
≤ 1900
≤ 2200
≤ 2500
≤ 3000
≤ 6000
0 250 500 750 1,000 Km
N
120°W
110°W
100°W
90°W
80°W
70°W
60°W
50°W
40°N
50°N
40°W
30°W
20°W
10°W
70°N
80°N
170°E
180°
170°W
160°W
150°W

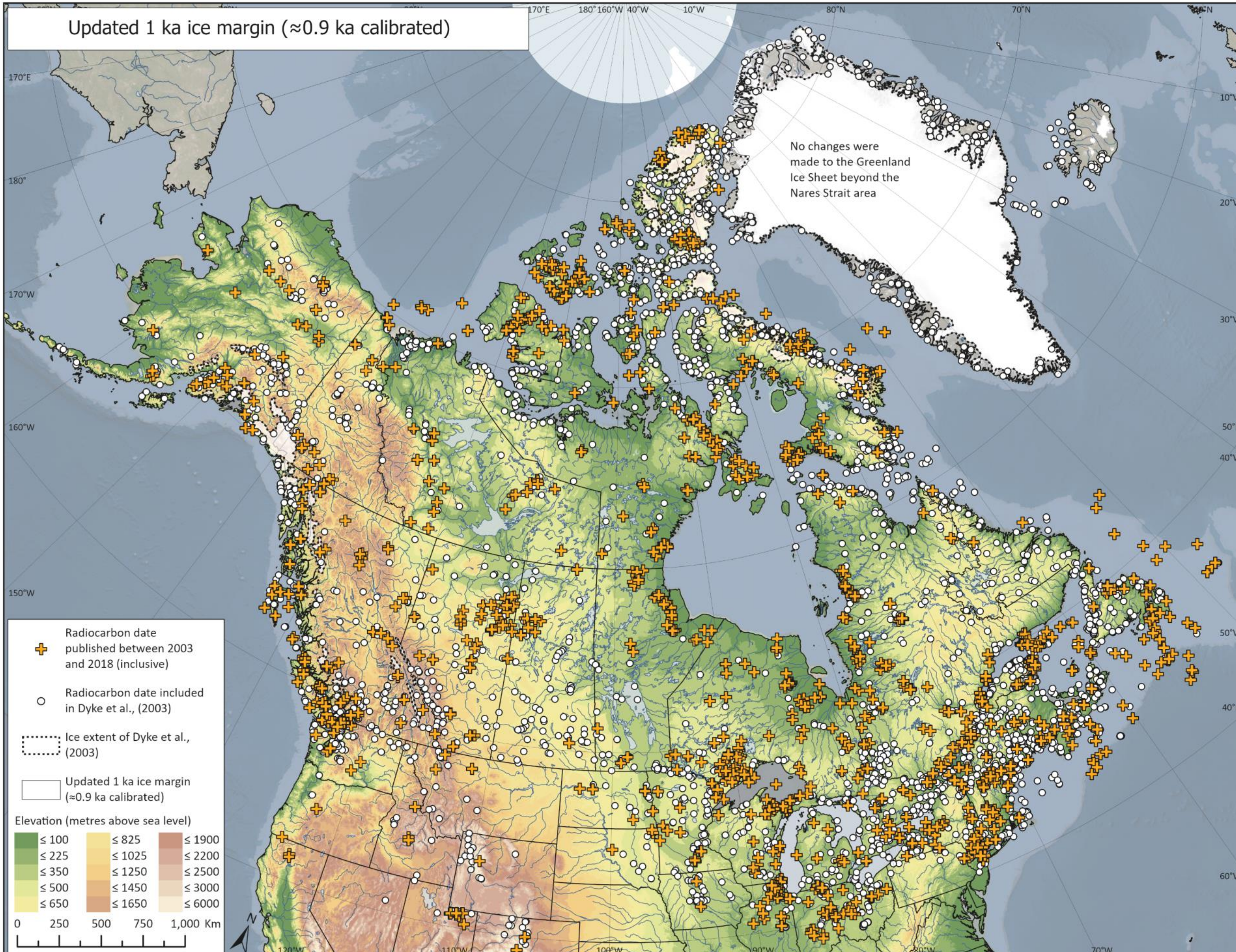
Updated 1 ka ice margin (≈0.9 ka calibrated)
No changes were made to the Greenland Ice Sheet beyond the Nares Strait area
Radiocarbon date published between 2003 and 2018 (inclusive)
Radiocarbon date included in Dyke et al., (2003)
Ice extent of Dyke et al., (2003)
Updated 1 ka ice margin (≈0.9 ka calibrated)
Elevation (metres above sea level)
≤ 100
≤ 225
≤ 350
≤ 500
≤ 650
≤ 825
≤ 1025
≤ 1250
≤ 1450
≤ 1650
≤ 1900
≤ 2200
≤ 2500
≤ 3000
≤ 6000
0 250 500 750 1,000 Km
N
120°W
110°W
100°W
90°W
80°W
70°W
170°E
180°
170°W
160°W
150°W
10°W
20°W
30°W
50°N
40°W
50°W
40°N
60°W
80°N
70°N